1-1-2012

A Phenomenological Investigation of Ignition and Combustion in Alternative-Fueled Engines

Saroj Kumar Jha

Follow this and additional works at: https://scholarsjunction.msstate.edu/td

Recommended Citation

Jha, Saroj Kumar, "A Phenomenological Investigation of Ignition and Combustion in Alternative-Fueled Engines" (2012). *Theses and Dissertations*. 225.
https://scholarsjunction.msstate.edu/td/225

A PHENOMENOLOGICAL INVESTIGATION OF IGNITION AND COMBUSTION

IN ALTERNATIVE-FUELED ENGINES

By

Saroj Kumar Jha

A Dissertation
Submitted to the Faculty of
Mississippi State University
in Partial Fulfillment of the Requirements
for the Degree of Doctor of Philosophy
in Mechanical Engineering
in the Department of Mechanical Engineering

Mississippi State, Mississippi

May 2012

A PHENOMENOLOGICAL INVESTIGATION OF IGNITION AND COMBUSTION

IN ALTERNATIVE-FUELED ENGINES

By

Saroj Kumar Jha

Approved:

_____
Kalyan K. Srinivasan
Assistant Professor of Mechanical
Engineering
(Major Advisor)

_____
Sundar R. Krishnan
Assistant Professor of Mechanical
Engineering
(Co-Major Advisor)

_____
Rogelio Luck
Professor of Mechanical
Engineering
 (Committee member)

_____
Rafael Hernandez
Associate Professor of Chemical
Engineering
(Committee member)

_____
Pedro Mago
Associate Professor of Mechanical
Engineering
(Committee member)

_____
Steven R. Daniewicz
Paccar Chair and Head of Mechanical
Engineering
(Graduate Coordinator)

_____
Sarah A. Rajala
Dean of Bagley College of Engineering

Name: Saroj Kumar Jha

Date of Degree: May 11, 2012

Institution: Mississippi State University

Major Field: Mechanical Engineering

Major Professor: Kalyan K. Srinivasan

Title of Study: A PHENOMENOLOGICAL INVESTIGATION OF IGNITION AND
                   COMBUSTION IN ALTERNATIVE-FUELED ENGINES

Pages in Study: 168

Candidate for Degree of Doctor of Philosophy

Current diesel technologies involve a broad spectrum of combustion regimes. Previous diesel combustion models either lack the universality across various combustion regimes or suffer computational cost. This dissertation discusses the development of a phenomenological framework to identify and understand key in-cylinder processes that influence the overall performance of a compression ignition engine. The first part of this research is focused on understanding the ignition delay (ID) of diesel fuel in a pilot-ignited partially premixed, low temperature natural gas (NG) combustion engine. Lean premixed low temperature NG combustion is achieved by using small pilot diesel sprays (2-3% of total fuel energy) injected during early compression stroke (about 60° BTDC). Modeling ignition delay at advanced pilot injection timings (50°-60°BTDC) presents unique challenges. In this study, single component droplet evaporation model in conjunction with the Shell hydrocarbon autoignition (SAI) model is used to obtain ignition delay predictions of pilot diesel over a wide range of injection timings (20°-60° BTDC). Detailed sensitivity analysis of several SAI model parameters revealed that the model parameter Aq, which influences chain initiation reactions, was most important to

predict ignition delays at very lean equivalence ratios. Additional studies performed to ascertain critical model parameters revealed that ignition delay was particularly sensitive to intake manifold temperature over the range of injection timings investigated. Finally, the validated SAI model was used to predict ignition delays of pilot diesel fuel at various exhaust gas recirculation (EGR) substitutions, intake manifold temperatures and engine loads (bmep = 6 bar and 3 bar, respectively).

The second part of this research involved the development of a phenomenological simulation of diesel/biodiesel combustion, which included sub-models for diesel spray entrainment, evaporation, ignition and premixed and mixing-controlled combustion. In the simulation, the cylinder contents consisted of an unburned zone, packet zones, and a burned zone. The simulation, after appropriate calibration, was capable of predicting cylinder pressure and heat release rates at different engine load conditions over the injection timing range of 0°BTDC to 10°BTDC. The total number of packets, droplet evaporation rates, air entrainment rates; ignition delay and premixed/mixing-controlled reaction rate parameters had a profound influence on combustion predictions.

ACKNOWLEDGEMENTS

I would like to express my deepest and everlasting gratitude to my parents, Sri Mani Kant Jha and Smt. Pramila Devi for their love, support and encouragement throughout my life.

I would like to dedicate this thesis to my wife, Sharada, for her love, sacrifice and devotion. Her contribution towards my thesis is immeasurable.

TABLE OF CONTENTS

LIST OF TABLES

LIST OF FIGURES

ix

CHAPTER I

INTRODUCTION

Background

The progressive evolution of diesel engine technologies has enabled engineers to overcome many barriers related to clean and efficient power generation. However, there are still several challenges that must be surmounted, including increasingly restrictive emissions norms and the need for better fuel conversion efficiencies. To reduce the adverse effects of particulate matter (PM) and nitrogen oxides (NO_x) emissions on human health and the environment, the US Environmental Protection Agency (EPA) has imposed very stringent emissions standards for heavy-duty diesel engines as shown in Figure 1.1. Moreover, since global crude oil resources are finite (Wood et al. 2004), energy security and sustainability concerns have dictated the search for alternatives to conventional petroleum-based fuels. Therefore, tough emissions regulations combined with diminishing crude oil resources provide ample justification for adopting advanced combustion strategies and alternative fuels.

Biodiesel is currently being considered as a sustainable alternative to conventional (petroleum) diesel fuel since it is produced from renewable sources. There are several advantages of using biodiesel as an alternative fuel in diesel engines. It is completely miscible with petroleum diesel fuel, hence different blends with varying percentages of biodiesel and diesel can be used. Biodiesel significantly reduces carbon dioxide (CO_2), carbon monoxide (CO), unburned hydrocarbon (UHC) and particulate matter (PM)

1

emissions (Agency 2002). The substantial reduction in net CO_2 by 78.45% is credited to biodiesel produced from crops that consume CO_2 from the atmosphere (Sheehan et al. 1998; Hill et al. 2006). Furthermore biodiesel is an oxygenated fuel, containing approximately 11% oxygen by weight (Yuan 2005). This is believed to yield more complete combustion, resulting in lower CO, UHC and PM emissions (Wang et al. 2000; USEPA 2002; McCormick et al. 2005).
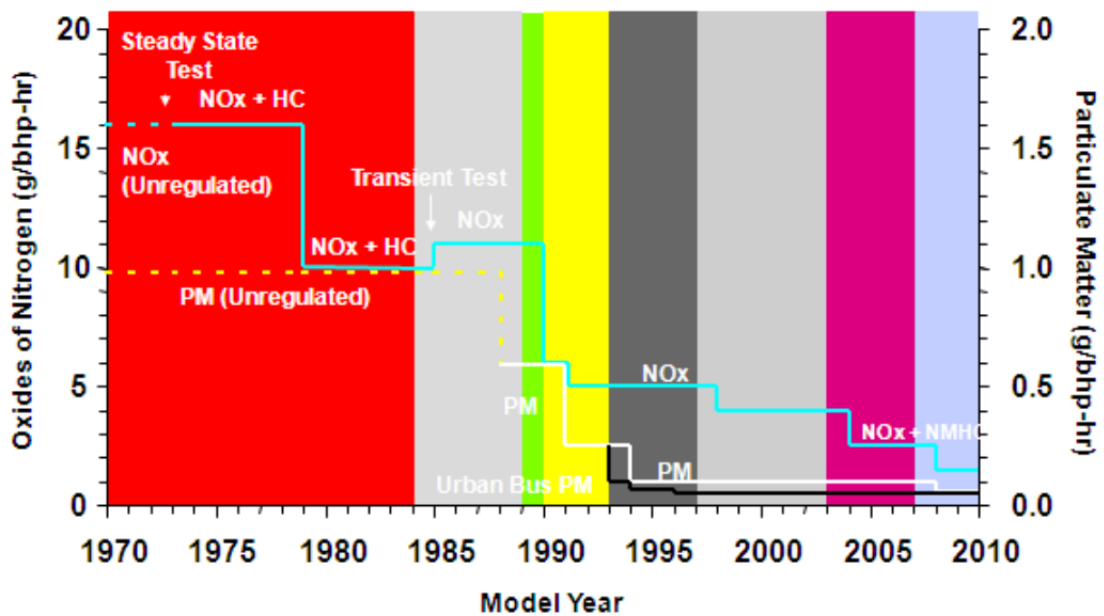
Figure 1.1   Heavy duty diesel engine emissions standards (US-EPA)
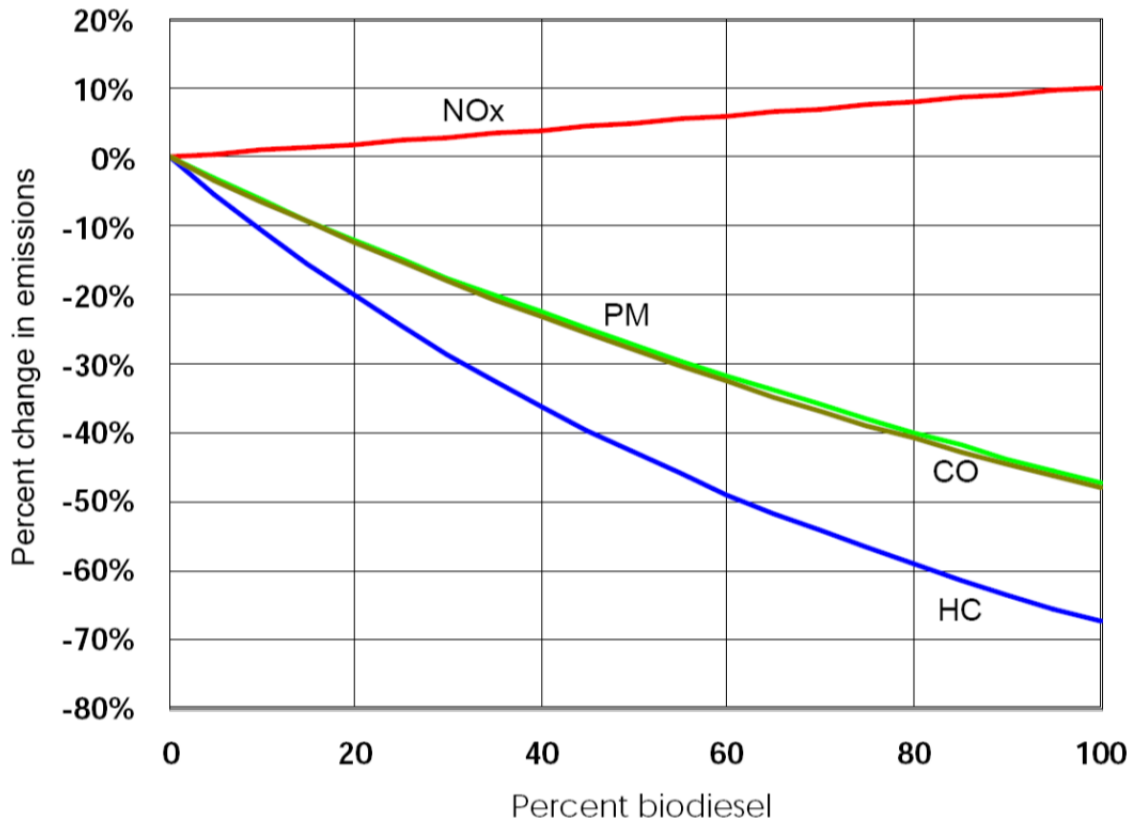
Figure 1.2   Average emission impacts of biodiesel for heavy-duty high-way engines

There are some disadvantages associated with biodiesel, including lower energy density and higher nitrogen oxides (NO_x) emissions than conventional diesel. The lower heating value of biodiesel is about 12% lower than that of diesel, which means that biodiesel has lower energy content. The lower heating value of diesel is approximately 43 MJ/kg while that of biodiesel is approximately 37 MJ/kg. Hence the fuel efficiency is reduced, which implies more biodiesel fuel (approximately 8%) (Tat 2003) is required to achieve the same amount of torque or power as compared to diesel fuel (Yuan 2005). Another problem faced in the use of biodiesel on unmodified diesel engines is higher smog-generating NOx emissions (Szybist et al. 2007). These biodiesel emissions trends are shown in Figure 1.2 for fuel blends from conventional diesel (B0) to 100% biodiesel (B100) (USEPA 2002).

Significant reductions in CO, PM and UHC emissions were observed with an increase in biodiesel blend ratio. In contrast, a 10% increase in NO_x emissions is typically observed with B100. Several different theories have been proposed as the cause for this biodiesel NOx effect increase (McCormick et al. 2001; Ban-Weiss et al. 2007). The NO_x increases observed in modern engines have been more significant (McCormick et al. 2005). Though diesel engines can be operated with biodiesel without any modifications to the engine hardware, significant variations in engine performance and emissions have been reported because of the inherent differences in physical and chemical properties between biodiesel and petroleum diesel (Knothe 2001; Rakopoulos et al. 2008). Several mechanisms have been hypothesized to explain these performance and emissions differences. These include the possible effects related to differences in viscosity (Patterson et al. 2006), bulk modulus (Szybist et al. 2005), boiling point (Choi et al. 1997), adiabatic flame temperature (Ban-Weiss et al. 2007), radiative heat loss (Szybist et al. 2007) and their effects on thermal NOx and/or prompt NOx production (Szybist et al. 2007). In general, it is reported that biodiesel usage in diesel engines leads to shorter ignition delays, which tend to decrease the level of premixed combustion, and also results in longer combustion durations relative to petroleum diesel (Hashimoto et al. 2002; Canacki 2007). Considerable research has been conducted in order to determine the cause of and to develop strategies for mitigating biodiesel-induced increases in NO_x emissions. The prime objective of such efforts has been to improve the combustion process by studying the effects of engine parameters on engine performances.

Both experiments and calculations can be used to evaluate the effects of individual parameters on engine performance and emissions. Experimental investigations provide relatively precise results for a specific test, but the cause and effect of individual

parameters in the test results are difficult to conclude when many parameters are involved. Therefore, time consuming and expensive experimental approaches are impractical to evaluate the combined effects of multiple variables. On the other hand, the numerical approach, although possibly less precise in prediction, is very useful in finding the impact of a particular parameter. Combustion models range from zero-dimensional and single-zone to quasi-dimensional, multi-zone and multi-dimensional models based their thermodynamic resolution of working mixtures.

Zero-dimensional single-zone models assume that the cylinder charge is uniform in both composition and temperature at all times during the cycle (Foster 1985; Assanis and Heywood 1986). Computationally efficient single-zone models have been widely used for predicting engine performance. However, it is difficult to use this type of model to account for fuel spray evolution and for spatial variations of mixture composition and temperature. On the other hand, multidimensional simulation (Amsden et al. 1985; Amsden et al. 1987; Patterson et al. 1994; Varnavas and Assanis 1996) resolves the space of the cylinder on a fine scale and solves governing equations of conservation of mass, momentum and energy, as well as governing equations for species and chemical kinetics. However, computational time and storage constraints prevent it from being used for the practical application of an engine simulation. Also, multidimensional models are not computationally efficient for engine cycle simulation and integrated vehicle system simulation.

On the other hand, quasi-dimensional, multi-zone models (Li and Assanis 1993; Tauzia et al. 2000), which are an intermediate step between zero-dimensional and multi-dimensional models, have been effectively used to model diesel engine combustion systems. These models need significantly less computing resources compared to

multidimensional models. Instead of solving the full momentum equation, which is one of the main reasons of computational inefficiencies of multi-dimensional models, these models depend on a blend of fundamental theory. Quasi-dimensional models can also offer the fastest and least expensive means of generating the spatial information required to predict emission products. Various quasi-dimensional models have been developed with different levels of complexity to predict engine combustion.

Many advanced combustion concepts such as homogeneous charge compression ignition (HCCI) (Epping et al. 2002), premixed charge compression ignition (PCCI) (Cao et al. 2009), etc. are being examined by researchers to meet NOx and PM emissions standards for heavy-duty diesel engines. Various low temperature combustion (LTC) strategies such as the Nissan modulated kinetics (MK) concept (Kimura et al. 1999) are used in modern diesel engines to control NO_x and PM emissions, and in all of these strategies, the phasing of the combustion process is of critical importance vis-à-vis engine performance and emissions. Studies have shown that the start of combustion and hence, the ignition delay, plays a very important role in the appropriate phasing of the combustion process with respect to the top dead center (TDC). For conventional diesel combustion, fuel injection timings and the start of combustion are usually close to TDC, and the fuel injection and combustion events may occur simultaneously; consequently, the associated NO_x emissions are relatively high. By comparison, for early injection timings associated with some LTC strategies, the fuel injection and combustion events are separated from each other, and therefore, the NO_x emissions are much lower. Clearly, direct control of the ignition delay period, which separates the fuel injection and combustion events, is critical for achieving LTC and reducing NO_x and PM emissions. Therefore, it is very important to understand the underlying processes governing fuel

6

autoignition and develop a robust ignition delay model to simulate the low temperature combustion process.

This dissertation focuses on the simulation of different combustion phenomena of diesel engines employing diesel and biodiesel as primary fuels. This work will also discuss the autoignition chemistry for diesel and biodiesel and demonstrate the need for change in the shell autoignition model to obtain accurate ignition delay predictions. The specific objectives of the present research effort are described in the next section.

Objectives

The principal motivation for the current research, as stated in the previous section, is to analyze the combustion process in a diesel engine with alternative fuels such as diesel, biodiesel and blends of diesel and biodiesel. To accomplis this, the dissertation focuses on numerical investigations of combustion in diesel engines with the following primary objectives:

Objective 1: To develop and validate a reduced-kinetic ignition delay model for conventional and low temperature diesel and alternative fueled combustion engines

Objective 2: To develop and validate a phenomenological simulation of diesel, and biodiesel combustion using models for physical processes such as fuel evaporation, air entrainment, ignition delay, premixed and mixing-controlled spray combustion.

Organization of the dissertation

This work is organized into four chapters. Chapter I provides the background, motivation and primary objectives of this research. Chapter II deals with detailed investigations of the ignition delay process of diesel fuel using the Shell Auto Ignition (SAI) model. This chapter first reviews past research published in the open literature on

chemical kinetic pathways to describe the ignition delay of diesel-like fuels. Later on, it discusses approaches to the modeling of autoignition and fuel evaporation and effect of different parameters on ignition delay using the SAI model. Chapter III discusses the phenomenological simulation of diesel and biodiesel combustion. This chapter starts with a literature review of diesel and biodiesel combustion. This is followed by a discussion of the development of a phenomenological simulation with detailed calibration of varioussub-models based on sensitivity analyses. Finally, the phenomenological diesel and biodiesel simulations are validated extensively against experimental measurements. The fourth chapter presents a summary of the simulation research efforts, and reiterates the main conclusions attained in this dissertation research. The final chapter itemizes some recommendations for future work on diesel and biodiesel combustion.

CHAPTER II

IGNITION PROCESS MODELING

Autoignition can be described as a phenomenon leading to the start of combustion in a reactive medium of an air-fuel mixture (Kuo 1986). At times autoignition is termed as spontaneous ignition, self-ignition or homogeneous ignition. Fuel-air mixture can be lit off by quick compression, as in diesel engines (or by pressure waves due to quick heat release, as in spark ignition engines). In diesel engines, there are several phenomena that lead to autoignition of a fuel vapor-air mixture along with evaporation of fuel droplets. It has been found that the fuel in evaporation rate influences vapor availability for the autoignition to take place. Moreover, increase in temperature during the autoignition process augments droplet heating and evaporation processes; therefore, the investigation of fuel droplet heating and evaporation in engine-like conditions should be coupled with the research of autoignition. In this chapter, the focus will be on the discussion of approaches to the modeling of autoignition and fuel evaporation.

Background

Estimation of ignition delay in diesel engines is of great significance because of its impact on startability, engine noise and pollutant formation. It is also important from the perspective of preparing the fuel before injecting into the engine. Ignition delay is the time from the instant when the first packet of fuel enters the combustion chamber (start of injection) to the moment when the first flame is observed in the spray (start of combustion). This delay period includes (a) physical delay, wherein atomization,

9

vaporization and mixing of air/fuel occur and (b) chemical delay attributed to pre-combustion reactions. Both physical and chemical delays occur simultaneously.

Many ignition delay correlations have been formulated based on experiments conducted in constant volume bombs, rapid compression machines and engines (Wolfer 1938; Halstead et al. 1975; Kadota et al. 1976; Hardenberg and Hase 1979; Watson et al. 1980; Hiroyasu et al. 1983; Schapertons and Lee. 1985; Lahiri et al. 1997; Assanis et al. 2003). Wolfer (1938) developed the earliest correlation for predicting ignition delay based on exponential dependence on temperature as in Arrhenius' equation for rate of reaction. Kadota et al. (1976) and Hiroyasu et al. (1983) further studied the effect of equivalence ratio on ignition delay prediction. In order to make the expression suitable for oxygenated fuels, Lahiri et al. (1997) modified the equivalence ratio used in expression by Hiroyasu et al. (1983) to fuel-oxygen ratio. However, these correlations are not robust enough to calculate the ignition delay under transient diesel engine conditions as they are based on experiments conducted in a constant volume bomb. Another reason for their limited predictability is their application outside the temperature and pressure range of their validity. On the other hand, a few correlations have been developed considering engine data under steady state operating conditions (Hardenberg and Hase 1979, Watson et al. 1980). These correlations also failed to yield accurate predictions under widely varying operating conditions. Assanis et al. (1999) later compared these correlations and presented a modified Watson correlation (1980).

Furthermore, numerous efforts have been devoted to understand the fundamental chemical reaction mechanisms governing the autoignition of hydrocarbon fuels and/or their surrogates (Minetti et al. 1995; Curran et al. 1998; Curran et al. 2002; Soyhan et al. 2002; Tanaka et al. 2003). These studies range from detailed kinetic mechanisms of

hydrocarbon oxidation (Minetti et al. 1995; Kumar et al. 2009; Westbrook et al. 2009) (applicable over a very wide range of temperature and pressure conditions) to reduced kinetic mechanisms (Halstead et al. 1975; Griffiths 1995; Soyhan et al. 2002; Tanaka et al. 2003; Ra and Reitz 2008) that are of a more limited scope. Since fuel ignition chemistry is quite complicated even for n-alkanes larger than C_5, reduced kinetic mechanisms are often desirable, especially when ignition chemistry is coupled with other combustion computations such as fluid and heat transport. Since the chemistry of fuel autoignition is very complex, simplifications are often necessary to simulate autoignition in practical combustion systems.

The Shell autoignition (SAI) model is one example of a simplified reduced kinetic model for hydrocarbon autoignition. The SAI model, originally proposed by Halstead et al. (Halstead et al. 1977) for simulating the onset of knock in spark ignition engines, is a generic reduced kinetic mechanism that is currently widely used to simulate autoignition in diesel engines. The original SAI model has been subsequently improved (Schapertons and Lee. 1985; Sazhin et al. 1999; Hamosfakidis and Reitz 2003) to account for mass conservation, overall energy balance, and preignition energy release calculations. Griffiths (Griffiths 1995) analyzed various reduced kinetic models for hydrocarbon oxidation including the SAI model and its subsequent development (Cox and Cole 1985; Hu and Keck 1987). Griffiths found that in fuels with two-stage autoignition, the shell model seemed to be biased towards longer duration of first stage evolution and towards shorter duration in the development of second stage. While the SAI model has been shown to predict ignition processes fairly accurately in engines for fuel injection timings close to top dead center (i.e. at high temperatures), its performance for early injection timings that involve low- and intermediate-temperature ignition chemistry is not very

11

well understood. The proposed work is an attempt to fill this knowledge gap in the applicability of the SAI model to LTC conditions.

In addition, physical properties such as Cetane number, fuel viscosity, injector nozzle-hole size, injected fuel quantity and injection pressure contribute to the delay phenomenon in diesel engines (Chandorkar et al. 1988). There is strong influence of injection parameters like the hole size, injection pressure and types of fuel on the ignition delay. These parameters have a cumulative consequence on atomization, vaporization and mixing of air/fuel vapor. Ignition delays due to these physical phenomena mentioned above are normally grouped together as physical delay (Thelliez and Ji 1987, Woschni and Anisits 1974). Among several phenomena, studies have shown that fuel droplet heating and evaporation have a lot of importance in diesel ignition/combustion study (Faeth 1983; Sirignano 1983; Kuo 1986). Some researchers (Aggarwal 1998; Chiu 2000; Babinsky and Sojka 2002) have discussed simplified models for droplet heating and evaporation. These models focused on simulating droplet convective and radiative heating, evaporation and the ignition of fuel vapor/air mixture. Loth (Loth 2000) and Orme (Orme 1997; Loth 2000) investigated the effects of the temperature gradient inside fuel droplets on droplet evaporation, break-up and the ignition of fuel vapor-air mixture based on a zero-dimensional code. Investigations (e.g., (Sazhina et al. 2000)) of ignition in a mono-disperse diesel spray have shown that for droplets with an initial radius of 6 μm or larger, the physical ignition delay due to droplet heating and evaporation dominated the chemical ignition delay. The present work describes an attempt to incorporate the effects of droplet evaporation and autoignition phenomenon into a comprehensive ignition delay model.

12

Advanced low Pilot-ignited natural gas LTC concept

The Advanced Low Pilot-Ignited Natural Gas partially premixed low temperature combustion (ALPING LTC) concept was demonstrated in previous research by extending conventional dual fuel combustion to very low pilot quantities and early (advanced) pilot injection (Krishnan et al. 2004; Singh et al. 2004; Srinivasan et al. 2006; Srinivasan et al. 2006).

Figure 2.1 shows a schematic of the ALPING LTC combustion process. The ALPING LTC process employs early injection (approximately 60° Before Top Dead Center) of small (pilot) diesel sprays (about 1-5 percent on an energy basis) to ignite homogeneous natural gas-air mixtures (greater than 90 percent on an energy basis). Early injection provides sufficient time for the pilot diesel spray to mix with the 'fuel-lean' natural gas-air mixture. When the charge is compressed further, the autoignition of diesel will ensure multiple, spatially distributed ignition centers (as opposed to a single, fixed ignition source in conventional spark-ignition), which in turn will ignite the natural gas-air mixture. Since this combustion strategy leads to locally-lean LTC, both PM and NOx emissions are reduced. The presence of distributed ignition centers accelerates overall combustion rates, resulting in high fuel conversion efficiencies. Since robust ignition is critical to achieving controlled ALPING LTC, it is necessary to understand the pilot ignition process over a range of engine operating conditions.

Description of quasi-two zone combustion model

The essential feature of ALPING LTC is the presence of 'distributed ignition centers' that enable faster combustion rates in lean, premixed natural-gas air mixtures (can be seen in figure 2.1). Distributed ignition centers present a unique challenge in

modeling ALPING LTC with a phenomenological approach. Several simplifying

assumptions have been made to model ignition phenomena in ALPING LTC.

1.   The quasi-two zone model considers the closed thermodynamic system

between IVC and SOC.

2.   The closed system is a mixture of ideal gases

3.   After BOI, the combustion chamber is divided into two zones as depicted

in Figure 2.2: the autoignition zone and the 'main reaction zone.'
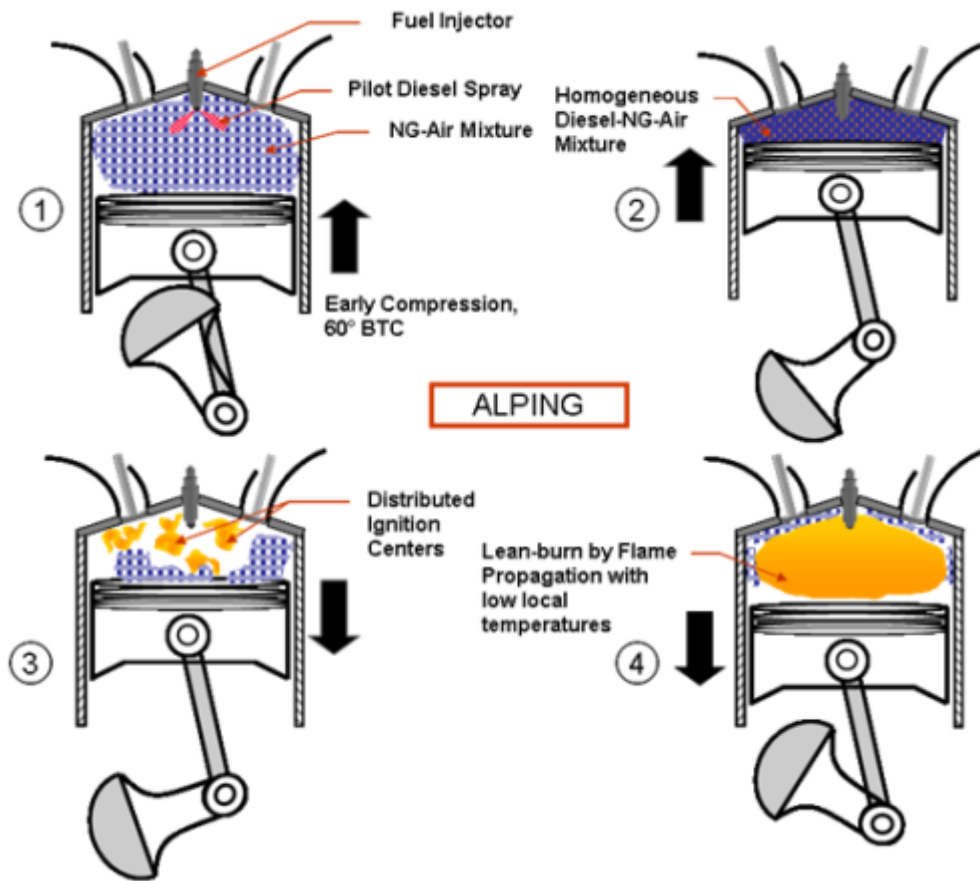
Figure 2.1   Schematic of ALPING combustion
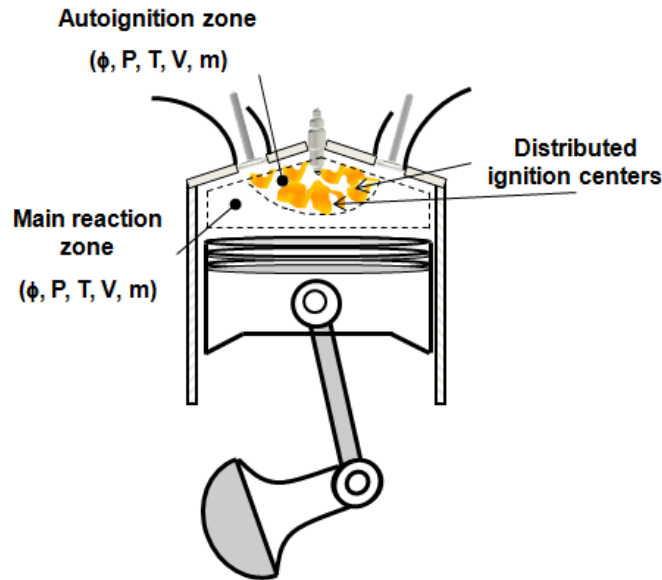
Figure 2.2   Schematic representation of quasi two-zone combustion model

4.   The quasi two-zone model is assumed to investigate the behavior of "knock-free" combustion conditions only. Therefore, the pressures of the autoignition zone and the main reaction zone are equal at any given crank angle.

In the autoignition zone, pilot diesel sprays undergo evaporation and ignition in the presence of natural gas and air. The autoignition zone is an ensemble of all the autoignition sites (distributed ignition centers) present in the combustion chamber. Diesel evaporation is modeled using an isolated droplet evaporation model. Further, the diesel sprays are assumed mono-disperse with droplets of uniform initial Sauter Mean Diameter (SMD). Finally, to capture the effect of distributed ignition centers without resorting to a detailed entrainment model, it is assumed that upon evaporation, diesel mixes adiabatically with the surrounding natural gas-air mixture at a user-specified autoignition zone equivalence ratio (φ_{auto}). Bulk of the combustion occurs in the main reaction zone, which includes unburned reactants, diluents (if EGR is present) and post-

combustion products. The autoignition zone ceases to exist as soon as pilot diesel ignites and combustion of the premixed natural gas-air mixture begins in the main reaction zone.

Ignition delay kinetic mechanisms

There is an ever-increasing need to utilize consistent complex chemical kinetic mechanisms in engine combustion modeling, particularly in the prediction of ignition timing. The complexity of the mechanisms ranges from tens of species to hundreds of species used in precise depictions of fuel ignition. Validation of these kinetic mechanisms over a wide range of engine operating conditions is necessary for predictive engine modeling. Engine measurements are in general not most favorable for testing and validating chemical kinetic mechanisms since there are several factors that affect the data in addition to chemical kinetics, such as turbulence, spray effects and heat loss. Consequently, it is universal to use better-controlled, fundamental laboratory experiments, such as ignition-delay measurements in closed and constant volume reactors for kinetic mechanism validation. Data for several fuels are available in the literature over a wide range of temperatures, pressures, and equivalence ratios and diluents concentrations using rapid compression machines, shock tubes and constant volume bombs. There have been several attempts to utilize these data to establish both detailed and reduced kinetic mechanisms for the calculation of ignition delay.

Detailed kinetic mechanisms

Detailed kinetic mechanisms aim to include all of the important elementary steps and many of the subsidiary processes for a given reaction system with appropriate rate data assigned; for example, the complete reaction mechanism for iso-octane oxidation includes 3,600 elementary reactions with 860 chemical species. There have been

16

substantial efforts to construct the detailed kinetic mechanism for hydrocarbon combustion over wide temperature ranges. Several numerical methods have been applied in the initial selection of reaction schemes and optimization of groups of rate parameters. The progress in the development of kinetic mechanism took the route from smaller hydrocarbon such as ethane, ethene, propane, n-butane and then proceeded to larger hydrocarbons such as heptanes and isooctane. Earlier, the major focus was towards high temperature mechanisms such as temperature beyond 1000K. Later on, after the analysis of butane oxidation by Pitz and westbrook (1986) at low temperature up to 600K, importance of low temperature mechanisms were addressed. The complexity of models increased henceforth.

At higher temperatures, unimolecular fuel and alkyl radical species decomposition and isomerization reactions are more important, while at low temperatures H atom abstraction from the fuel molecule and successive additions of alkyl radicals to molecular oxygen, leading to chain branching, dominate the oxidation process. The degradation of the hydrocarbons tend to follow a sequential breakdown of the carbon backbone (such as $C_4 \rightarrow C_3 \rightarrow C_2 \rightarrow C_1$) rather than fragmentation into smaller carbon containing units that may occur at high temperature ($C_4 \rightarrow 2C_2$). In addition, the selectivity of different propagating free radicals (especially OH, HO_2, RO_2 or RO) is emphasized at low temperature and the reactivity at particular C-H bonds of the alkane may differ appreciably. These kinetic aspects have an increased importance at low temperature because the relative magnitudes of rate constants for individual reactions are more dependent on the activation energies in the Arrhenius expression at lower temperatures.

Previous experimental studies have focused on shock tubes (Bilger et al. 1991; Warnatz 1992), jet-stirred reactors (Ritter and Bozzell 1991), rapid compression

machines, flow reactors [Griffiths and Scott, 1989], amongst others. All of these systems demonstrate phenomena such as self-ignition, cool flame, and negative temperature coefficient (NTC) behavior. Furthermore, variation in pressure from 1 to 45 bar changes the temperature range over which the NTC region occurs. Ranzi et al. used a semi-detailed model to simulate the oxidation of PRF mixtures (Ranzi et al. 1997). Curran et al. (Curran et al. 1998) used a detailed chemical kinetic mechanism to simulate the oxidation of PRF mixtures. Many works have been documented previously for different fuels such as propane (Koert et al. 1996), neopentane (Curran et al. 1996 and Wang et al. 1999), the pentane isomers (Ribaucour et al. 2000), the hexane isomers (Curran et al. 1996), n-heptane (Curran et al. 1998), and primary reference fuel blends (Curran et al. 1998).

Reduced Kinetic mechanisms

Effective computer modeling of ignition process requires a simple, robust and efficient autoignition model. At the same time, it should adequately describe the main features of the process. This clearly shows the need of reduced kinetic models of autoignition despite the development of many detailed kinetic models discussed above. In fact, it is required that a reduced kinetic model, with parameters fitted to a certain range of fuels, should allow wider range of fuels and physical conditions. These prerequisites have been attempted to be satisfied in the Shell autoignition model (Halstead et al. 1975). It has remained most popular since its inception largely due to its simplicity, combined with a generalized description of the kinetic mechanism, which proves to be satisfactory for many applications. The reduced kinetic mechanisms developed by other authors have considerably more reactions and species than the Shell

model (Griffiths et al. 1994 and Sahetchian et al. 1995). This makes them substantially

more complicated for practical implementation. Some of the models (Cox and Cole,

1985; Hu and Keck 1987) were derived largely as a further development of the Shell

model. They incorporate more explicit representations of the elementary reactions of the

low temperature oxidation of alkanes (Griffiths 1995) and contain considerably more

reactions than the Shell model.

An alternative to the Shell model for practical applications was suggested by

Schreiber et al. (1994), which comprises five species in six reactions. Muller et al.

(1992) suggested an even simpler approach to autoignition modeling, but this model was

developed only for n-heptane.

The Shell autoignition model, which was originally designed to simulate the

autoignition for spark-ignition gasoline engines, was successfully extended to modeling

the combustion of diesel fuels (Theobald 1986, Kong et al. 1996). At the same time, the

validation of the autoignition of diesel fuels is highly complicated, since we need to take

into account the uncertainty of the available models of spray atomization, evaporation

and mixing with air. This means that, autoignition modeling for diesel sprays is

intrinsically multi-phenomenal. In contrast to the well-defined conditions in an RCM, the

autoignition in diesel spray occurs over a wide range of equivalence ratios and

temperatures due to fuel evaporation and mixing. This obviously hinders the validation

of the numerical models for diesel fuels.

Arrhenius type empirical ignition delay correlations

Several Arrhenius-type ignition delay correlations have been proposed by various

researchers based on experimental data from constant volume pressure vessels, steady

flow reactors, rapid compression machines, and IC engines for different fuels as shown in

Table 2.1. All of these correlations are based on the estimation of pre-ignition reaction

rates, which are a function of the pressure, temperature, and equivalence ratio. Ignition

delay is inversely proportional to the rate of pre-ignition reactions prior to the combustion

process. A general form of Arrhenius-type ignition delay correlations is given by

$$\tau(P,T,\phi) = A \cdot P^{-n} \cdot \phi^{-m} \cdot e^{\frac{E_a}{R_u T}} \qquad \qquad 2.1$$

$$\int_{t_o}^{t_i} \frac{dt}{\tau(P,T,\phi)} = 1 \qquad \qquad 2.2$$

where τ is the ignition delay time, P is the pressure, T is the temperature, φ is the

equivalence ratio, A is the pre-exponential factor, E_a is the activation energy, R_u is the

universal gas constant and m and n are model parameters. These ignition delay

correlations can be used to determine the ignition delay using instantaneous pressure,

temperature and equivalence ratio following Livengood and Wu's (Livengood and Wu

1955) method (Equation 2.2).

Figure 2.3 shows ignition delay behavior predicted using Arrhenius-type

empirical ignition models and experimental results at 6 bar BMEP and 1700 rev/min for

ALPING LTC combustion in a single-cylinder engine. As evident from these results, the

ALPING LTC experiments covered a wide range of pilot injection timings. At most of

these injection timings, the empirical Arrhenius-type models were unable to predict

ignition delays satisfactorily except at the most advanced injection timing of 60° BTDC.

One reason for the poor performance of these models is perhaps the fact that the

pressures, temperatures, and equivalence ratios spanning the wide range of injection

timings are beyond the range of their validity. Most Arrhenius-type ignition delay

correlations were formulated for typical end-of-compression conditions of temperature

and pressure in diesel engines. All these models except Watson et al. (1980) over

predicted ignition delays and led to an almost linear ignition delay trend with respect to

injection timing. Even the inclusion of an equivalence ratio term in ignition delay models

like Hiroyasu et al. (1980) and Hernandez et al. (2010) did not help in modeling ALPING

ignition delays satisfactorily.

Table 2.1   Parameters of Arrhenius-type ignition models

References	Temperature Range	Arrhenius Equation Parameters			
		A	E_A/R (K)	m	n
Hernandez et al (2010)	Low	$e^{-18.98}$	10915.8	1.5573	0.493
	Intermediate	$e^{0.7156}$	-1959.0	1.5715	1.269
	High	$e^{-21.3}$	17324.5	0.6101	0.520
Spadaccini & Tvelde (1982)	Low – High	2.43×10^{-9}	20895	-2	0
Hiroyasu et al. (1980)	Low – High	0.845	4350	-1.31	-2.02
Watson (1980)	Low – High	3.45	2100	-1.02	0
Wolfer (1938)	Low – High	0.44	4650	-1.19	0
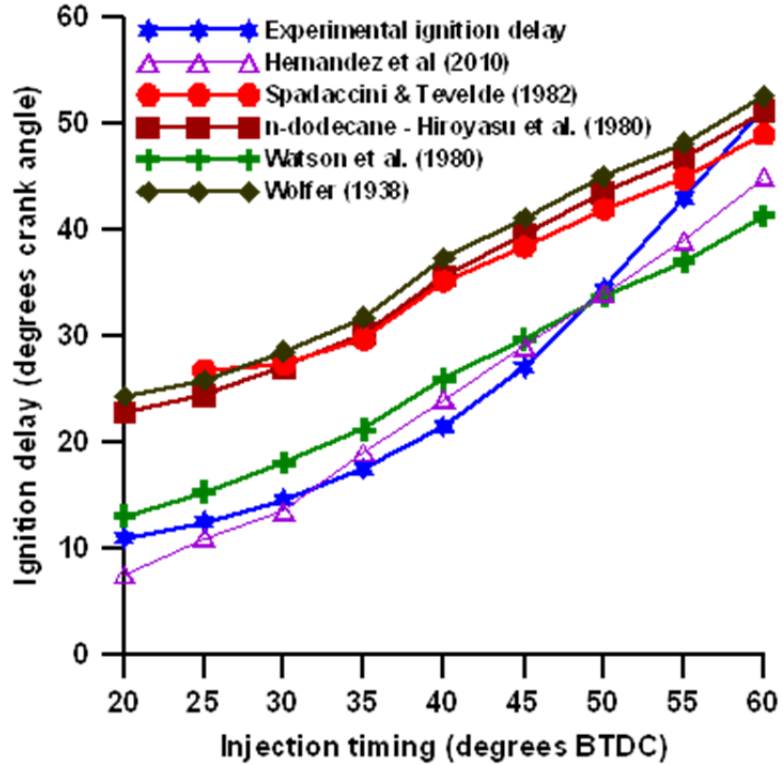
Figure 2.3   Comparison of ignition delay predictions from various Arrhenius-type ignition delay correlations(Wolfer 1938; Hiroyasu et al. 1980; Watson et al. 1980; Spadaccini and TeVelde 1982) with experimental ignition delay values

Ignition Delay Model Development

Shell Autoignition (SAI) mechanism

The original SAI model developed by Halstead, Kirsch and Quinn is based on a reduced mechanism for cool flames and two-stage ignition of non-aromatic saturated hydrocarbons (Halstead et al. 1975; Halstead et al. 1977). This model was validated using experiments performed on a rapid compression machine. The eight-step chain-branching reaction schemes involved in this model are shown here:

Initiation:

$$RH + O_2 \xrightarrow{k_q} 2R^*$$ 2.3

Propagation:

$$R^* \xrightarrow{\quad k_P \quad} R^* + P + q \qquad\qquad 2.4$$

$$R^* \xrightarrow{\quad f_1.k_p \quad} R^* + B \qquad\qquad 2.5$$

$$R^* \xrightarrow{\quad f_4.k_p \quad} R^* + Q \qquad\qquad 2.6$$

$$R^* + Q \xrightarrow{\quad f_2.k_p \quad} R^* + B \qquad\qquad 2.7$$

Branching:

$$B \xrightarrow{\quad k_b \quad} 2R^* \qquad\qquad 2.8$$

Termination:

$$R^* \xrightarrow{\quad f_3.k_p \quad} out \qquad\qquad 2.9$$

$$2R^* \xrightarrow{\quad k_t \quad} out \qquad\qquad 2.10$$
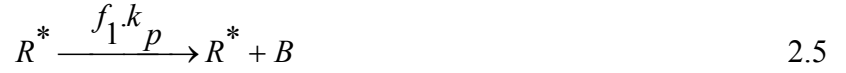
Here RH represents hydrocarbon fuel (C_nH_{2m}), R* the radical, B the branching species, Q the intermediate species, and P the products. A very notable assumption in the SAI model is that although the radicals R* refer to different radicals encountered before ignition; they are treated as a single group.

The five conservation equations that describe the above mechanisms are as follows:

$$\frac{d[R^*]}{dt} = 2(k_q[RH][O_2] + k_B[B] - k_t[R^*]) - f_3 k_p[R^*] \qquad\qquad 2.11$$

$$\frac{d[B]}{dt} = f_1 k_p[R^*] - k_B[B] + f_2 k_p[Q][R^*] \qquad\qquad 2.12$$

23

$$\frac{d[Q]}{dt} = f_4 k_p [R^*] - f_2 k_p [Q][R^*]$$

2.13

$$\frac{d[O_2]}{dt} = -pk_p [R^*]$$

2.14

$$RH = \frac{[O_2] - [O_2]_{t=0}}{pm} + [RH]_{t=0}$$

2.15

The specific reaction rate obtained using Arrhenius expressions with pre-exponential

factors (A) and activation energies (E) are expressed as $k_i = A_i exp(-E_i/RT)$. On the other

hand, the rate constant, k_P in the rate expressions is obtained as $k_p = (1/(k_{P1}[O_2]) + 1/k_{P2}$

$+ 1/(k_{P3}[RH]))^{-1}$. The factor f_i can be expressed as $f_i = A_{fi}.exp(-E_i/RT).[O_2]^{xi}.[RH]^{yi}$.

Exothermicity, q, of the reaction is calculated as the heat release during the propagation

cycle for oxidation of a single -CH2- fuel molecule from the fuel assuming a fixed

proportion (λ) of CO and CO_2 in the products. Effect of species R*, B and Q were

neglected in the energy and mass balances in the original SAI model. The oxygen

consumption rate which is one of the important rate determining steps is defined as

$$p = \frac{[n(2 - \lambda) + m]}{m}$$

2.16

Twenty six kinetic parameters were used and optimized for the simulation of autoignition

in the original SAI model.

Modifications to the SAI mechanism

Schapertons and Lee (S&L) (Schapertons and Lee. 1985) later modified the

elementary steps in the original SAI model to account for mass conservation and

proposed the main propagation cycle as follows

$$R^* + (\Lambda + 1)\left(\frac{1}{m}C_nH_{2m} + pO_2\right) \rightarrow R^* + qP + f_1B + f_4Q + heat \qquad 2.17$$
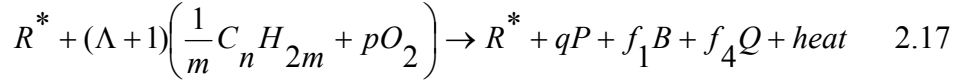
where, $\Lambda = (f_1W_B + f_4W_Q)/(W_{CnH2m}/m + pW_{O2})$ and $q = 1 + n/m$. Molecular weight of generic species R^*, B and Q is given by $W_{R*} = (W_{CnH2m} + W_{O2})/2$, $W_B = 2W_{R*}$ and $W_Q = W_B$. The modified propagation cycle results in increased fuel consumption and consequently, a factor of $(\Lambda + 1)$ increase in pre-ignition energy release. In addition, the reaction rates were frozen to their corresponding values at 950 K even if the actual temperature was higher. As seen in Equation 2.17, the elementary steps have been incorporated into the main propagation cycle. Finally, for mass conservation purposes the two termination reactions were assumed to lead to nitrogen.

$$\text{Linear termination:} \qquad R^* \rightarrow \frac{W_{R^*}}{W_{N_2}}N_2 \qquad 2.18$$

$$\text{Quadratic termination:} \qquad R^* \rightarrow 2\frac{W_{R^*}}{W_{N_2}}N_2 \qquad 2.19$$
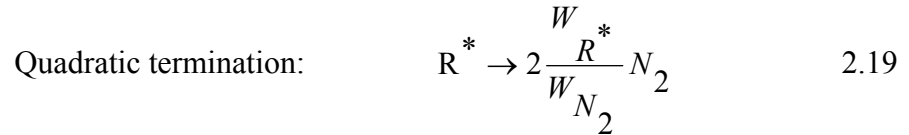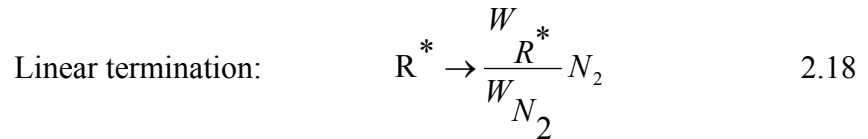
More recently, Hamosfakidis and Reitz (Hamosfakidis and Reitz 2003) suggested additional modifications to remove three deficiencies associated with the SAI model. First, instead of using a constant CO/CO_2 ratio (constant λ), they employed the following energy balance to calculate heat release.

$$\frac{1}{m}C_nH_{2m} + p(O_2 + c_{N_2}N_2 + c_{H_2O}H_2O + c_{CO_2}CO_2) \rightarrow$$
$$n_{O_2}O_2 + n_{N_2}N_2 + n_{H_2O}H_2O + n_{CO_2}CO_2 + n_{CO}CO + n_{H_2}H_2 + n_{C_nH_{2m}}C_nH_{2m} \qquad 2.20$$
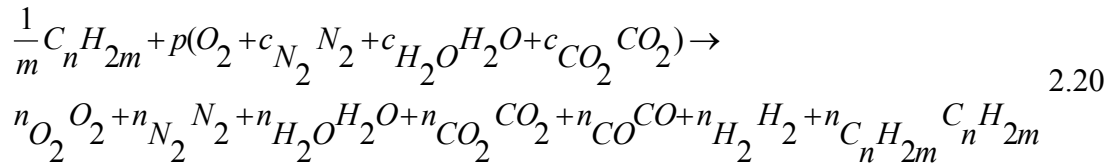
where, $p = (n/m + 0.5)/\varphi$ and φ is the equivalence ratio of the mixture. The coefficients c in the reactant side is based on molar ratio of corresponding reactant species with respect

to coefficients of the constituents of the product. Thus the energy release of the reaction

at temperature T can be given by

$$\Delta H_{r,T} = \sum_{i=1}^{N_P} n_i{}''(\Delta H_{f,i}^0 + \Delta h_{s,i}^0) - \sum_{i=1}^{N_r} n_i{}'(\Delta H_{f,i}^0 + \Delta h_{s,i}^0) \qquad 2.21$$

where, $\Delta H^0{}_{f,i}$ represents the enthalpy of formation and $\Delta H^0{}_{s,i}$ represents the sensible

enthalpy of the species i. With Equation 2.21, the propagation cycle proposed by

Schapertons and Lee can be altered into the following Equation

$$R^* + (\Lambda + 1)\left(\begin{array}{c} \frac{1}{m}C_n H_{2m} + p(O_2 + c_{N_2} N_2 \\ + c_{H_2O}H_2O + c_{CO_2}CO_2) \end{array} \right) \rightarrow R^* + P + f_1 B + f_4 Q + heat$$

$$2.22$$
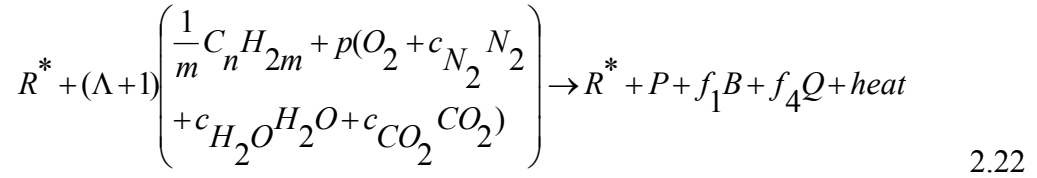
where, $p = n_{O2}.O_2 + n_{N2}.N_2 + n_{CO2}.CO_2 + n_{CO}.CO + n_{H2}.H_2 + n_{CnH2m}.C_nH_{2m}$.

The second modification in the Hamosfakidis and Reitz (H&R) model was based

on the assumption that autoignition and combustion are closely related phenomena.

Thus, instead of converting radicals into inert N_2, the same products can be assumed in

radical termination reactions from combustion of the same reactants, excluding nitrogen

in the product side. . In the original SAI and Schapertons and Lee models, the species

contributions were only considered in the mass balance. In this study, the H&R model,

with only the activation energy (A_q) for the chain initiation reaction modified (Table A2

(Appendix)), was used to predict ignition delays for ALPING LTC.

Diesel evaporation model

An isolated droplet evaporation model based on Kanury (1975) is used to

calculate droplet evaporation rates. Quasi-steady conditions are assumed with the

evaporation rates corresponding to temperature and species concentration changes. The

liquid diesel in droplet form is not considered to be active part of the autoignition zone. Only evaporated diesel is allowed to enter the autoignition zone. In order to further simplify the model all fuel droplets are assumed to have the same initial sauter mean diameter (SMD) of 30 microns.

The steady-state energy and species (diesel) conservation equations (in spherical coordinates) for evaporation of a single diesel droplet, assuming constant properties and no combustion, are

$$K_g \frac{d}{dr}(4\pi r^2 \frac{dT}{dr}) - C_g \frac{d}{dr}([W"4\pi r^2]T) = 0$$

2.23

$$\rho_g D_F \frac{d}{dr}(4\pi r^2 \frac{dY_F}{dr}) - \frac{d}{dr}([W"4\pi r^2]Y_F) = 0$$

2.24

where T is the temperature, Y_F is the mass fraction of diesel; K_g, C_g, and ρ_g are thermal conductivity, specific heat at constant-pressure, and density of diesel-air mixture in autoignition zone, respectively; and D_F is the diffusion coefficient of diesel vapor in the diesel-air mixture. The mass of liquid evaporated from the diesel droplet per unit droplet area per unit time is given by W". The first terms in Equations 2.23 and 2.24 represent conductive heat flux and diffusive mass flux, respectively, while the second terms represent convective heat and mass fluxes. Equations 2.23 and 2.24 can be written in terms of normalized temperature (b_T) and diesel mass fraction (b_D) as follows:

$$\rho_g \alpha_g \frac{d}{dr}(r^2 \frac{db_T}{dr}) - \frac{db_T}{dr}[W"r^2] = 0$$

2.25

$$\rho_g D_F \frac{d}{dr}(r^2 \frac{db_D}{dr}) - \frac{db_D}{dr}[W"r^2] = 0$$

2.26

27

where, α_g is the thermal diffusivity of gas in autoignition zone and R is the instantaneous diesel droplet radius. The subscript W refers to droplet "wall" conditions at r = R, where T = T_W, Y_F = Y_FW.

$$b_T = \frac{C_g(T - T_\infty)}{L + C_l(T_W - T_R)}$$

2.27

where T_∞ is the temperature of gas "away" from droplet surface ($r \rightarrow \infty$), T_R is the interior temperature of the droplet ("liquid reservoir"), C_l is the specific heat of liquid diesel, and L is the latent heat of vaporization of diesel.

$$b_D = \frac{Y_F - Y_{F\infty}}{Y_{FW} - Y_{FR}}$$

2.28

Equations 25 and 26 are subject to the following boundary conditions:

At r = R, $b_T = b_{TW}$, $b_D = b_{DW}$ and as r →∞, $b_T = b_T\infty = 0$ and $b_T = b_T\infty = 0$

Also,

$$W''_W = \rho_g \alpha_g \left. \frac{\partial b_T}{dr} \right|_W = \rho_g D_F \left. \frac{\partial b_D}{dr} \right|_W$$

2.29

The final expression for evaporated diesel mass per unit droplet area per unit time is

$$W''^*_W = \frac{\bar{h}^0}{C_g} \ln(1 + B)$$

2.30

where, $\bar{h}^0$ is the average heat transfer coefficient for heat transfer between droplet and surroundings which is evaluated with a Nusselt number value of 2 (which is the conduction limit value for low Reynolds number flows), and assuming that the diesel

droplets are very small and are carried along with the mean gas flow. B is the mass transfer number, which is defined as follows for Le = 1:

$$B = \frac{C_g(T_\infty - T_W)}{L + C_l(T_W - T_R)} = \frac{(Y_{F\infty} - Y_{FW})}{(Y_{FW} - T_{FR})}$$

2.31

In Equation 2.31, the middle term is from energy considerations (B_T) and the last term is from species considerations (B_D). In this chapter, only diesel evaporation without combustion is considered.

Sensitivity analysis

Sensitivity analysis is a valuable tool in model assessment as it shows how the model behavior responds to changes in parameter values. It helps in establishing confidence in the model by studying the uncertainties associated with parameters in models. Sensitivity analysis can also specify which parameter values are reasonable to use in the model. If the model performs as expected from experimental observations, it indicates that the parameter values replicate at least in part the desired output. In this study, the sensitivity analysis was performed with ignition delay as the model output of interest.

For performing the sensitivity analysis, the ignition delay is expressed as a function of different parameters:

$$ID = f(x_1, x_2 \ldots x_n)$$

2.32

where, x_i refers to different experimental variables and model parameters on which ID depends. First, the sensitivity of ID to different variables is determined. Then, uncertainty magnification factors (UMF) that indicate important model parameters are estimated. Subsequently, uncertainties in the ID are determined due to each variable.

29

Finally, the uncertainty percentage contributions (UPC) of different variables are quantified. The sensitivities (S_i), uncertainty magnification factor (UMF_i), the overall uncertainty (U_{ID}) and the uncertainty percentage contribution (UPC_i) can be evaluated as follows (Coleman and Steele 1999)

$$S_i = \frac{ID(x_i + \Delta x_i) - ID_0}{\Delta x_i}$$ 2.33

$$UMF_i = \frac{x_i}{ID} S_i$$ 2.34

$$U_{ID} = \sqrt{\sum_{i=1}^{n}(S_i . U_{xi})^2}$$ 2.35

$$UPC_i = \left(\frac{S_i . U_{xi}}{U_{ID}}\right)^2$$ 2.36

where, U_{xi} are the estimated uncertainties in the variable x_i. In Table 2.2, several experimental variables are presented with their nominal values and their estimated uncertainties based on measurement and expected errors.

Table 2.2   Estimated Uncertainties for Experimental Variablesand Model Parameters

Parameter	Nominal	Estimated
Inlet Pressure	203.7 kPa	2%
Initial Temp.	348 K	2%
Engine Speed (N_e)	1700 rpm	1%
Wall Temp (T_{wall})	400 K	5%
Compression Ratio	14.5	1%
Bore	0.13716 m	0.1%
Stroke (s_c)	0.16510 m	0.1%
Connecting Rod	0.26162 m	0.1%
n_{RH}	14	1
m_{RH}	30	2
Air flow rate, m_a	0.062 kg/s	1%
Diesel flow rate,	5.58×10^{-5}	1%
NG flow rate, m_{NG}	1.35×10^{-3}	1%
Droplet diameter	3×10^{-5} m	5×10^{-6} m
φ_{auto}	1.0	1%

Results and discussions

Studies of Ignition delay using rapid compression machine

Experimental RCM results (Halstead et al., 1977) are compared to model predictions for primary reference fuels (PRF) RON90 and RON70 in Figure 2.4. The experimental conditions used in the Thornton RCM experiment (Halstead et al., 1977) (Φ = 0.9, compression ratio = 9.6:1, pre-compression pressure 103.42 kPa) are used to estimate the ignition delay. The end-of-compression molar concentration of the mixture was 0.324 kmol/m^3. The end-of-compression pressure was calculated using the ideal gas equation of state. The temperature and the concentration of all generic species were calculated using SAI model. It can be inferred from Figure 2.4 that fuel reactivity plays an important role in the ignition mechanism, and therefore, a separate set of model parameters is needed to predict ignition delays for different fuels even though other experimental variables remain same. Also, the values of the parameters used in the shell

model are subjective (Hamosfakidis and Reitz 2003) and their selections can be done independently, after having assigned values to the other parameters.

Hamosfakidis and Reitz (2003) modified the Shell model to decrease the number of model parameters from twenty-six to twenty and thus reduced the computational efforts. Unlike constant end-of-compression molar concentration in the Thornton RCM experiment (Halstead et al. 1977), constant end-of-compression pressure (80 bar) was used as in (Hamosfakidis and Reitz 2003) as an initial condition to compute ignition delays. Figure 2.5 shows the comparison of ignition delay predictions using original SAI model and the modified SAI model (Hamosfakidis and Reitz 2003). It can be seen that the relative error is higher at high and low temperature where as error reduces at medium temperature. Also, shown in this figure are presumably more accurate ID results from CHEMKIN with detailed kinetics incorporated for n-tetradecane. In all cases the original SAI model underpredicted the actual ignition delay whereas the modified SAI model matched the CHEMKIN predictions.
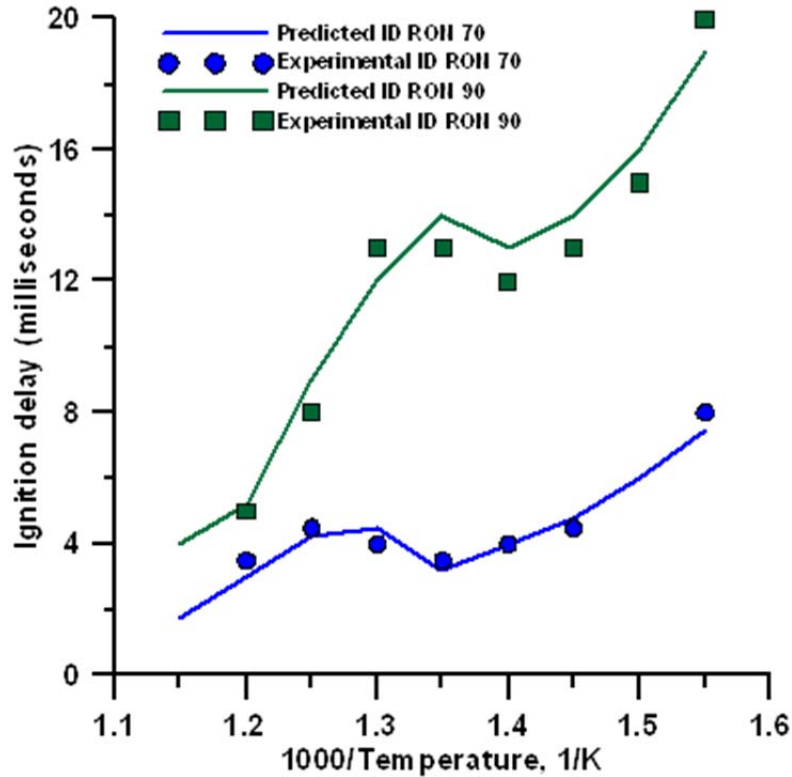
Figure 2.4   Comparison of experimental IDs (Halstead et al. 1977) and model predictions showing the effect of temperature on ignition delay for PRF RON 70 and PRF 90 ($\Phi = 0.9$, compression ratio 9.6:1, wall temperature = 373 K)

In order to further verify the SAI model, experimental autoignition data for n-heptane obtained from measurements in the Lille RCM (Minetti et al. 1995) for an initial pressure at the start of combustion of 17.33 kPa and 21.74 kPa are used. In Figure 2.6, the experimental ignition delays and ID predictions with the modified SAI model (Hamosfakidis and Reitz 2003) are plotted against the end-of-compression temperatures for the Lille RCM. In addition, Figure 2.6 also includes pressure dependence of ignition delays in a rapid compression machine. Here, increase in pressure led to increase in charge density, which has profound effect on chain initiation and chain propagation reactions. As the end-of-compression pressure is reduced, ignition delay increased and negative temperature coefficient (NTC) region became more prominent. The NTC region

is the range of temperature where increase in temperature leads to increase in ignition

delay as can be seen in the Figure 2.6 (between 750 K and 850 K).
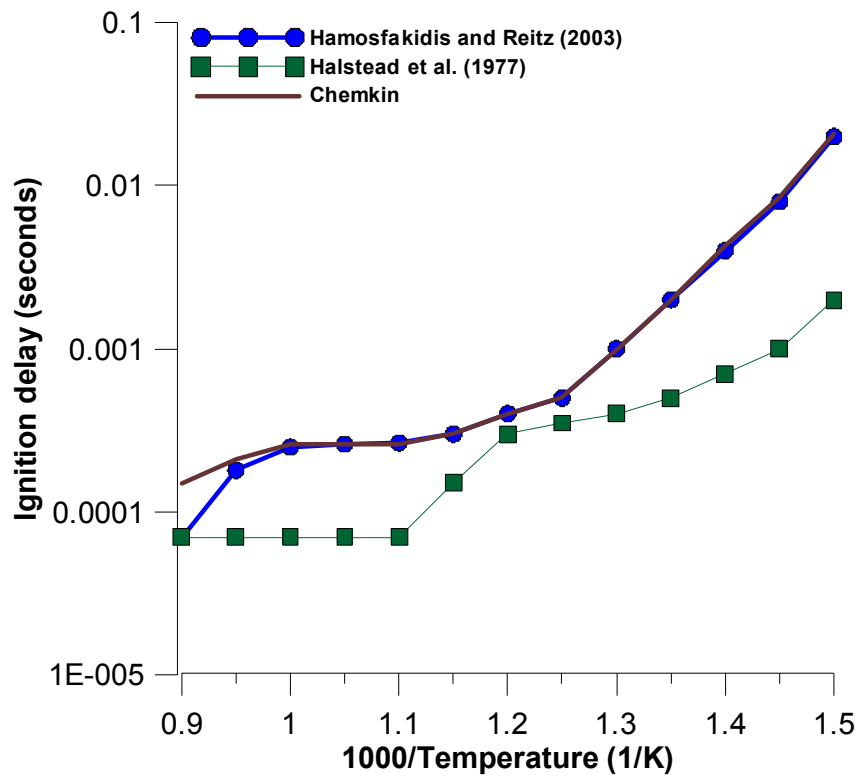
Figure 2.5   Ignition delay vs. inverse temperature for n-tetradecane for stoichiometric
mixture at 8 MPa (Hamosfakidis and Reitz 2003)
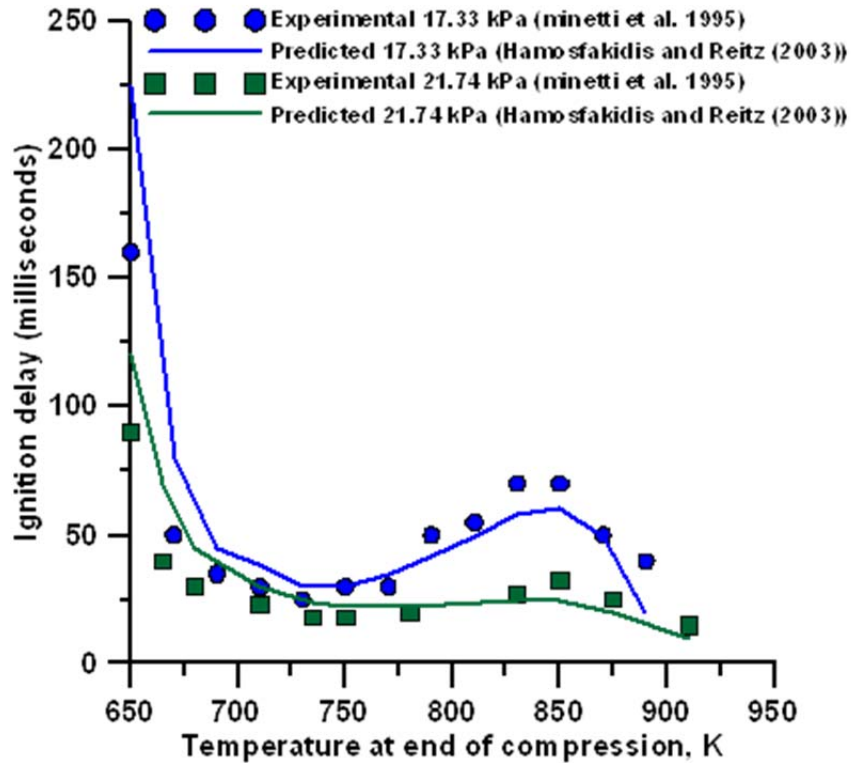
Figure 2.6   Measured and predicted ignition delays for stoichiometric n-heptane-air mixtures plotted as functions of core gas temperature T in the Lille RCM (compression ratio, r = 9.8 and T, = 355 K) (Minetti et al. 1995)

Further, ignition delays predicted by the original SAI model (Halstead et al. 1977) are compared to experimental results from the Leeds RCM [24] (with compressed gas densities of about 0.131 kmol/m3) as shown in Figure 2.7. The agreement between original SAI model predictions for PRF RON 70 and experimental results was good at for temperatures higher than 750 K but less satisfactory at lower temperatures. Short ignition delays throughout the entire temperature range and lower threshold compressed gas temperature for the onset of ignition are evident from the high reactivity of n-C_7H_{16}.
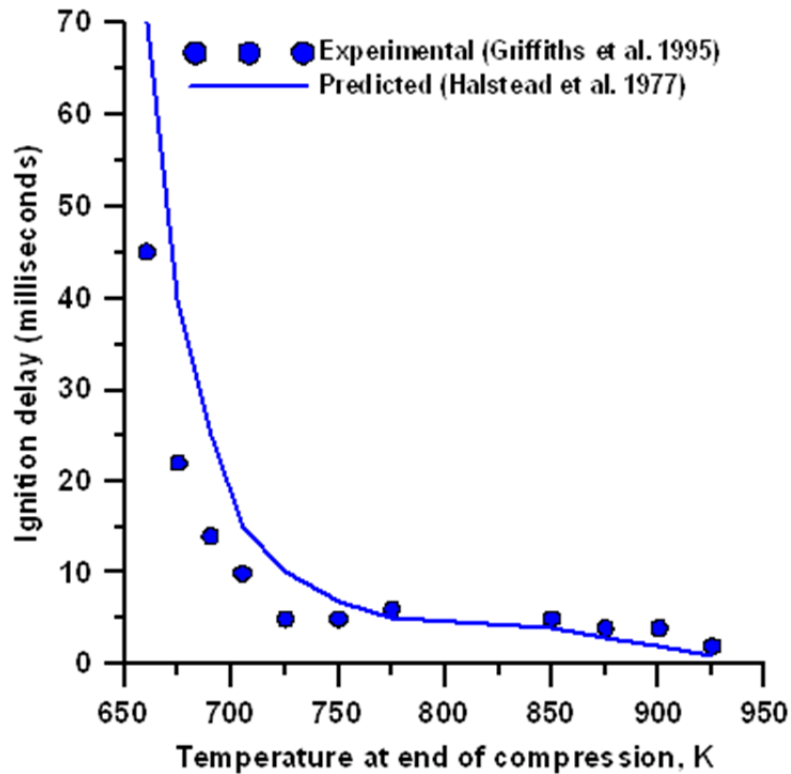
Figure 2.7   Ignition delay variation with compressed gas temperature for n-heptane
              (Griffiths 1995)

Delineation of temperature regime for autoignition phenomenon

In the section above ignition delay prediction using SAI model was compared to several RCM experiment results. These RCM experiments were performed in order to capture the chemistry of autoignition . However, due to certain assumptions associated with RCM, it is necessary to study the difference in ignition delays obtained from the RCM and those obtained from anengine. Figure 2.8 shows the ignition delays of 70 RON PRF in a rapid compression machine (RCM) environment for end-of-compression RCM conditions similar to the start of injection conditions for ALPING LTC in the single-cylinder engine. Also illustrated in Figure 2.8 are the predicted and measured ignition delays (re-plotted in milliseconds) for ALPING LTC engine operation. The modified SAI model by Hamosfakidis and Reitz (Hamosfakidis and Reitz 2003) was used to

predict ignition delays in both the RCM and engine cases. It was observed that for the range of injection timings considered (20°-60° BTDC), the temperatures at the start of injection in ALPING combustion fall under the low temperature regime or negative temperature coefficient regime, that is, less than 800 K. In the RCM, preignition reactions occur in the fuel-air mixture at constant volume (after compression) whereas in the engine, the volume continues to decrease (due to compression) after the start of injection when preignition reactions begin. Thus, in the engine, apart from the energy release due to preignition reactions, compression also leads to a further increase in temperature and charge density, resulting in shorter ignition delays compared to the RCM. Moreover, in ALPING combustion, physical phenomena such as fuel spray formation, droplet atomization, droplet evaporation, air entrainment and mixing with fuel result in a significant physical ignition delay. In contrast, in the RCM, fuel and air mixture at the end of compression are considered to be evaporated and homogeneously mixed. It can be noticed from the figure that as injection timing is retarded towards TDC, the engine ignition delays approach the RCM ignition delays. These trends show that the SAI mechanism, which was originally developed and calibrated with experimental ID results from an RCM, may be more suitable for engine ignition delay predictions at high temperatures (towards the end of compression).
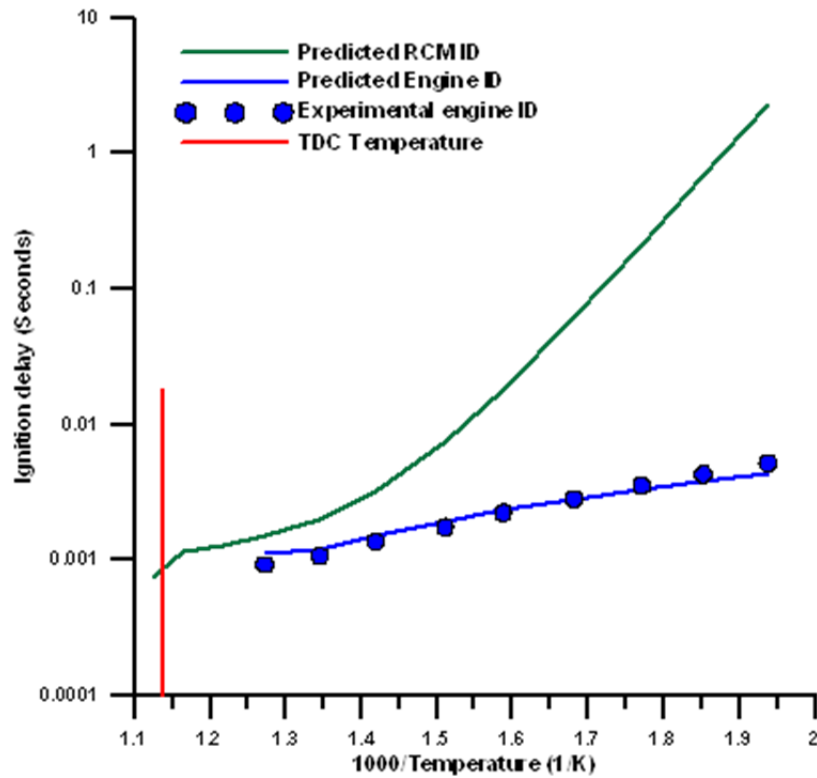
Figure 2.8   Ignition delay vs. temperature in RCM(Halstead et al. 1977) and ALPING
combustion engine

Uncertainty Analysis

In the section above, it was shown that for similar experimental conditions, there
were differences between actual experimental ALPING ignition delays and predicted
ignition delay predictions from the RCM ALPING-like conditions. Since the SAI model
involves 26 model parameters to predict the ignition delay based on RCM autoignition
kinetics, it is necessary to understand the sensitivity of these parameters for tuning the
ignition delay model to match experimental ALPING IDs. Sensitivity analysis will help
in finding how the model behavior responds to changes in parameter values and will also
help in creating confidence in the model by studying the uncertainties associated with
parameters in models.

Figures 2.9 and 2.10 illustrate the sensitivities of predicted IDs to the SAI model parameters. The Arrhenius reaction rate expressions ($k_i = A_i \exp(-E_i/RT)$) in the SAI model (Halstead et al. 1977; Hamosfakidis and Reitz 2003) use two sets of constants, viz., pre- exponential factors (A_i) and activation energies (E_i). It can be seen that among A_i, the predicted IDs were most sensitive to A_{P3}, A_q, A_{f1} and A_{f3} at all end-of-compression temperatures in the RCM and for all injection timings in the engine. Among E_i, the IDs were most sensitive to E_q, E_{P3}, E_b and E_{f3}. In both the RCM and the engine, comparing sensitivity of all the parameters, it can be seen that ID was most sensitive to E_q. All of these model parameters (e.g., A_q and E_q) showed higher sensitivities at the retarded BOI of 20° BTDC. By comparison, ID sensitivities at 60° BTDC BOI was moderate, while 40° BTDC BOI showed very low sensitivities.

In engine combustion simulations, since model parameters play a crucial role in the accuracy of model predictions, the uncertainty analysis outlined above provides a basic framework for discerning the most sensitive parameters and the largest contributors to model uncertainties. While experimental input variables cannot be modified, model parameters can be calibrated. Clearly, as demonstrated in Figures 2.9 and 2.10, proper choice of the most sensitive model parameters such as A_{P3}, A_q and A_b can ensure the best ID predictions under ALPING LTC conditions.
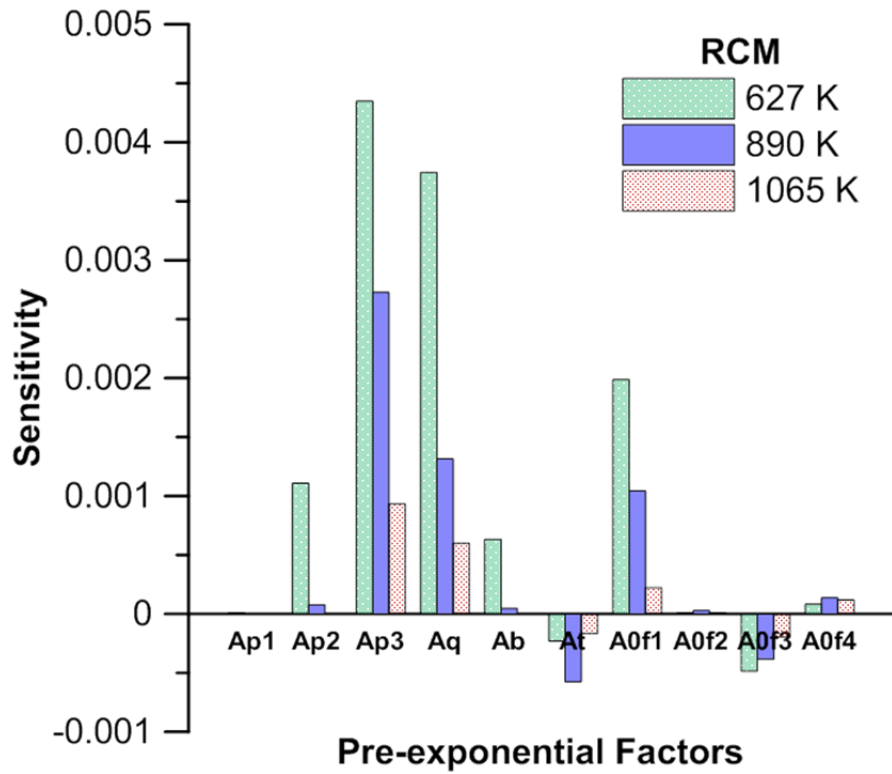
Figure 2.9   Sensitivities of predicted IDs at different end-of-compression temperature inside RCM to pre-exponential factors used in modified H&R model.
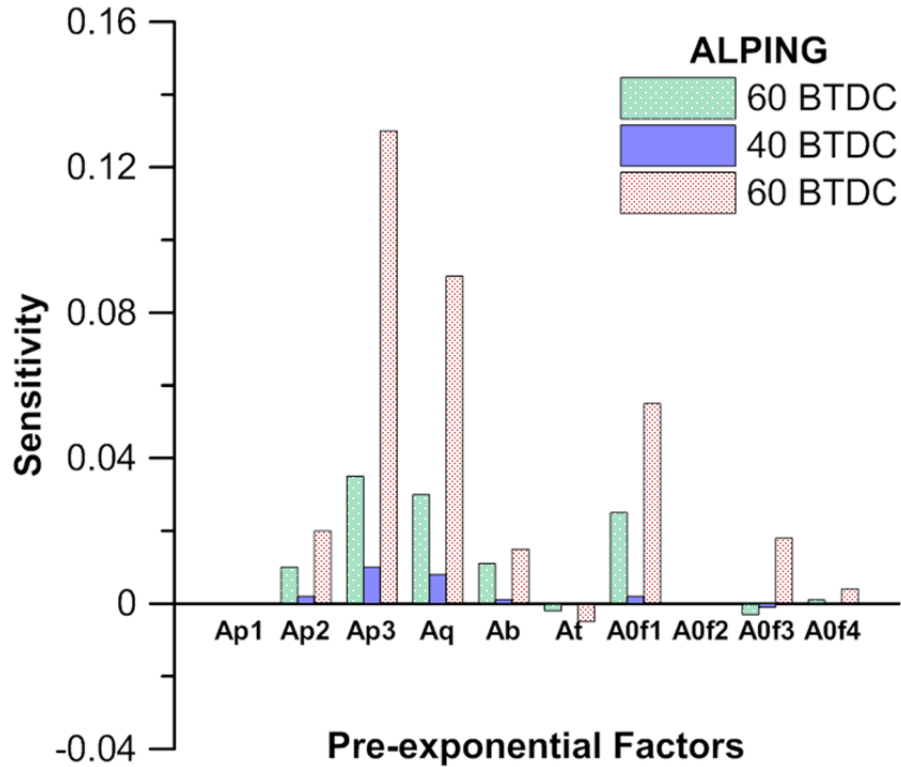
Figure 2.10   Sensitivities of predicted IDs at different BOIs to pre-exponential factors used in modified H&R model.

Validation of ignition delay prediction using modified SAI model from ALPING engine

Ignition delay in diesel engines typically includes both physical and chemical components. In general, the physical delay is a consequence of the finite time taken for spray atomization, evaporation, and fuel-air mixing while the chemical delay is due to the finite rate of preignition reactions. In this analysis, n-tetradecane ($C_{14}H_{30}$) is considered as the surrogate for diesel fuel. Ignition delay is defined as the period (in crank angle degrees) between BOI and the onset of ignition in the autoignition zone, which is assumed to occur when its temperature increases above 1100 K or the rate of increase of its temperature exceeds 10^7 K/s. The predicted and measured ID results were obtained at

a medium load (BMEP = 6 bar), engine speed of 1700 rpm, and intake manifold temperature (Tin) of 75°C.

Figure 2.11 compares the ID predictions from the modified H&R model (present work) and the original H&R model (Griffiths 1995) to the experimental IDs obtained for ALPING LTC. It must be noted that the experimental IDs were obtained over a range of injection timings, 20° BTDC – 60° BTDC at a medium load (BMEP = 6 bar), a constant speed of 1700 rpm, and fixed intake manifold conditions (PIVC = 212 kPa, Tin = 75° C). The model inputs were fixed: SMD= 30 μm, φauto = 1.0, and EGR = 0%. It is clear that the original H&R model (Hamosfakidis and Reitz 2003) systematically over-predicted IDs throughout the range of BOIs.

The original H&R model was developed for diesel-type combustion and was fitted well at relatively high SOI temperatures . To improve ID predictions for low and intermediate SOI temperatures, several parametric studies were performed with the original H&R model constants as the baseline. A parametric study showed that A_{P3} and A_q were the most sensitive model parameters that affected ignition delay predictions. Therefore, A_q was modified to the value shown in Table A2 (APPENDIX) so as to minimize the difference between experimental and predicted IDs. The parameters Aq in the model determine the rate of the initiation reaction (Theobald and Cheng 1987). Increasing A_q to 2.5×10^{13} (instead of the baseline H&R value of 5.74×10^{12}) resulted in a better match between predicted and experimental IDs as shown in Figure 2.11.
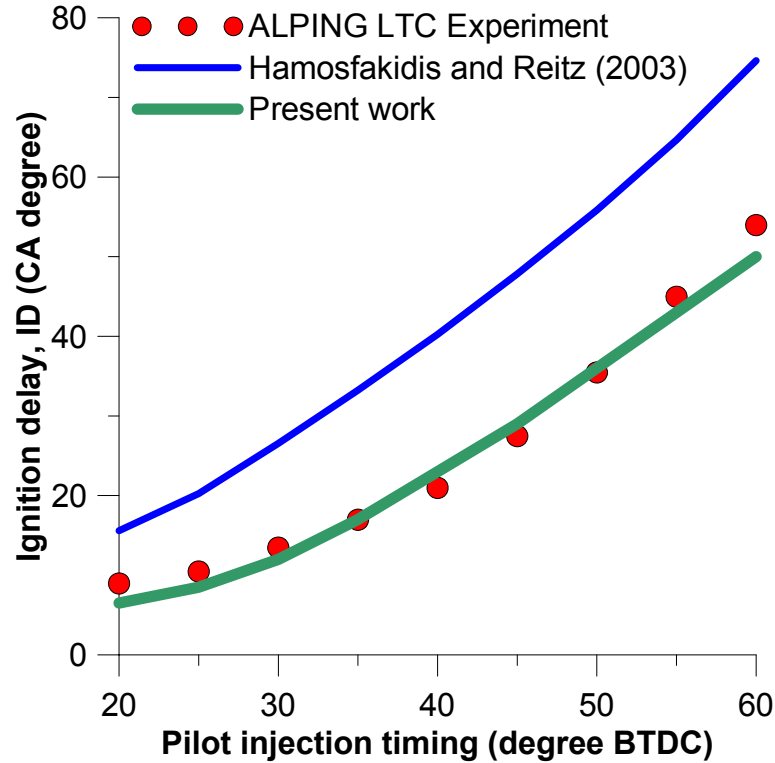
Figure 2.11   Comparison of predictions from H&R model and present work (A_q = 2.5 × 10^{13}) with experimental ID values for ALPING LTC at different BOIs, half load (BMEP = 6 bar; 1700 rpm, PIVC = 212 kPa, Tin = 75° C, SMD= 30 µm, φ_{auto} = 1.0, EGR = 0%)

Parametric studies based on simulation

In Figures 2.12 to 2.15, variations in ID and $\Delta\theta_{evap}$ are analyzed over a range of BOIs for different parameters such as initial droplet SMD, intake temperature, autoignition zone equivalence ratio (φ_{auto}), and EGR. In all of these parametric studies, it was found that evaporation duration ($\Delta\theta_{evap}$) and ID increased as the BOI was advanced from 20° BTDC to 60° BTDC. This is due to the progressive decrease in temperature at the time of injection as BOI occurs earlier with respect to TDC. Since both evaporation and ignition are temperature-dependent phenomena, higher temperatures closer to TDC lead to accelerated evaporation rates and pre-ignition energy release rates, thereby leading to shorter $\Delta\theta_{evap}$ and ID.

Effect of Initial Droplet Sauter Mean Diameter (SMD)

Figure 2.12 shows the predicted ID and $\Delta\theta_{evap}$ as a function of BOI for three

initial droplet SMD values: 10, 30, and 50 microns. For this study, the engine speed of

1700 rpm , P_{IVC} of 212 kPa, T_{in} of 75°C, and mass of diesel injected per cycle (m_d) of

3.94 mg/cycle were held constant. The autoignition zone equivalence ratio (please see

figure 2.2 for details of the autoignition zone) was fixed at unity (stoichiometric) with no

EGR. Larger droplet SMDs decreased evaporation rates, thereby resulting in longer

$\Delta\theta_{evap}$. Similarly, larger SMDs also led to longer IDs for BOIs closer to TDC. However,

as BOI was advanced beyond 35° BTDC, there was no significant impact of SMD on the

predicted IDs, which remained approximately constant. For the retarded BOIs (20°-30°

BTDC), the onset of ignition occurred even before evaporation was complete for the

SMD of 50 microns.
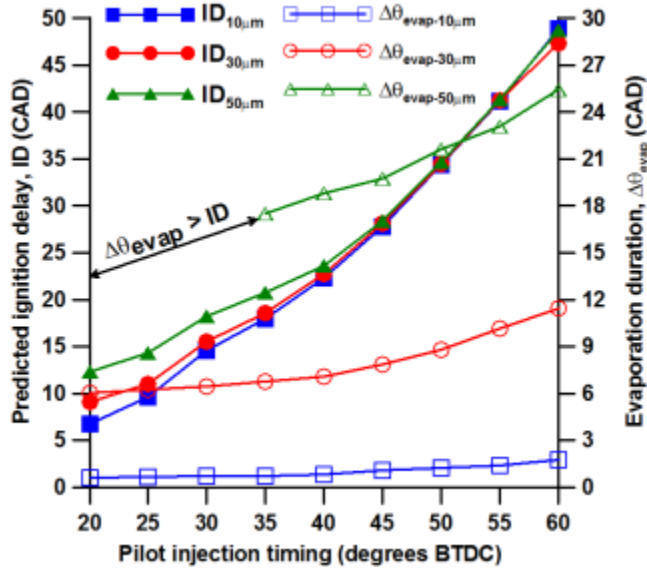
Figure 2.12   Ignition delay and $\Delta\theta$evap vs. BOI for different diesel droplet diameters at
half load (BMEP = 6 bar), 1700 rpm, PIVC = 212 kPa, Tin = 75° C, φauto
= 1.0, EGR(%) = 0

Shorter evaporation durations and shorter IDs were observed for smaller SMDs for different reasons. For constant diesel injected mass, smaller SMDs led to more droplets having larger total surface areas at identical in-cylinder conditions. Larger droplet surface areas resulted in faster evaporation rates. A visible difference was observed in IDs for different SMDs at retarded BOIs because at these timings, evaporation was incomplete due to longer $\Delta\theta_{evap}$ for larger SMDs. Slower evaporation rates of droplets with larger SMDs resulted in longer $\Delta\theta_{evap}$ and slower increase of diesel and oxygen concentrations in the autoignition zone. These effects decreased radical formation rates for droplets having larger SMDs, thus increasing IDs for retarded BOIs. The SMD effect diminished as BOI was advanced beyond 40° BTDC due to the fact that $\Delta\theta_{evap}$ was shorter than the ID. Therefore, relatively small changes in $\Delta\theta_{evap}$ caused by changes in SMD did not have any significant impact on ID since the chemical component of ID overshadowed the physical component at advanced BOIs.

<center>Effect of Intake Charge Temperature</center>

Intake charge temperature is considered to be one of the most important factors affecting IDs and $\Delta\theta_{evap}$ (Sazhin 2005) In Figure 2.13, at the effect of different intake temperatures (50°, 75° and 100°C) on ID and $\Delta\theta_{evap}$ is presented. Again, at different intake temperatures, other engine variables were held constant: N_e = 1700 rpm, P_{IVC} = 212 kPa, m_d = 3.94 mg/cycle, SMD= 30 μm, φ_{auto} = 1.0, and EGR = 0%. It can be observed that for each intake temperature chosen in the study, $\Delta\theta_{evap}$ and ID increased as the BOI was advanced from 20° to 60° BTDC. Also, ID and $\Delta\theta_{evap}$ decreased with increasing intake temperature at all BOI. This may be explained from the preignition reaction rate expressions ($k_i = A_i.exp(-E_i/RT)$), where higher temperatures led to faster

<center>45</center>

reaction rates, thus decreasing IDs. This relation between intake temperature and ID has

been observed by several researchers in the past (Halstead et al. 1977; Schapertons and

Lee. 1985; Sazhin et al. 1999; Hamosfakidis and Reitz 2003). Also from Equations 25

and 26, it can be seen that the evaporation rates increase with increasing temperature,

thereby reducing the total $\Delta\theta_{evap}$ at higher temperatures.
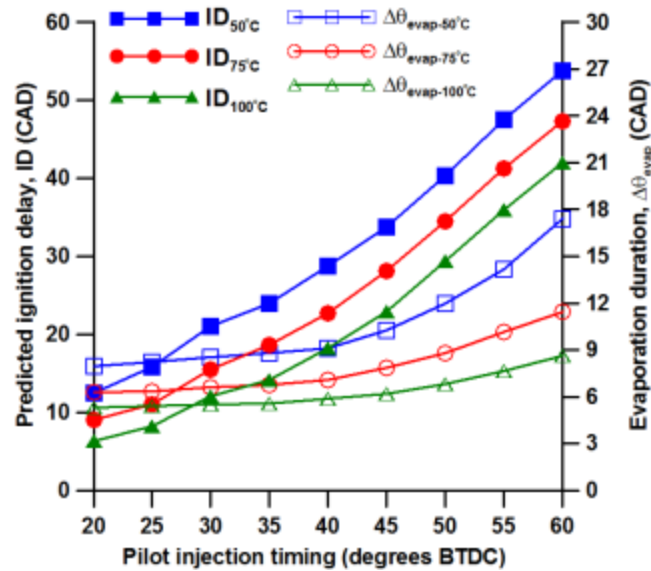
Figure 2.13   Ignition delay and $\Delta\theta$evap vs. BOI for different intake temperatures at half
load (BMEP = 6 bar); 1700 rpm, PIVC = 212 kPa, SMD = 30 μm, φauto =
1.0, EGR(%) = 0

Effect of Autoignition Zone Equivalence Ratio (φ_auto)

The autoignition zone equivalence ratio (φ_{auto}) is an important model parameter in

the quasi-two-zone combustion model. The effect of φ_{auto} on ID predictions is shown as

percent relative error trends in Figure 2.14. Relative error in ID was calculated as the

difference between predicted ID and experimental ID for a given BOI and φ_{auto},

normalized with the experimental ID, and expressed as a percent relative error in

predicted ID. For this parametric study, φ_{auto} was varied from lean to rich values while

other engine variables were held constant: N_e = 1700 rpm, P_{IVC} = 212 kPa, T_{in} = 75° C,

SMD = 30 μm, m_d = 3.94 mg/cycle, and EGR = 0%. The purpose of this study was to

determine the optimal φ_{auto}, which provided the least percent relative error over the range

of BOIs encountered in ALPING LTC. From Figure 2.14, it can be seen that

stoichiometric autoignition zone equivalence ratio (φ_{auto} = 1.0) resulted in the least error

(±10%) in predicted IDs between 20° and 60° BTDC injection timings. Consequently,

the optimal φ_{auto} for the present model (all results shown except Figure 2.14) was

assumed to be 1.0 over the range of BOIs in ALPING LTC. The percent relative error

trends also show that the impact of φ_{auto} variation on predicted IDs was more pronounced

at retarded BOIs, possibly due to the increased importance of the physical component of

ID at retarded BOIs.
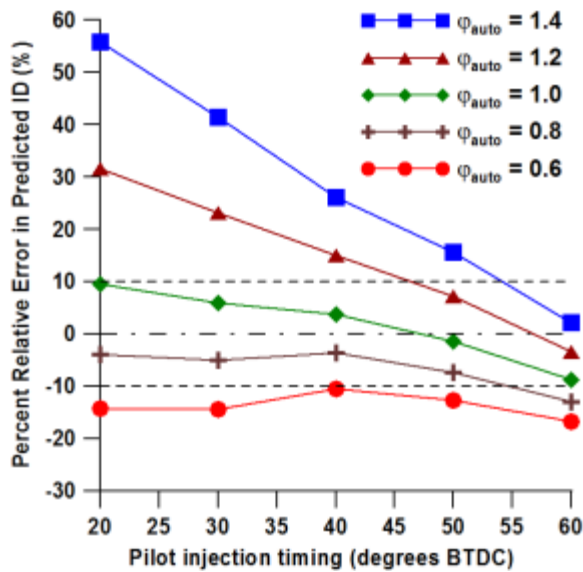
Figure 2.14   Relative error in predicted ignition delays vs. BOI for different autoignition
zone equivalence ratios (φauto) at half load (BMEP = 6 bar); 1700 rpm,
PIVC = 212 kPa, SMD = 30 μm, Tin = 75° C, EGR(%) = 0

Effect of EGR

Exhaust gas recirculation (EGR) involves slip-streaming some of the exhaust back into the intake manifold to mix with fresh intake charge to reduce NO_x emissions. The amount of EGR in the total intake charge is usually expressed as EGR %, which is defined as:

$$EGR(\%) = \frac{m_{EGR}}{m_i} \times 100 \qquad\qquad 2.37$$

where $m_i = m_a + m_{NG} + m_{EGR}$ and m_{EGR} is the mass of EGR. Since diesel engines do not employ any intake throttling, they operate at 95-100 percent volumetric efficiencies at most engine operating conditions. The use of EGR results in displacement of a portion of air causing a reduction in the air available for combustion. This decreased combustion air lowers the air–fuel ratio at which the engine operates and can affect exhaust emissions significantly. Also, when uncooled EGR is mixed with the air delivered to a diesel engine, the temperature of the charge increases and can considerably affect the compressed charge temperature and the combustion process (Mitchell et al. 1993; Ladommatos et al. 1998). The displacement of intake charge with CO_2 and H_2O can impact the combustion process in many ways. For instance, addition of EGR can lead to a net reduction in intake oxygen concentration, which influences the flame temperature and thus NO_x emissions (Mitchell et al. 1993). On the other hand, the higher specific heats of both CO_2 and H_2O in comparison to that of O_2 and N_2 being displaced results in a net diluent effect. In ALPING LTC, when the intake natural gas-air mixture mixes at intake temperature (T_{in}) with recycled, uncooled, exhaust gas at a higher temperature (T_{EGR}), the resulting natural gas-air-EGR mixture temperature (T_{mix}) will be higher. An important effect while using EGR can be a net stratification in temperature and/or

48

composition of the final intake mixture. However, the extent of homogenization of the in-cylinder mixture is dependent on available mixing times (Srinivasan et al. 2007).

Figure 2.15 shows both experimental and simulated IDs as a function of BOI at different EGR substitutions. A reduction in experimental ID was observed with increasing percent EGR for the entire range of BOIs, except at the most retarded BOI of 20° BTDC. There may be several competing factors that led to this behavior. For example, increasing hot EGR substitutions led to higher intake charge temperatures, thereby causing shorter ignition delays for most BOIs. On the other hand, oxygen concentrations also decreased as percent EGR was increased; therefore, the charge was hotter and depleted of oxygen when it entered the combustion chamber. Also, the higher specific heats (C_p) of CO_2 and H_2O introduced by EGR increased the effective C_p of the intake mixture. This increase in effective C_p resulted in lower temperatures at the time of pilot diesel injection. Lower temperatures at BOI coupled with oxygen depletion resulted in lower preignition energy release in the autoignition zone. This decrease in preignition energy release competed with the effects of higher intake charge temperatures at different BOIs, affecting the actual ignition delay times. However, from Figure 2.15 it is clear that ID decreases with increasing EGR substitutions for most BOIs. This demonstrates that for most BOIs, the most significant effect of uncooled EGR is a net increase in intake charge temperature, and therefore, a net reduction in IDs However, the simulated IDs do not follow the experimental trends for 20° BTDC BOI but continue to show a decreasing trend with increasing EGR. These differences indicate a shortcoming of the present model.
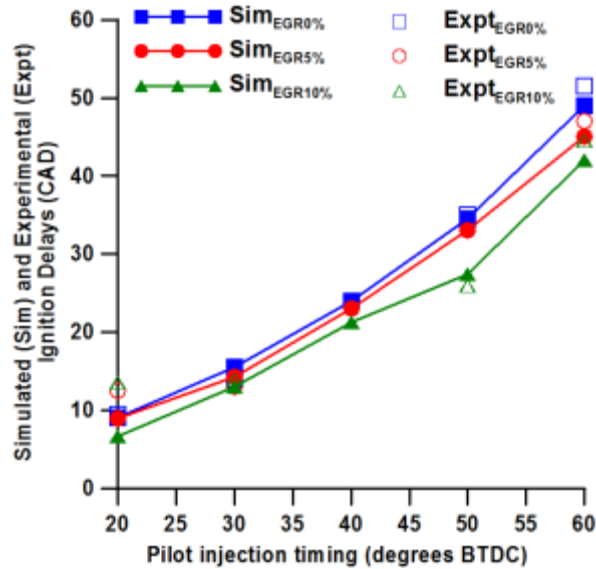
Figure 2.15   Ignition delay and Δθevap vs. BOI for different EGR (%) at half load (BMEP = 6 bar); 1700 rpm; PIVC = 212 kPa, Tin = 75° C, SMD = 30 μm, φauto = 1.0

Ignition delay of biodiesel

Chemical kinetic studies of biodiesel combustion, either experimentally or using computational modeling are very limited. The most important reason for this is that the chemical structure of biodiesel considerably differs from that of fossil fuels due to the inclusion of oxygen atoms into the alkyl chain. Biodiesel in general is composed of several fatty acid methyl esters. Therefore modeling biodiesel ignition kinetics is complicated. In addition, the large fuel molecules of biodiesel make the capabilities of kinetic modeling even more difficult. A general method used to get rid of this problem is to choose a surrogate molecule that corresponds to the chemical properties of the real fuel to be studied (Herbinet et al. 2010; Westbrook et al. 2011). Consequently, related research has followed two major pathways. In order to address the *ester* component of major constituents of biodiesel, experiments and kinetic modeling of smaller methyl esters have been performed. Methyl butanoate is the largest methyl ester that has been

50

studied kinetically and it is concluded that this fuel reproduces kinetic features of the oxidation of the ester component of biodiesel molecules. On the other hand, combustion of large biodiesel molecules has been studied by assuming that large methyl esters can be considered as being fundamentally the same as large *n-alkanes*. Other researchers have used kinetic models for *n-alkanes* as large as *n-hexadecane* to simulate the combustion of the large methyl ester molecules in actual biodiesel fuels. A brief review of past work in the area of methyl ester combustion is presented here.

A detailed chemical kinetic mechanism for the combustion of methyl butanoate was developed by Fisher et al. (Fisher et al. 2000), which was validated against the limited available data obtained under low-temperature, subatmospheric conditions in closed vessels, using pressure measurements as the main diagnostic. Later, Metcalfe and co-workers studied the oxidation of methyl butanoate and ethyl propanoate in a jet-stirred reactor (Metcalfe et al. 2007). A revised detailed kinetic mechanism based on the work of Fisher et al. (Fisher et al. 2000) for methyl butanoate and a new sub-mechanism for ethyl propanoate were used to simulate measured ignition delay times. Gaïl and co-workers carried out a wide-ranging kinetic modeling study of the oxidation of methyl butanoate using a jet-stirred reactor, a variable-pressure flow reactor, and an opposed-flow diffusion flame (Gaïl et al. 2007). Sarathy et al. (Sarathy et al. 2007) performed an experimental study of methyl crotonate ($C_5H_8O_2$ unsaturated methyl ester) in a jet-stirred reactor and an opposed-flow diffusion flame. Vaughn et al. studied the combustion of biodiesel fuel droplets in microgravity and measured ignition times of methyl esters (such as methyl butanoate, methyl decanoate, methyl dodecanoate, and methyl oleate) and commercial soy oil methyl esters (Vaughn et al. 2006). Ignition delay times obtained during this study showed that methyl decanoate and methyl dodecanoate are better

surrogates for commercial soy oil methyl esters than methyl butanoate, in agreement with conclusions of Fisher et al. (2000) and Gaïl et al. (2007).

Dagaut et al. studied the oxidation of rapeseed oil methyl ester (RME) in a jet-stirred reactor (JSR) at 1–10 atm over the temperature range 800–1400 K (Dagaut et al. 2007). Experimental data obtained were compared with computational mechanisms for oxidation of *n-hexadecane* and has been confirmed against experiments in a JSR (Ristori et al. 2001). The agreement was reasonable and *n-hexadecane* was considered to be a good surrogate for rapeseed oil methyl ester under the conditions of the study. However, the *n-hexadecane* mechanism was unable to predict the early production of CO_2 that was observed in experiments.

Ignition delay model for methyl butanoate

A good knowledge of the kinetics of the reaction of biodiesel fuels at both high and low temperature is necessary to perform reliable simulations of ignition, combustion, and emissions in diesel engines. Modeling of the oxidation of methyl butanoate provided a better understanding of the chemistry of methyl ester combustion (Dooley et al. 2008).

As mentioned earlier, the multistep SAI model containing 26 model parameters can be tailored to model a particular fuel. The model parameters include the activation energy, E, the pre-exponential factor, A, and the exponents x and y of the reaction rate equation for each of the reactions in the model: $k_i = A_i exp(-E_i/RT)$. Among 26 parameters adjustable to each fuel, there is kinetic information available to the rates of the chain propagation steps, which are related to alkyl peroxy isomerization theory (Halstead et al. 1977). Thus, the values of Ap_1, Ep_1, Ap_2, Ep_2, Ap_3, and Ep_3 used here were those used by Halstead et al. (1977) from literature data and were not altered, as

although methyl butanoate shows only single stage ignition, other longer chain methyl-esters components of biodiesel do show negative temperature coefficient behavior (Dooley et al. 2008). Among PRF 90 and PRF 100 parameters published by Halstead et al. (1975) the remaining 20 constants were individually increased and decreased to determine their effect on the ignition delay and this information was then used to match the ignition delay found from detailed CHEMKIN modeling (Toulson et al. 2010).

Summary

This chapter reviewed literature on autoignition mechanisms of diesel surrogate fuels in RCMs, shock tubes and constant volume pressure vessels. The shortcomings of traditional Arrhenius type ignition delay model fits were addressed in the context of advanced low temperature combustion, such as lean premixed natural gas combustion using very small diesel pilot sprays. The need for reduced chemistry-based autoignition models such as the Shell Auto Ignition (SAI) model and several modifications made to the original SAI was established to capture the ignition delay behavior at low temperature conditions. Further, the modified SAI model proposed by Hamosfakidis and Reitz (2003) was identified as a suitable candidate to estimate ignition delays at low temperature conditions. Detailed examination of model parameters using sensitivity analysis indicated that preexponential factors such as Ap3 and Aq exerted maximum influence on ignition delay predictions. Finally, parametric studies to investigate intake charge pressure, temperature and amount of exhaust gas recirculation were performed and the predictions of the modified H&R model were validated against experimental data at various operating conditions.

CHAPTER III

MULTI-ZONE MODELING OF DIESEL AND BIODIESEL COMBUSTION

In diesel engines, fuel is injected into the engine cylinder near the end of the compression stroke. During a phase known as ignition delay, the fuel spray atomizes into small droplets, vaporizes, and mixes with air. As the piston continues to move closer to top dead center, the mixture temperature reaches the fuel's auto-ignition temperature range, causing ignition of some premixed quantity of fuel and air. The remaining fuel that had not participated in premixed combustion is consumed in the mixing-controlled combustion phase. In this chapter, the combustion behavior of diesel andbiodiesel fuels in a compression ignition engine will be studied. The chapter will begin with a review of the research on combustion models for the conventional diesel engine. Thereafter, properties of diesel andbiodiesel with associated combustion phenomena will be described. Later, model formulation and the simulation results of the different phases of combustion and experimental data will be compared.

Diesel Combustion Process

Combustion in diesel engines is very complex and until recently, its detailed mechanisms were not well understood. Since engine performance, fuel consumption, and emitted pollutants depend on the combustion process in the engine, it is necessary to understand the mechanisms of combustion in diesel engines. The basis of diesel combustion is its unique way of releasing the chemical energy stored in the fuel. To perform this process, oxygen must be made available to the fuel to facilitate combustion.

54

One of the most important aspects of this process is the mixing of fuel and air, which is a process often referred to as mixture preparation.

In diesel engines, fuel is often injected into the engine cylinder near the end of the compression stroke, just a few crank angle degrees before top dead center (Heywood 1988). The liquid fuel when injected through small orifices or nozzles atomizes into small droplets and penetrates into the combustion chamber. The atomized fuel which is heated by the hot air at or near TDC, vaporizes, and mixes with the surrounding air. The mixture temperature continues to rise until it reaches the fuel's autoignition temperature. Some premixed fuel and air ignites immediately thereafter. This rapid ignition is considered the start of combustion and is marked by a sharp pressure rise in cylinder pressure. The delay between start of combustion and the start of injection is termed as Ignition Delay as described in chapter II. Increased pressure resulting from the premixed combustion compresses and heats the unburned portion of the charge and shortens the delay. It also increases the evaporation rate of the remaining fuel. Atomization, vaporization, fuel vapor-air mixing, and combustion continue until all the injected fuel has combusted. Therefore, inducted charge air and injected fuel play primary roles in the diesel combustion process. It is therefore important to study the effect of the inducted charge air temperature, the injected fuel's atomization, spray penetration, temperature, and chemical reaction characteristics. While these two factors are most important, there are other parameters that may play important role in the combustion process. For instance, intake port design, intake valve size, compression ratio, injection pressure, nozzle hole geometry, spray geometry, valve configuration and top piston ring position have a significant impact on combustion. Therefore, it is significant to realize that the combustion system of the diesel engine is not limited to the combustion bowl, injector

sprays, and their immediate surroundings. Rather, a combination of various systems and
processes may affect the final outcome of the combustion process.

Heat Release Rates in DI Diesel Engines

Many researchers have studied cylinder pressure traces to determine heat release
rates (Austen and Lyn 1961; Lyn 1963; Shipinski et al. 1968; Henein and Patterson 1972;
Barba et al. 2000; Chmela and Orthaber 2004). Figure 3.1 shows an example of a rate of
net heat release diagram (Q_n) together with cylinder pressure (P), and fuel injection rate
(m_{fi}) (Heywood 1988). Details of the work done to obtain these traces were given by Lyn
(Lyn 1963). The initial sharp rise in the heat release rate results from burning the
premixed portion of the fuel. During the ignition delay period which is the time between
start-of-injection (SOI) and the time at which the net rate of heat release returns to zero,
evaporation from the spray forms a fuel rich fuel vapor-air mixture, first at the sides and
then at the tip of the fuel jet. The negative heat release after the start of injection is due
mainly to the heat transfer from the air to the evaporating liquid fuel.
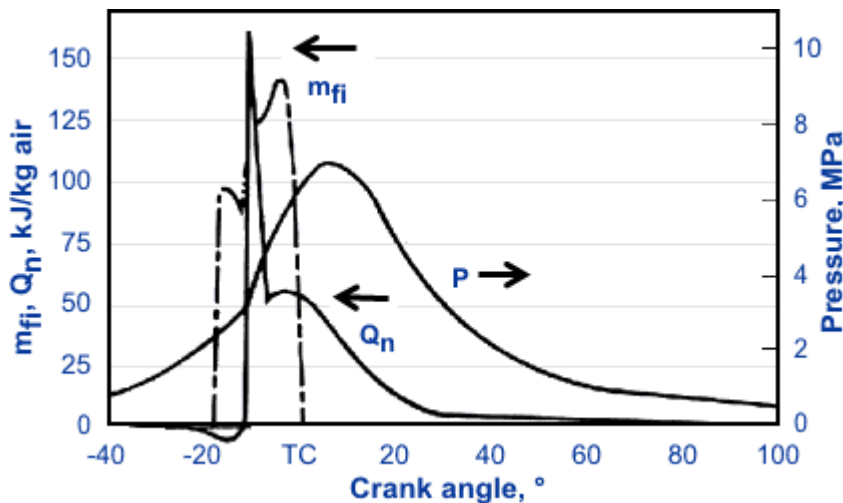
Figure 3.1   Heat Release Rate, Cylinder Pressure, and Injection Rate (Heywood, 1988)

At the point of maximum heat release rate, the cumulative heat release is about 5% of the total computed heat release (Xingcai et al. 2006; García et al. 2009). This percentage reflects the approximate portion of fuel burned soon after ignition. However, this portion may vary according to the fuel properties, engine design choices and engine operating conditions.

Three Phases of Diesel Combustion

Diesel combustion includes both physical and chemical phenomena that have been described by many researchers (Henein and Patterson 1972; Heywood 1988). The combustion process is usually described in terms of three distinct phases, namely, ignition delay, premixed combustion and mixing-controlled combustion (Figure 3.2).
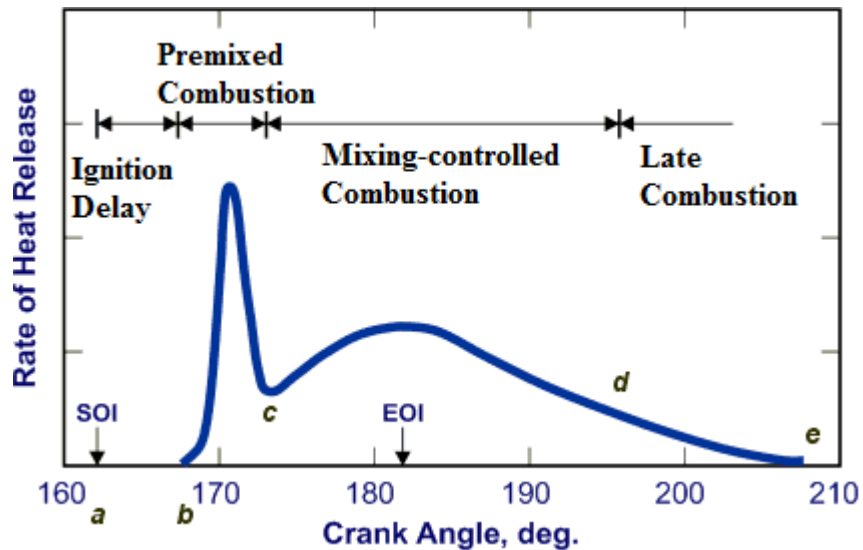
Figure 3.2   Different Phases of Combustion in Diesel Engines (Heywood, 1988)

Ignition Delay

Ignition delay in diesel engine combustion is the time between the start of injection and the start of detectable combustion (a → b in Figure 3.2). There are several

ways to identify the start of combustion which include abrupt changes in cylinder pressure, light emission from combustion reactions, temperature rise due to combustion, combustion of a defined amount of fuel and a fixed point on the heat release rate curve (Heywood 1988). One of the many definitions for ignition delay is the time between start-of-injection (SOI) and the time at which the net rate of heat release returns to zero. It is the time when the integrated amount of heat released by reactions becomes equal to that absorbed by the evaporated fuel. Net heat release rate is normally negative shortly after injection due to liquid fuel heating and evaporation (Figure 3.1).

Depending on methods used for the measurement of start-of-injection, ignition delay may include injector lag—the time taken between the injector receiving the signal driving it open and fuel exiting the injector nozzle into the combustion chamber. For example, using a Hydraulically-actuated Electronic Unit Injection (HEUI) injector with a maximum injection pressure of 142 MPa, an injector lag of about 1.5 ms was measured (Cheng et al. 2007). Others have measured injection lags in common rail systems ranging from 0.30 to 0.75 ms (Laguitton et al. 2002; Kastengren et al. 2008). The duration of the ignition delay is an important variable. It has a significant impact on the combustion process, mechanical stresses, engine noise and exhaust emissions. Figure 3.3 gives a summary of the physical and chemical steps before and after autoignition.
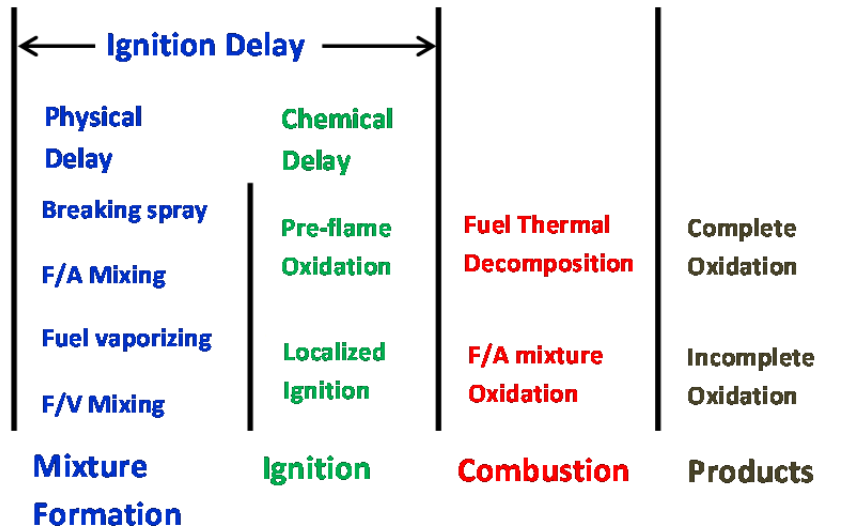
Figure 3.3   Steps Before and After Autoignition (Henein and Patterson 1972)

The physical processes involved in the ignition delay period (ID) are spray break up, droplet formation, fuel and air mixing, heating of the liquid fuel and evaporation, mixing of the vapor and air to form a combustible mixture. The chemical processes that take place in the ignition delay period are pre-ignition reactions that break-down the hydrocarbon fuel and generate radicals and localized ignition that takes place in several areas within the combustion chamber. The early stages of pre-ignition can be considered to be dominated by the physical processes that result in the formation of a combustible mixture and the later stages by the chemical changes which lead to autoignition (Henein and Patterson 1972).

While it is difficult to draw a distinct line separating the physical and chemical processes because they overlap, an estimate can often be made of the point at which the chemical process starts to dominate. In addition to the fuel type (chemical structure), temperature, and pressure conditions, ignition delay is also affected by injection pressure and injector nozzle orifice diameter (Kobori et al. 2000).

Premixed Combustion

The term premixed combustion refers to the rapid premixed combustion of a portion of the fuel injected during the ignition delay period. This period is indicated as b→c in Figure 3.2. This portion of the fuel would have undergone atomization, evaporation, and the pre-ignition chemical reactions. It would also have mixed with air to form a fuel-rich mixture that is ready to ignite once the autoignition temperature is reached. When autoignition occurs, the premixed fuel burns at a very high rate, producing high temperature and high rates of pressure rise in the combustion chamber (Gerpen 2001). The rate of premixed burning is governed mainly by chemical kinetics. Engine speed, load and injection timing can all affect the proportion of fuel burned in this premixed phase. An examination of several correlations found that the mass of fuel burned in the premixed burn phase increased linearly with the product of engine speed and ignition delay time (Alkidas 1987).

Mixing-Controlled Combustion

In the mixing-controlled combustion phase, the consumption rate of this fuel is controlled by its rate of injection and subsequent mixing with air. The mixing-controlled combustion phase is represented by the curve between c→d in Figure 3.2. The combustion paths of three types of mixtures—rich, stoichiometric, and lean—are presented in Figure 3.4 (Gerpen 2001).
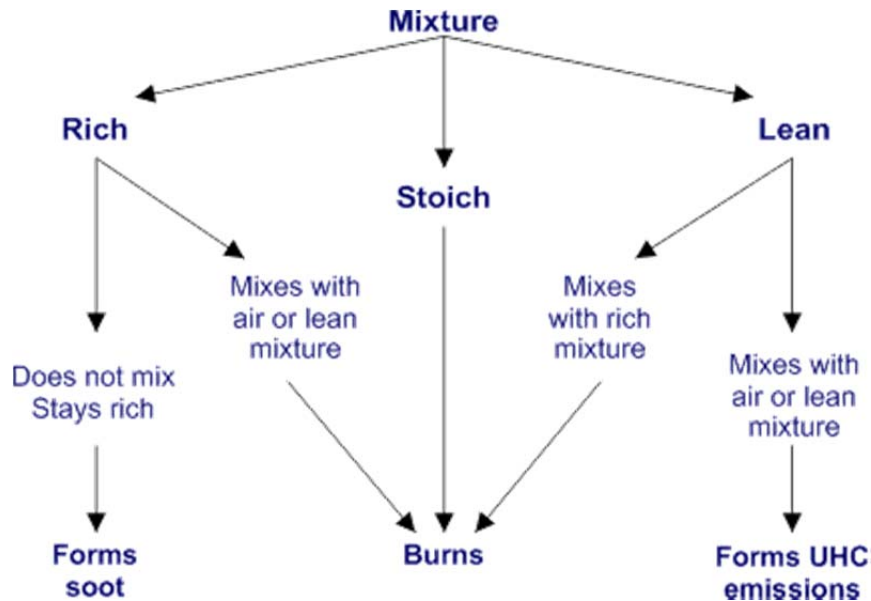
Figure 3.4   Three Paths from Mixture to Combustion (Gerpen, 2001)

While the combustion process has been treated as consisting of three distinct phases, a fourth phase can also be defined that describes the activity in the final stages after the end of injection and prior to opening the exhaust valve. In this final phase any remaining fuel that has not been consumed will continue to burn, perhaps at a much lower rate as shown in Figure 3.2 (d → e). Therefore, as long as fluid motion still exists inside the cylinder, mixing will continue to occur and provide opportunities for the fuel as well as partially-burned products to completely burn.

Conceptual Diesel Combustion Model – the current view

The understanding of the phases of the "conventional" diesel combustion process discussed above advanced significantly in the 1990s with the application of laser-sheet visualization techniques with optical access into the combustion chamber (Dec 1997; Flynn et al. 1999). Earlier, it was assumed that the quasi-steady portion of diesel combustion shortly after ignition and up to the end of injection was in steady-state such as those found in furnaces and gas turbines. These early models of diesel combustion had

three important characteristics. First, the liquid phase penetrated with fuel droplets being present up to or within the combustion zone. Second, after the premixed burn, combustion occurred solely in a diffusion flame and was confined to the peripheral region of the jet. Third, soot occurred mainly in the shell-like region around the jet periphery.

Early laser-sheet imaging studies showed features inconsistent with early conceptual models. According to these studies, soot is distributed throughout the cross section of the downstream portion of the reacting diesel jet. There are no liquid fuel droplets in the reacting jet. Also, soot particles in the upstream portion of the jet are much smaller than those in the head vortex region. Further imaging studies provided additional details which lead to significant changes in the conceptual model of the conventional diesel combustion process as can be seen in Figure 3.5. The belief that ignition occurs at a few locations around the periphery turned out not to be the case. Ignition actually occurs at multiple points across the downstream regions of the jet. Rather than penetrating to the end of the reacting jet, the length of the liquid portion of the jet core is actually very short in normal burning. Even after the end of the premixed burn phase, fuel is partially consumed through rich premixed burning before the fuel reaches the diffusion flame where burning is completed.
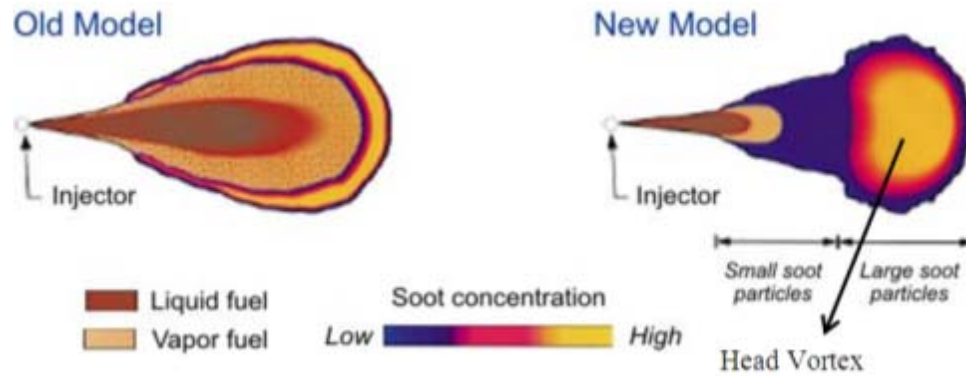
Figure 3.5   Comparison Between "Old" and "New" Diesel Combustion Models (Dec 1997)

Spray Characterization

The role of injection system characteristics has been widely studied. Empirical and semi-empirical correlations between macroscopic and microscopic spray features and injection parameters are available in literature (Naber and Siebers 1996; Arrègle et al. 1999; Gupta et al. 2000; Morgan et al. 2001).

The macroscopic description of a diesel spray generally emphasizes the interaction of the latter and the control volume where it is injected and mixed. The diesel spray is often described by three parameters namely, spray tip penetration, spray angle and break up length. Several researchers have studied the front penetration and have found a series of correlations that allow us to establish the main variables that affect or favor the penetration of a pulsed diesel spray (Dent 1971; Hay and Jones 1976).

The microscopic description is characterized by the content of droplets of diverse sizes and the changes in their special kinetics. For example, the atomization mechanism is responsible for distribution of the droplet sizes in the injection. Generally, the quality of the atomization of a liquid spray can be estimated on the mean diameter of the droplets. One common indicator of mean droplet size is the Sauter mean diameter

(SMD). The SMD can be viewed as the diameter of a droplet that has the same surface-to-volume ratio as that of the entire spray. In DI diesel engines equipped with modern fuel injection systems that provide high injection pressures, SMD can be as low as 6 to 15 microns (Henein and Patterson 1972; Heywood 1988). The diameter of the droplets obtained as a result of atomization is based on a series of parameters such as rate of injection, working fluid temperature, spatial evolution of the size of the drops and evolution of the diameter of droplets during time (Hiroyasu et al. 1989).

A greater number of smaller size droplets leads to a greater surface area that facilitates heat transfer from the hot compressed air to the small fuel volume contained in those droplets. It is also important to note that the injection process is not a steady stabilized process during which pressure, effective spray hole geometry, and injection rate are fixed. In fact, they do vary from the start to the end of injection. Therefore, one might expect the droplet size distribution to vary during the injection process. To further complicate the combustion process, temperature inside the combustion chamber is non-uniform and this non-uniformity varies throughout combustion. Therefore, mixing rates vary according to many parameters such as droplet size distribution, temperature distribution within the combustion chamber, spray penetration and atomization, fuel quality and its evaporation rates, as well as many other parameters (EL-Hannouny et al. 2007). The ability to model or to simply understand diesel combustion depends to a great extent on the ability to define each of the parameters involved in this process including droplet size distribution.

Air Entrainment

As the air-fuel mixing process is a key event in diesel combustion, a good understanding of the spray formation is essential to improve mixing efficiency. The spray penetration length and spray penetration rate from a fuel injector are the two important parameters to evaluate fuel spray performance. The significance of high or low penetration mainly depends on engine design and geometry. Shorter spray penetration may be suitable to reduce fuel impingement, but in larger engines may slow down maximum air utilization (Bergstrand and Denbratt 2001). It has been found that liquid and vapor penetration is dependent on ambient density and injection pressure. Initial researches of spray performance were focused on low-pressure sprays injected into ambient or low density conditions (Kuniyoshi et al. 1980). Investigations by Hiroyasu and Arai (1990), Naber and Siebers (1996) have shown a strong dependency of spray penetration upon both in-cylinder pressure and fuel injection pressure (Hiroyasu and Arai 1990; Naber and Siebers 1996). Hiroyasu and Arai (1990) showed that the spray behavior is strongly dependent on in-cylinder density and found that in a higher density environments, wider dispersion of the spray occurred with increased amounts of air entrainment. This entrainment had a direct effect on the momentum of the spray and hence reduced the penetration rate of the spray.

Hiroyasu and Arai (1990) also observed that the in-cylinder temperature has a significant effect on spray penetration, reducing the penetration by as much as 20% compared to sprays injected at non-evaporating conditions. Dent (1971) included a term to compensate for these temperature effects (Dent 1971). However, the observations of Naber and Siebers (1996) and Morgan *et al.* (2001) showed that this term does not fully compensate for the temperature effect on the liquid phase penetration(Naber and Siebers

1996; Morgan et al. 2001). Modern common rail fuel injection equipment was used in the investigations of Naber and Siebers (1996) and Morgan *et al.* (2001), while injecting into high-density environments. Their results showed that this correlation over-predicts the liquid penetration length. It is clear that although the influence of injection parameters has been widely investigated, information on the effects of in-cylinder density and fuel rail pressure on spray and fuel vapor distribution are still not conclusive.

It has also been shown that injection rate profile and injection nozzle geometry have a major influence on both the penetration and distribution of the fuel spray within the cylinder (Bae and Kang, 2000). The decreased size of droplets produced by smaller diameter nozzle causes faster mixing and evaporation and thus leads to shorter ignition delays. Change in the nozzle orifice diameter has also been shown to have an effect on the emissions (Bergstrand & Denbratt, 2001). The internal flow structures within the nozzle are also thought to affect the spray performance. Hence different spray structures may not be attributed to differences in nozzle diameter alone, but also to the nozzle type and internal nozzle geometry. Investigations into these flow processes have been undertaken in both large scale and full size nozzles (Soteriou et al. 1995; Badock et al. 1999). The variation in the behavior of various nozzle types and the influence of injection rate may help explain the apparent differences in the correlations for penetration with time and dispersion found in the literature. This, again, highlighted the strong dependence of the fuel spray behavior on the nozzle geometry and hence the dangers of applying generic correlations derived from experiments based on a limited specific nozzle type.

The fuel evaporation, penetration with time and dispersion is important to the combustion process as it provides the transport of the fuel vapor into the chamber. The

66

ambiguity over the effect of nozzle types on liquid phase penetration also extends to the vapor phase propagation. It is therefore clear that the effect of nozzle type and in-cylinder conditions on the injection and mixing processes are not fully understood.

Biodiesel—Mono Alkyl Esters

Global crude oil resources are finite (Wood et al. 2004); energy security and sustainability concerns have dictated the search for alternatives to conventional petroleum-based fuels. Therefore, tough emissions regulations combined with diminishing crude oil resources provide ample justification for adopting advanced combustion strategies and alternative fuels. Biodiesel is currently being considered as a sustainable alternative to conventional (petroleum) diesel fuel since it is produced from renewable sources. In the following, section, a review on biodiesel properties and its effect on engine performance and emissions will be discussed.

Bio-fuels in diesel engines have been used since the invention of diesel engine by Rudolph Diesel. While unprocessed vegetable oils are useful for some diesel engine applications (Cloin 2007), pure or partially esterified oils may cause a variety of engine problems such as long-term engine deposits, piston ring sticking, fuel injector plugging, or lube oil gelling which can cause engine failure or require more frequent maintenance and shorter engine overhaul intervals. Exhaust from engines fueled with raw vegetable oils can also have more adverse health effects compared to exhaust from the same engine using diesel fuel (Bunger et al. 2007). Unprocessed or partially esterified vegetable oils are therefore, generally considered unsuitable as diesel fuels and do not meet the requirements set by existing biodiesel standards and specifications. Eventually, biodiesel research focused on alkyl esters in the recent past due to their properties similar to diesel.

Many vegetable oils and animal fats have been suggested and investigated as feedstocks for the production of diesel fuel substitutes. The most common source of biodiesel in the USA is soybeans. Other significant biodiesel resources are greases and animal fats (Tyson et al. 2004). In Europe, the main source of biodiesel is rapeseed. Oil from jatropha (Jatropha curcas) nuts is an increasingly important biodiesel feedstock in tropical climates (Openshaw 2000) in India and in some African countries. Palm (Elaeis guineensis) oil is another cost effective biodiesel feedstock. Palm oil biodiesel has been increasingly produced in Southeast Asia (Malaysia, Indonesia) and in South America. If the demand for biodiesel continues to increase, the capacity to grow bio-oil plants for fuel may become limited. Methods have also been developed to make diesel fuel substitutes from oils naturally produced by certain species of algae (Sheehan et al. 1998). These oils, made of fatty acid triglycerides are converted into methyl esters before they are used as diesel fuel.

In the USA, the ASTM (American Society for Testing of Materials) Biodiesel Task Force adopted a definition of biodiesel that limited it to "mono alkyl esters of long chain fatty acids derived from renewable lipid feedstocks, such as vegetable oils and animal fats, for use in compression ignition (diesel) engines" (Howell 1997). The mono alkyl ester definition eliminates pure vegetable oils as well as monoglycerides and diglycerides from consideration as biodiesel.

Biodiesel due to its renewable character and greenhouse gas (GHG) emission reduction potential is favorable as an alternative to diesel fuel. However, high prices often present a barrier for widespread biodiesel use. Renewable fuel feedstocks, such as vegetable oils, have been supported by legislation and incentive programs in a number of countries. In markets with no government subsidies, the initial retail prices of biodiesel

are typically about 2 to 3 times higher compared to petro-diesel. As the volumes increase and the technology for producing fuel grade materials matures, the price may be reduced.

A common approach to reduce cost and maximize potential engine compatibility is blending biodiesel with petroleum diesel fuels. Such blends are commercialized as diesel fuel in many parts of the world. Blend levels in the USA vary from a few percent up to 20% biodiesel and 80% conventional petrodiesel. This is sometimes referred to as B20 (under the same convention, neat biodiesel is termed B100). In Europe, biodiesel is largely used as low level blends. Blends of up to 5% biodiesel in petrodiesel are broadly accepted for use in existing diesel engines by engine and fuel injection equipment manufacturers (FIE 2007).

Properties and Specifications

The ASTM specification D6751 for biodiesel was adopted in the USA in 2002 (ASTM 2002). The D6751 standard covers biodiesel (B100) for use as a blend component with petroleum diesel fuels. No standards currently exist in the USA that cover B100 for use as an automotive fuel. The D6751 specification is modified based on the existing ASTM standard for petrodiesel, D975. Development work on new analytical methods for a number of biodiesel properties was initiated in relation to the ASTM biodiesel standard (Stavinoha and Howell 1999). In 2008, D975 was modified to allow up to 5% biodiesel to be added to diesel fuel, and a B6 to B20 standard, D7467, was adopted. In Europe, biodiesel quality is described by the European standard EN 14214. This standard applies to neat biodiesel used as both *automotive fuel* and a *blend component*. The diesel fuel standard, EN 590, allows up to 7% biodiesel. Selected requirements for biodiesel blend stock, as defined by ASTM, and for biodiesel fuel

according to the European standard are listed in Table 3.1 (NREL 2009). Average

properties of neat biodiesel fuels compiled from various literature data are compared with

those of petroleum diesel in Table 3.2 (EPA 2002; Kinast 2003; McCormick et al. 2005).

The biodiesel data included soybean and rapeseed oil based fuels, as well as animal-based

biodiesels. Bio-fuels made from different feedstocks tend to show variations in

properties.

     In comparison with petrodiesel, biodiesel is characterized by: lower heating value

(by about 10-12%), higher cetane rating (typically 45-60), about 11% oxygen content by

weight (petro-diesel contains no oxygen), no aromatic content (and no PAHs), no sulfur

or ultra low sulfur content, better lubricity, higher viscosity, higher freezing temperature

(higher cloud point, pour point,...), higher flash point, higher boiling temperature (T10,

T50, T90), lower toxicity, rapid biodegradability and different corrosive properties.

Table 3.1   Biodiesel Standard Specifications (NREL 2009)

Parameter	Value (Method)	Value (Method)
Flash Point (°C), min	93 (ASTM D93)	120 (EN ISO 3679)
Water & Sediment (% vol), max	0.050 (ASTM D2709)	-
Kinematic viscosity (mm^2/s) @ 40°C	1.9 - 6.0 (ASTM D445)	3.5 - 5.0 (EN ISO 3104)
Sulfated Ash (% wt), max	0.020 (ASTM D874)	0.020 (EN ISO 3987)
Sulfur, max	0.0015 or 0.05% (wt) (ASTM D5433)	10 mg/kg (EN ISO 20846/84)
Copper Strip Corrosion, max	No. 3 (ASTM D130)	Class 1 (EN ISO 2160)
Cetane Number, min	47 (ASTM D613)	51 (EN ISO 5165)
Carbon Residue (% wt), max	0.05 (ASTM D4530)	0.3 (EN ISO 10370)
Acid Number (mg KOH/g), max	0.5 (ASTM D664)	0.5 (EN 14104)
Free Glycerin (% wt), max	0.02 (ASTM D6584)	0.02 (EN 14105/6)
Total Glycerin (% wt), max	0.24 (ASTM D6584)	0.25 (EN 14105)
Distillation, 90% recovered, max	360°C (ASTM D1160)	-

Table 3.2   Comparison between Biodiesel and Petro-diesel properties

Property	Biodiesel	Petrodiesel
Natural Cetane Number	55	44
Sulfur, ppm	9	333
Nitrogen, ppm	18	114
Aromatics, vol%	0	34
T10, °C	346	217
T50, °C	351	263
T90, °C	359	317
Specific Gravity	0.88	0.85
Kinematic Viscosity @40°C, mm^2/s	4.2	2.6

In comparison with petrodiesel, biodiesel is characterized by: lower heating value (by about 10-12%), higher cetane rating (typically 45-60), about 11% oxygen content by weight (petro-diesel contains no oxygen), no aromatic content (and no PAHs), no sulfur or ultra low sulfur content, better lubricity, higher viscosity, higher freezing temperature (higher cloud point, pour point,...), higher flash point, higher boiling temperature (T10, T50, T90), lower toxicity, rapid biodegradability and different corrosive properties.

Typical *heating value* (LHV) for biodiesel is 32.6 MJ/litre (117,000 BTU/gal), as compared to 36.2 MJ/litre (130,000 BTU/gal) for the US No. 2 diesel (McCormick 2002). As a result, a loss of engine power of about 8% is measured with neat biodiesel, and of about 2% with the B20 blend (Sharp et al. 2000). Fuel consumption penalties of 13% and higher have been reported with heavy-duty engines over the US FTP Transient test cycle (Sharp et al. 2000).

Emissions

Several studies have been conducted on the tailpipe exhaust emissions from biodiesel fuels and their blends. The results of these studies are often inconclusive or contradictory due to various reasons, making it difficult to quantify emission trends. Variability exists between the properties of various biodiesel fuels, especially in their cetane number, as well as between properties of the petroleum blending stock in the case of blends. Studies have been conducted on different types of engines (heavy-duty onroad, nonroad, light-duty) which, in general, may show different emission trends with biodiesel. Studies use different test cycles, including an array of steady-state and transient testing conditions which result in obvious emission differences. Relative emission effects reported with biodiesel may be distorted due to the use of different

baseline fuels. For a valid emission comparison, engines should be recalibrated to their

original power output to account for the lower heating value of biodiesel—a requirement

that is too often neglected.

A comprehensive summary of biodiesel emission effects was compiled by the US

EPA as guidance for States in claiming emission credits for the use of biodiesel and its

blends (EPA 2002). Figure 3.6 illustrates the correlation between the percentage

emission impact and the biodiesel content in the blend.

NO$_x$ Emissions

NO$_x$ emissions with B100 typically increase by about 10-30% relative to diesel

fuel (Gragg 1994; Krahl et al. 1995; Sharp et al. 2000; McCormick et al. 2005). NOx

emissions with B20 biodiesel blends are typically increased by 1-7% (McCormick 2002;

Sze et al. 2007). There are also claims that on average, there is no increase in NOx

emissions up to blend levels as high as B20 (McCormick 2006).
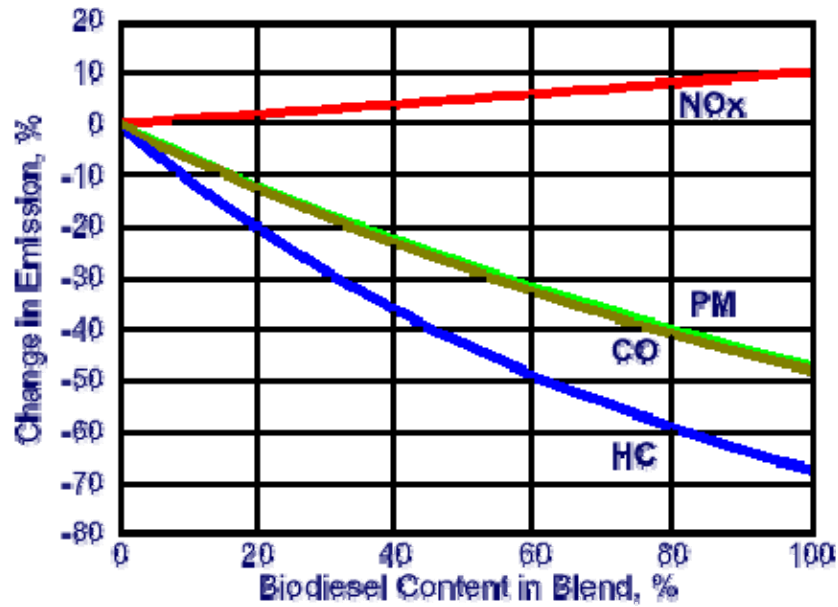
Figure 3.6   Average Impact of Biodiesel on Emissions from Heavy-Duty Engines
(NREL 2009)

The NOx increase depends on the type of the biodiesels feedstock; the highest

NOx emissions were reported with the most highly unsaturated fuels (soybean, rapeseed,

and soapstock-based) (Graboski et al. 2003). Biodiesel from more saturated feedstocks,

such as animal fats, yields a smaller NOx increase.

The NOx increase also depends on the engine technology. According to a study

with two heavy-duty engines meeting US 2004 emission standards—one with a common

rail and one with an electronic unit injector (EUI) fuel system—the NOx increase effect

can be higher in newer engines, where a 30% NOx emission increase was measured with

B100 fuel over the FTP cycle (McCormick et al. 2005).

The biodiesel NO_x increase has been shown to be test cycle specific. The

difference in NO_x emissions between diesel fuel and biodiesel blends has been shown to

correlate very well with average cycle power regardless of whether the test is carried out

on a chassis or engine dynamometer. As average drive cycle power increases, the NO_x

74

emissions increases with biodiesel fuelling(Sze et al. 2007). This is consistent with steady state tests with biodiesel blends, which show that NOx emission increases with biodiesel are highest at high loads. At low loads, increases are much smaller, and in some cases NOx emissions can be lower than with diesel fuel (McGill et al. 2003).

Explanation for the NOx increases observed with biodiesel is still unclear. Rather, NOx increases can occur for multiple reasons, the relative importance of which is dependent on both the particular engine being considered and its operating condition (Cheng et al. 2006; Sze et al. 2007).

Start of Combustion

Because of its higher specific gravity, the bulk modulus of compressibility of biodiesel is 5-10% higher that of diesel fuel (Tat 2003; Tat and Gerpen 2003; Boehman et al. 2004). This difference in bulk modulus can result in a more rapid transfer of the pressure wave from the fuel pump to the injector needle and an earlier needle lift (Morgan et al. 2001; Szybist and Boehman 2003). The effect would be most noticeable in pump-line-nozzle mechanical injection systems where pressure waves must travel relatively long distances. Injection timing advances of up to 2.3 degrees have been observed (Monyem et al. 2001). Unit injector systems show very little change in start of injection timing due to differences in fuel bulk modulus (Cheng et al. 2006). Common rail systems are expected to show little impact as well since the injector opening is controlled electronically.

Engine control systems may also advance timing to compensate for the ~10% lower energy density of biodiesel or for differences in other fuel properties. Increased fuel delivery may have various performance and emissions effects, including, in some

75

injection systems, injection timing advance. Some researchers, who modeled fuel injection and combustion with biodiesel, suggested that the high kinematic viscosity of biodiesel may also be responsible for the increased NOx through fuel injection system interactions [May 1998]. The mechanisms involved, however, are complex and ultimately difficult to explain. In the experimental part of the same work, some biodiesel fuels were found to cause the opposite effect of delayed injection timing and decreased NOx in certain low speed/load areas of the engine map. Biodiesel also has a higher cetane number than diesel fuel which can reduce ignition delay and also advance the start of combustion.

Changes in Other Controlled Parameters

To maintain a given load, a higher volume of biodiesel must be injected into the cylinder because of the lower volumetric heating value. On newer electronic diesel engines, the ECM can interpret the increased injector opening time as an increased load, and adjust injection timing, rail pressure, EGR, and other parameters accordingly.

Premixed Burn Fraction

A relation between premixed burn fraction and NOx emissions has been widely reported with increased premixed burn fractions resulting in increased NOx emissions. While the premixed burn is generally too rich to produce NOx [Dec 1997], it can affect the time-temperature history of the combustion process and in this way impact NOx emissions. Based on the higher cetane number of biodiesel, the ignition delay could be shorter and premixed burn fraction lower. This may offset increases in NOx due to other factors. Cetane number, however, may not accurately reflect the ignition delay behavior of fuels whose ignition characteristics have a temperature dependence different from the

primary reference fuel blends used in ASTM D 613 (Taylor 2004). Other fuel properties like ester group attached to the biodiesel molecule, lesser aromatic hydrocarbon etc. could yield a higher premixed burn fraction and higher NOx for biodiesel/diesel fuel blends in spite of the higher cetane number.

Diffusion Flame Temperature

Diesel engine NO_x formation is exponentially affected by the temperature of the diffusion flame. Oxygenated fuels such as biodiesel produce less soot in the combustion zone. Soot particles are important in radiating heat away from the flame region and providing some reduction in flame temperature. With less soot in the combustion zone, even a small increase in temperature due to lower heat transfer would result in some NOx emissions increase (Guo et al. 2004).

It is well known that adiabatic flame temperatures increase as the number of unsaturated carbon-carbon bonds in a molecule increases (Ban-Weiss et al. 2007). Since biodiesel is rich in unsaturated fatty acid esters, it may be reasonable to assume that this could result in a measurable increase in adiabatic flame temperature over diesel fuel. While calculating adiabatic flame temperatures is relatively straight forward, the challenge is the lack of the detailed thermophysical data for biodiesel components. Thermophysical data are available for methyl oleate (one unsaturated bond and the predominant ester in rapeseed methyl ester) and a calculation of adiabatic flame temperature for methyl oleate and primary reference fuel blends showed that there is no discernible difference (Cheng et al. 2006). It should be kept in mind however that soy based biodiesel is predominantly methyl linoleate (2 unsaturated bonds) and thus may give different results from methyl oleate. Commercial diesel fuels also contain

significant aromatics which would increase adiabatic flame temperatures for diesel fuels relative to the primary reference fuels used by (Cheng et al. 2006). It is not clear what effect biodiesel would have on the flame temperature when blended with diesel fuel with significant aromatics.

Mixture Stoichiometry and Combustion Chemistry

Differences in fuel properties such as viscosity, density, surface tension and volatility can influence fuel spray parameters and evaporation rates. Fuel mass injection rates and spray tip penetration can increase when biodiesel is blended with diesel fuel. This could influence fuel-air mixing and the stoichiometry of the fuel-rich premixed burn and change species concentrations and the relative importance of the prompt NO formation mechanism. The stoichiometry of the pre-mixed burn has a strong influence on soot formation.

While there are several factors that can impact NOx emission differences between petroleum diesel and biodiesel, some of them would be dependent on engine design parameters and thus highly variable. Where as, differences in flame temperature and mixture stoichiometry and chemistry, is more fuel specific and therefore less likely to vary. In order to determine if there are fundamental factors tied to the fuel itself that contribute to NOx emission differences, Cheng (2006) maintained a constant start-of-combustion and premixed burn fraction between the biodiesel and primary reference diesel fuels. It was found the NOx still increased by ~10% with biodiesel (B100). While it was not possible to positively identify the specific cause of the difference, the results strongly suggested that reduced soot radiative heat transfer from the combustion zone (resulting in higher flame temperatures) and mixture stoichiometry at the lift-off length

78

are both important. Further work is needed to better understand the relative importance of these two factors.

CO & HC Emissions

There is widespread agreement in the literature that biodiesel and its blends decrease CO and HC emissions. This effect is attributed to the oxygen content in biodiesel, which enables more complete oxidation in the engine cylinder. The magnitude of these reductions varies. A comprehensive study by SwRI reported a 40% CO emission reduction and total elimination of HCs with neat biodiesel (Sharp et al. 2000). According to the EPA correlations, CO emissions are reduced by 12% using the B20 blend, and by 48% using B100.

It was also suggested that higher CO and HC emission reductions are seen at higher engine loads. A study investigating the effects of biodiesel on a diesel engine emissions at different engine operating conditions found an increase of both CO and HC at low loads (Choi et al. 1997).

PM Emissions

Biodiesel decreases the carbon particulate emissions and increases the SOF. As a result, the visible smoke and opacity are decreased. The effect of biodiesel on total particulate matter (TPM) depends on the composition of diesel particulates, and so it is specific to the engine and the test cycle. Most studies reported a decrease in TPM emission with biodiesel, in some cases by as much as 25-50% (Sharp et al. 2000). The EPA analysis (Fig. 3.6) found that PM emissions were reduced by 12% using the B20 blend, and by 47% using B100. Increased TPM emissions, however, are also possible (Schroeder et al. 1999).

PM emission reductions in a study with two US 2004 engines were significantly larger than those in old engines (McCormick et al. 2005). Particulate matter (PM) emissions were reduced by 25% using B20 blends; PM emission reductions in excess of 70% were seen with neat biodiesel.

The PM reduction with biodiesel can be attributed to a combination of factors. First, a dilution effect which provides a reduction in the concentration of compounds found in diesel fuel, such as aromatics, that are more prone to generating soot. These are replaced with compounds, such as the straight chain hydrocarbon attached to the ester group in biodiesel, which are less prone to generating soot (Pepiot-Desjardinsa et al. 2008). Second, an oxygen effect which increases the probability that fuel carbon atoms attached to fuel oxygen, in the ester functional group of biodiesel, for example, will be converted directly to CO before finally being converted to CO_2. Without the oxygen present, there is a higher likelihood of fuel carbon generating soot precursors before the conversion to CO and then ultimately to CO_2 (Pepiot-Desjardinsa et al. 2008).

When compared to EPA certification diesel fuel with 350 ppm sulfur, two straight chain hydrocarbons (hexadecane ($C_{16}H_{34}$) and dodecane ($C_{12}H_{26}$)) resulted in PM reduction of about 45-50%. Soy-based biodiesel, methyl oleate (C18:1), methyl palmitate (C16:0) and methyl laurate (C12:1) showed PM reductions of about 75-85% reductions relative to EPA certification fuel (350 ppm sulfur) (Knothe et al. 2006). The shift of PM emission towards higher SOF content, as well as the absence of sulfur, make biodiesel compatible with diesel oxidation catalysts, which can maximize the PM benefit by controlling SOF.

Thus, we can say that although biodiesel is quite similar in physical properties of diesel, there are some distinct properties of biodiesel which can have different impact on

the combustion phenomenon. In the following section, model development for different

phenomena associated with diesel and biodiesel combustion will be discussed.

Sub-Model Development for Multi-zone Combustion

A multi-zone phenomenological combustion model that simulates closed cycle

engine operation has been developed. When the simulation starts, the air inside the

cylinder constitutes the unburned zone. The initial charge in the cylinder is assumed not

to have any residual exhaust gas from the previous engine cycle. Mass is transferred

from the unburned zone to the packet zone after the start of injection (SOI). The state of

the unburned zone, primarily it's mass and temperature amongst other properties, is

calculated as long as there is some unburned mass in the cylinder. Conceptual schematic

of zone evolution (Krishnan 2005) is shown in figure 3.7.

At SOI, the packet zones that account for the combustion of diesel-air mixture

entrained in the diesel spray, come into existence. Fuel injected into the combustion

chamber during each time step is divided into small packets that are distributed in the

radial direction. The total number of packets in the spray direction is determined by the

injection duration and the computational time step. Each packet is assumed to have the

same mass of fuel. No mixing and heat or mass transfer among packets is considered.

Each individual packet experiences its own history of temperature, pressure and

equivalence ratio. However, the total number of packets in the radial direction is fixed

regardless of amount of fuel injected, the injection duration or time step.

| Unburned zone | Packet zone | Burned zone |
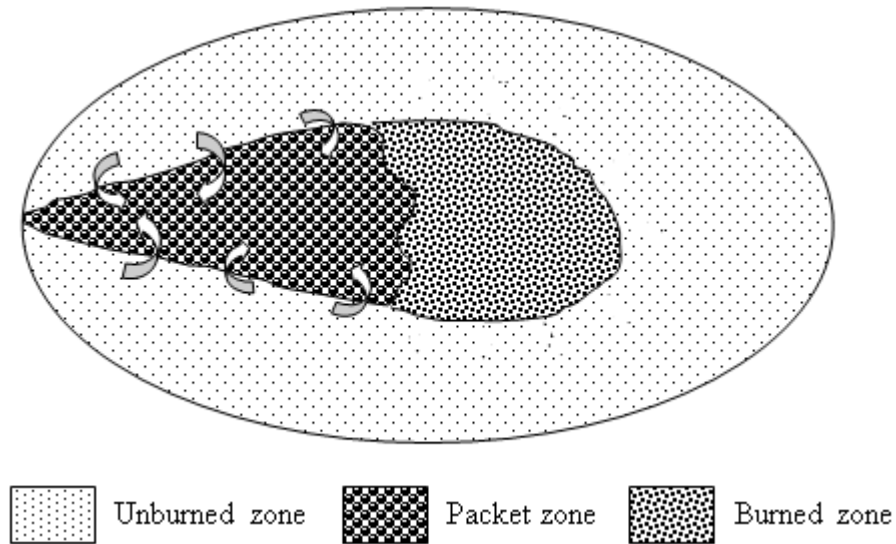
Figure 3.7   Conceptual schematic of zone evolution (Krishnan, 2005)
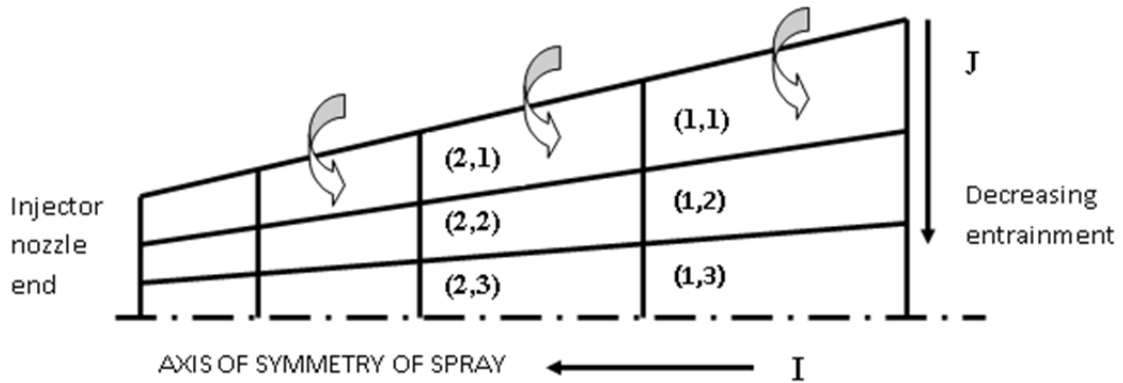
Figure 3.8   Division of spray into packet zones at a certain instance (Krishnan 2005)

Packets are classified based on their time of entry into the cylinder (I) and the stratification in unburned mixture entrainment across the spray (J) (shown in Fig 3.8). Although actual packet locations are not determined in this model, this method of packet identification allows for appropriate stratification of mixture entrainment across the spray, i.e., in this sense, the entrainment model is "quasi-dimensional."

The fuel injected into the chamber is initially assumed to form a liquid column at a speed equal to the fuel injection speed until the fuel break-up time. After that, the injected fuel is distributed, which is unique to each packet and varies from one time step

to another depending on the injection pressure and the cylinder conditions. The velocity of each packet is calculated from the spray tip penetration correlations.

It is assumed that the fuel atomizes to droplets with a diameter equal to the Sauter mean diameter. The effect of droplet size distribution within a packet is neglected. However, the droplet sizes in different packets may change depending on in-cylinder conditions at the start of injection. All the calculations related to the droplet evaporation are based on this Sauter mean diameter.

The air entrainment rate depends on the physical position of each packet, with centre line (innermost) packets receiving the least and the peripheral (outermost) packets receiving the most air. The amount of entrained air is calculated based on characteristic entrainment time and momentum conservation within each packet. It is assumed that the momentum of the packet at the exit of a nozzle is equal to that of the packet at every subsequent instant. Since the mass of the fuel and the injection velocity of each packet is initially determined, and the velocity of the packet can be calculated. Thus, the amount of air entrained can be obtained by the momentum conservation equation.

Evaporation of fuel is considered to begin immediately after the break-up. Both heat and mass transfer for a single evaporating droplet are considered in order to compute the instantaneous droplet temperature, rate of evaporation and droplet diameter.

The ignition delay is measured from the point of injection and is calculated with packet temperature and pressure. During the ignition delay period, some of the injected fuel is evaporated and mixed with air, forming a combustible mixture. Combustion is assumed to start individually in each packet after the ignition delay period. In the early stage, combustion occurs under premixed conditions. The premixed combustion in each packet is assumed to take place until the amount of fuel evaporated at the end of ignition

delay period of the corresponding packet has been consumed. Diesel evaporated in each packet after the occurrence of ignition is assumed to burn in the mixing-controlled phase. In this study, both premixed and mixing-controlled phase of combustion are considered to start simultaneously at the onset of ignition. During the combustion process, pollutant emissions can be calculated from the known pressure, temperature and composition of each packet. Each packet is "dumped" or adiabatically mixed with the remaining combustion products and ceases to exist as an individual packet when certain "dumping criteria" (to be discussed later) are satisfied. Some key assumptions (similar to the assumption considered by Krishnan (2005) of the model include the following:

1. Each zone is treated as an open thermodynamic system. However, the cylinder as a whole is a closed system.

2. Heat transfer occurs only between each zone and the cylinder walls. Although, mass transfer is allowed between zones, inter-zonal heat transfer is neglected.

3. When diesel burns it is assumed to be converted into products of complete combustion (CO_2 and H_2O).

4. Spatial variations in instantaneous cylinder pressure are negligible.

5. End of combustion is attained when the unburned zone mass becomes very small (less than 0.1 percent of its initial value) or more than 99.9 percent of the total entrained air has been consumed.

6. Crevice flows are neglected; therefore, the entire cylinder contents are treated as a closed system present within the combustion chamber.

The simulation starts from intake valve closure (IVC) and proceeds until exhaust valve opening (EVO). The cylinder pressure and temperature at intake BDC are

specified. Depending on the stage of the simulation, the cylinder contents are divided

into an unburned zone, packets and burned zone. In the following sections, detailed

mathematical expressions for the essential processes are presented.

Fuel Injection

The rate of fuel injected into the chamber and the injection timing affect the spray

dynamics and combustion characteristics. If the pressure upstream of the injector nozzle

is known, and the flow through each nozzle is quasi-steady, incompressible and one

dimensional, the mass flow rate of fuel injected through the nozzle is given by

[Heywood, 1988]:

$$\dot{m}_i = C_D A_n \sqrt{2 \rho_l \Delta P}$$

3.1

Where C_D = a discharge coefficient

A_n = nozzle hole area

ΔP = pressure drop across the injection nozzle.

Since $\dot{m}_i = \rho_l A_n u_i$, the fuel injection velocity, u_i, can be expressed as:

$$u_i = C_D \sqrt{2 \Delta P / \rho_l}$$

3.2

Spray penetration

The multi-zone model depends on an empirical correlation for spray evolution

and therefore the validity of the spray penetration model is critically important for

accuracy. The break-up length, l_b, of a liquid jet is given by [Levich, 1962]:

$$l_b \approx u_b t_b \approx \alpha \sqrt{\frac{\rho_l}{\rho_a}} d_n$$

3.3

Where u_b = jet velocity within the intact core

t_b = breakup time

α = a constant

d_n = nozzle hole diameter.

With the assumption that jet velocity within the intact core, u_b, is equal to the initial jet

velocity, u_i, the breakup time can be expressed as follows:

$$t_b = \frac{\alpha \rho_l d_n}{\sqrt{2 C_D^2 \rho_a \Delta P}}$$

3.4

Based on continuous jet theory, the spray tip penetration can be expressed as:

$$S = \beta \sqrt{t}$$

3.5

The expression for β can be obtained from the condition of $S = l_b$ at $t = t_b$.

$$\beta = 2^{0.25} \left(\alpha C_d d_n \right)^{0.5} \left(\frac{\Delta P}{\rho_a} \right)^{0.25}$$

3.6

Hiroyasu and Arai (1980) determined α and C_D from the experimental data as:

$$\alpha = 15.8$$

$$C_D = 0.39$$

With these values of α and C_D, they proposed the following correlation for spray

penetration before and after the spray breakup.

a. Before breakup, $0 < t < t_b(I)$ $S = 0.39 \left(\frac{2\Delta P}{\rho_l} \right)^{0.5} t$

3.7

b. After breakup, $t_b(I) < t$ $S = 2.95 \left(\frac{\Delta P}{\rho_l} \right)^{0.25} \left(d_n t \right)^{0.5}$

3.8

Where $t_b = 28.65 \dfrac{\rho_l d_n}{\sqrt{\rho_a \Delta P}}$

3.9

These correlations have been widely used in multi-zone models (Hiroyasu et al. 1983; Bazari 1992). However, considering that the nozzle discharge coefficient depends on the nozzle geometry and that the discharge coefficient of injector nozzles of modern diesel engines is usually between 0.6 and 0.8, the discharge coefficient of 0.39 seems too small. Schihl et al. (1996) developed a phenomenological cone penetration model and compared their model with Hiroyasu's model (Hiroyasu, 1983) and several experimental data sets from different sources. Discharge coefficients of the nozzles in the experimental data sources ranged from 0.64 to 0.74. Since Schihl's model is not valid before or near the breakup region, they compared the penetration after the breakup time. The comparison shows that Hiroyasu's model exhibits fairly good agreement with experimental data sufficiently long after the breakup time.

Dan et al. (1997) measured the temporal change in spray tip penetration with injection pressure and the discharge coefficient of the nozzle in the correlation used by them is 0.66. The discharge coefficient in Dent's correlation (Dent 1971) is 0.8. Jung (Jung 2001) showed that the correlation by Hiroyasu and Arai (1983) fits the experimental data better that the other correlations. The spray penetration after the breakup is valid for nozzles with different discharge coefficients. However, the penetration correlation before breakup is not applicable in those cases, since the injection velocity is directly a function of discharge coefficient. Therefore, Jung and Assanis (2001) proposed a modified penetration correlation to allow the correlation to handle different nozzles with an arbitrary discharge coefficient. They proposed the following correlation for spray penetration:

a. Before breakup: $\quad S = C_D \left(\dfrac{2\Delta P}{\rho_l} \right)^{0.5} t$

$$3.10$$

b. After breakup:
$$S = 2^{0.25}(\alpha C_D)^{0.5}\left(\frac{\Delta P}{\rho_a}\right)^{0.25}(d_n t)^{0.5}$$

    3.11

Where α is given by

$$\alpha = \frac{2.95^2}{2^{0.5}C_D}$$

    3.12

Hence, the velocity of the spray, V(J) is derived from the temporal differentiation of the equation of the spray tip penetration as follows:

a. Before breakup, $0<t<t_b(J)$
$$S = C_D\left(\frac{2\Delta P}{\rho_l}\right)^{0.5}t$$

    3.13

$$V(J) = C_D\left(\frac{2\Delta P}{\rho_l}\right)^{0.5}$$

    3.14

b. After breakup, $t_b(J)<t$
$$S = 2.95\left(\frac{\Delta P}{\rho_l}\right)^{0.25}(d_n t)^{0.5}$$

    3.15

$$V(J) = 1.48\left(\frac{\Delta P}{\rho_a}\right)^{0.25}(d_n)^{0.5}[t + t_b(1) - t_b(J)]^{-0.5}$$

    3.16

where the index J stands for the J-th packet in radial direction. Since the breakup time at the edge of the spray is shorter than that at the centre, the radial variation of the breakup time in the spray is incorporated as follows:

$$t_b(J) = 4.351\frac{\rho_l d_n}{C_D^2(\rho_a \Delta P)^{0.5}}Y(J)$$

    3.17

$$Y(J) = \exp\left[-0.8557\left(\frac{J-1}{J_t}\right)^2\right]$$

    3.18

Where J_t is the total number of packet in radial direction.

Droplet diameter after breakup

The droplet size distribution within the packet is neglected. All droplets in a packet are assumed to have the same diameter equal to the Sauter Mean Diameter. The number of droplets in each packet can be determined from the Sauter mean diameter and the total mass of fuel in the packet. The Sauter mean diameter, SMD, in the packet located along the spray centerline, is calculated by following equation (Jung and Assanis, 2001).

$$\frac{SMD}{d_n} = MAX(\frac{SMD^{LS}}{d_n}, \frac{SMD^{HS}}{d_n}) \qquad\qquad 3.19$$

$$\frac{SMD^{LS}}{d_n} = 4.12\,\mathrm{Re}_i^{0.12}\,We_i^{-0.75}\left(\frac{\mu_l}{\mu_a}\right)^{0.54}\left(\frac{\rho_l}{\rho_a}\right)^{0.18} \qquad 3.20$$

$$\frac{SMD^{HS}}{d_n} = 0.38\,\mathrm{Re}_i^{0.25}\,We_i^{-0.32}\left(\frac{\mu_l}{\mu_a}\right)^{0.37}\left(\frac{\rho_l}{\rho_a}\right)^{-0.47} \qquad 3.21$$

Where
$$\mathrm{Re}_i = \frac{\rho_l u_i d_n}{\mu_l} \qquad\qquad 3.22$$

$$We_i = \frac{\rho_l u_i^2 d_n}{\sigma} \qquad\qquad 3.23$$

And μ_l = viscosity of liquid

σ = surface tension

Air entrainment based on characteristic entrainment time

Air entrainment rate into the diesel spray is simultaneously governed by several factors (Krishnan, 2005). Entrainment rate is proportional to the available air (unburned zone mass, m_u) and all of this available air can be estimated to be entrained into the spray

in a time period to penetrate a distance equal to the cylinder bore radius known as the

characteristic entrainment time, (θ_{ch}). Spray penetration is determined using the

correlation recommended by Dent (1971). The total unburned entrained air is distributed

amongst a total number of $I_{tot} \times J_{tot}$. Decay in air entrainment towards the center of the

radial axis and with the progress in injection process must be captured.

The mass of air entrained (m_{ent}) into any packet (I, J) in one calculation step $(\Delta\theta)$

is expressed as follows (Bell 1985):

$$m_{ent}(I,J) = K \frac{m_u}{I_{tot}.J_{tot}.(1+Y)} \frac{\Delta\theta}{\theta_{ch}} \exp\left(-\frac{I}{I_{tot}} \frac{J}{J_{tot}}\right)$$

3.24

where K is the entrainment constant, Y is the ratio of time elapsed since SOI to total

injection duration, and I_{tot} and J_{tot} are the highest values of I and J, respectively. The

exponential term in Equation above accounts for stratification of entrainment in the radial

(J) direction and gradually lower entrainment in packets in the spray direction (higher I

values). It can be seen that the term $(1+Y)$ has been added in to the expression in order to

ensure that the overall rate of air entrainment in the spray decreases with increasing

elapsed time since SOI.

Air entrainment based on momentum equation

Another way of estimating air entrainment rate into the spray is using the

conservation of packet momentum. It is assumed that the momentum of the spray at the

exit of a nozzle is equal to the momentum of spray at any distance i.e.

$$m_f u_i = (m_f + m_a)\frac{dS}{dt}$$

3.25

Where m_f is the mass of fuel in a packet and m_a is mass of air in the packet. Therefore,

$$m_a = m_f\left(u_i \frac{dt}{dS} - 1\right)$$

3.26

The air entrainment rate can be obtained as (Jung and Assanis, 2001)

$$\overset{*}{m}_a = \frac{m_f u_i}{\left(dS\big/dt\right)^2} \frac{d^2S}{dt^2}$$

3.27

m

Combustion model

Combustion models range from zero-dimensional and single-zone to quasi-dimensional, multi-zone and multi-dimensional models based their thermodynamic resolution of working mixtures. The simplest single-zone combustion model specifies the heat release pattern in advance so that the cycle calculation merely involves adding energy to the cylinder contents in a pattern at the appropriate points in the calculations. This approach considers the cylinder contents to be a homogeneous mixture of air and gases that are always in thermodynamic equilibrium and deals as ideal gases. However, it is difficult to use this type of model to account for fuel spray evolution and for spatial variations of mixture composition and temperature. On the other hand, multidimensional simulation (Amsden et al. 1985; Amsden et al. 1987; Patterson et al. 1994; Varnavas and Assanis 1996) resolves the space of the cylinder on a fine scale and solves governing equations of conservation of mass, momentum and energy, as well as governing equations for species and chemical kinetics. However, computational time and storage constraints prevent it from being used for the practical application of an engine simulation.

In contrast, quasi-dimensional, multi-zone models (Li and Assanis 1993; Tauzia et al. 2000; Jung 2001), as an intermediate step between zero-dimensional and multi-dimensional models, have been effectively used to model diesel engine combustion

91

systems. These models need significantly less computing resources compared to multidimensional models. Instead of solving the full momentum equation, which is one of the main reasons of computational inefficiencies of multi-dimensional models, these models depend on a blend of fundamental theories. In the following section, first Wiebe's combustion function for single-zone combustion model and then two-phase heat release function for multi-zone model will be presented.

Wiebe's combustion function

Probably the most widely used heat release model is based on the Wiebe's combustion function. Weise specifies function to represent combustion curve, for the cumulative fuel burnt, as a function of the total fuel injected,

$$x = 1 - \exp(-a.y^{n+1})$$
3.28

Alternatively, in differential form (fuel burnt rate):

$$\frac{dx}{dy} = a(n+1).y^n.\exp(-a.y^{n+1})$$
3.29

The variable x represents the fraction of the mass of fuel burnt relative to the fuel injected and the variable y the time relative to the duration of combustion. The parameters a and n characterizes the shape of combustion curve. Therefore, the heat release pattern is defined by the total amount of fuel injected, the start of combustion, the combustion duration and the shape parameters of Wiebe function. The combustion duration is an arbitrary period in which combustion must be completed. The actual point at which combustion ceases has little real significance since the combustion rate decays exponentially to almost zero long before combustion really stops.

Parameter a in the Wiebe function can be considered as a combustion efficiency term, since the fraction of the cumulative fuel burnt to the total fuel injected is only dependent upon the parameter a. Therefore a may be chosen such that all the fuel is burnt at the end of combustion duration (for example, $x = 0.99$ at $y = 1$ if a 6.9). Then one may easily have a good approximation of a heat release pattern by varying the shape parameter n.

Two-phase Heat Release

During the ignition delay period, some of the injected fuel is evaporated and mixed with air, forming a combustible mixture. In the early stage, combustion occurs under premixed conditions at a rate equal to the following Arrhenius type equation (Nishida and Hiroyasu, 1989):

$$RR_p = B_l \cdot \rho_{mix}^2 \cdot x_{fv} \cdot x_{ox}^5 \cdot \exp\left(-\frac{1200}{T_p}\right) V_p$$

3.30

Where RR_p = reaction rate during premixed combustion phase

B_l = frequency factor

ρ_{mix} = density of the mixture

x_{fv} = the mass fraction of the fuel vapor

x_{ox} = the mass fraction of oxygen

T_p = temperature of the packet

V_p = volume of the packet

Equation 3.30 is assumed valid until the amount of fuel evaporated at the end of the ignition delay period in each packet has been consumed. Generally, the combustion during the second phase is mixing limited, so the availability of fuel vapor and entrained

air determine its rate. Mixing-controlled combustion is assumed to start simultaneous to the premixed phase. During this phase, the combustion kinetics proceeds at very high rate. However, the combustion kinetics slows down exponentially during this phase when the gas temperature becomes low and when the mixture is very lean. The combustion rate for the mixing controlled phase, RR_m, is governed by (Jung and Assanis, 2001):

$$RR_m = B_2 . m_{fv} . \frac{P_{ox}}{P} P^{0.25} . \exp\left(-\frac{2500}{T_p} \right)$$

3.31

Where B_2 is a constant; m_{fv} is mass of fuel vapor, P_{ox} is oxygen partial pressure; P is total pressure.

Heat Transfer Model

The heat transfer coefficient correlation of Woschni (1967) is used to calculate the spatially-averaged instantaneous heat transfer rate from the cylinder gases to the cylinder walls. Thereafter, the overall heat transfer rate with the corresponding area and temperature of the zone is weighted to find heat transfer rate from each zone.

$$\frac{dQ_i}{d\theta} = \frac{dQ_{tot}}{d\theta} \frac{V_i^{2/3}(T_i - T_{wall})}{\sum_i V_i^{2/3}(T_i - T_{wall})}$$

3.32

where $dQ_{tot}/d\theta$ is the overall heat transfer rate, $dQ_i/d\theta$ is the heat transfer rate from zone i, V_i is the zone volume, T_i is the zone temperature, and T_{wall} is the specified cylinder wall temperature.

Solution Procedure

In this section, the implementation of the multi-zone combustion model into the thermodynamic simulation is presented. Each packet can be treated as an open thermodynamic system. Each packet zone includes the entrainment of air from the unburned zone and mass transfer of fuel vapor from the liquid fuel spray by evaporation. Heat transfer takes place between the zones and the cylinder wall while the heat transfer between zones is ignored. The conservation equations for the gaseous contents of an open thermodynamic system are described in the following sections.

Conservation of mass

The rate of change of total mass in an open system is equal to the sum of the mass flow rates into and out of the system.

$$\dot{m}_\iota = \sum_j \dot{m}_{\iota,J} \quad \ldots \tag{3.33}$$

Where i denote i-th zone and j denotes mass flow to and from the zone. Once the fuel is injected, air entrainment is the mass flow for each packet zone and unburned zone. In particular, conservation of fuel species can be expressed as:

$$\dot{m}_{f,\iota} = \sum_j \dot{m}_{f,\iota,J} \tag{3.34}$$

Where $m_{f,i}$ denotes the fuel content in the i-th zone.

An average fuel-air equivalence ratio, φ can be defined as

$$\varphi = \frac{m_f/m_a}{\left(m_f/m_a\right)_{stoich}} \tag{3.35}$$

Where m_a is the mass of air in the system and subscript *stoich* denotes the stoichiometric fuel to air ratio.

Conservation of Energy

The first law of thermodynamics for the entire chamber as an open system is:

$$E = \dot{Q} - \dot{W} + \Sigma_j \dot{m}_j h_j \qquad 3.36$$

where last term in the equation above is the net rate of influx of enthalpy; $\dot{Q}$ is the total

heat transfer to the system; and $\dot{W}$ is the rate at which the system does work by boundary

displacement. The dot denotes differentiation with respect to time. Thus, the generic

form of the energy equation for any zone and the specific energy equations for different

zones are given below:

Generic form
$$\frac{d(m_i C_{vi} T_i)}{d\theta} = \sum_{netin} \frac{dQ_i}{d\theta} - \frac{P dV_i}{d\theta} + \sum_{netin} h_i \frac{dm_i}{d\theta} \qquad 3.37$$

Unburned zone
$$\frac{dT_u}{d\theta} = \frac{1}{m_u C_{pu}} \left[\frac{m_u R_u T_u}{P} \frac{dP}{d\theta} - \frac{dQ_u}{d\theta} \right] \qquad 3.38$$

Packet zones
$$\frac{dT_{ij}}{d\theta} = \frac{1}{m_{ij} C_{pij}} \left[\begin{array}{c} \dfrac{m_{ij} R_{ij} T_{ij}}{P} \dfrac{dP}{d\theta} - C_{pij} T_{ij} \dfrac{dm_{ij}}{d\theta} + C_{pu} T_u \dfrac{dm_{u-ij}}{d\theta} \\[2mm] - \dfrac{dQ_{ij}}{d\theta} - \dfrac{dQ_{ij-evap}}{d\theta} + \dfrac{dQ_{ij-comb}}{d\theta} \end{array} \right] \qquad 3.39$$

Burned zone
$$\frac{dT_b}{d\theta} = \frac{1}{m_b C_{pb}} \left[\begin{array}{c} \dfrac{m_b R_b T_{bj}}{P} \dfrac{dP}{d\theta} - C_{pb} T_b \dfrac{dm_b}{d\theta} + \\[2mm] \displaystyle\sum_{n=dump} C_{pij} T_{ij} \left(\dfrac{dm_{ij}}{d\theta} \right)_{dump} - \dfrac{dQ_{ij}}{d\theta} \end{array} \right] \qquad 3.40$$

In equations given above, the subscripts u, ij, and b refer to the unburned, packet

(I, J) and burned zones, respectively. In general, the variables m, R, T, P, cp, and Q refer

to the mass, characteristic gas constant, temperature, pressure, specific heat at constant

pressure, and heat transfer (from a given zone to the cylinder walls) associated with a

zone, respectively. The subscripts u-ij signifies the mass transferred from the unburned

zone to packet (I, J). The energy transferred out of packet (I, J) due to diesel evaporation is denoted by the subscript ij-evap and the energy release accompanying combustion in packet (I, J) is denoted by the subscript ij-com. The summation term in equation above accounts for the total energy associated with dumped packets (variables identified by the subscript dump) that is transferred to the burned zone.

Simulation procedure

First, using the mass conservation equations, the masses of all zones are calculated.Then the energy conservation equations for all the zones (after BOI) are numerically integrated and zone temperatures are determined using the Livermore Solver for Ordinary
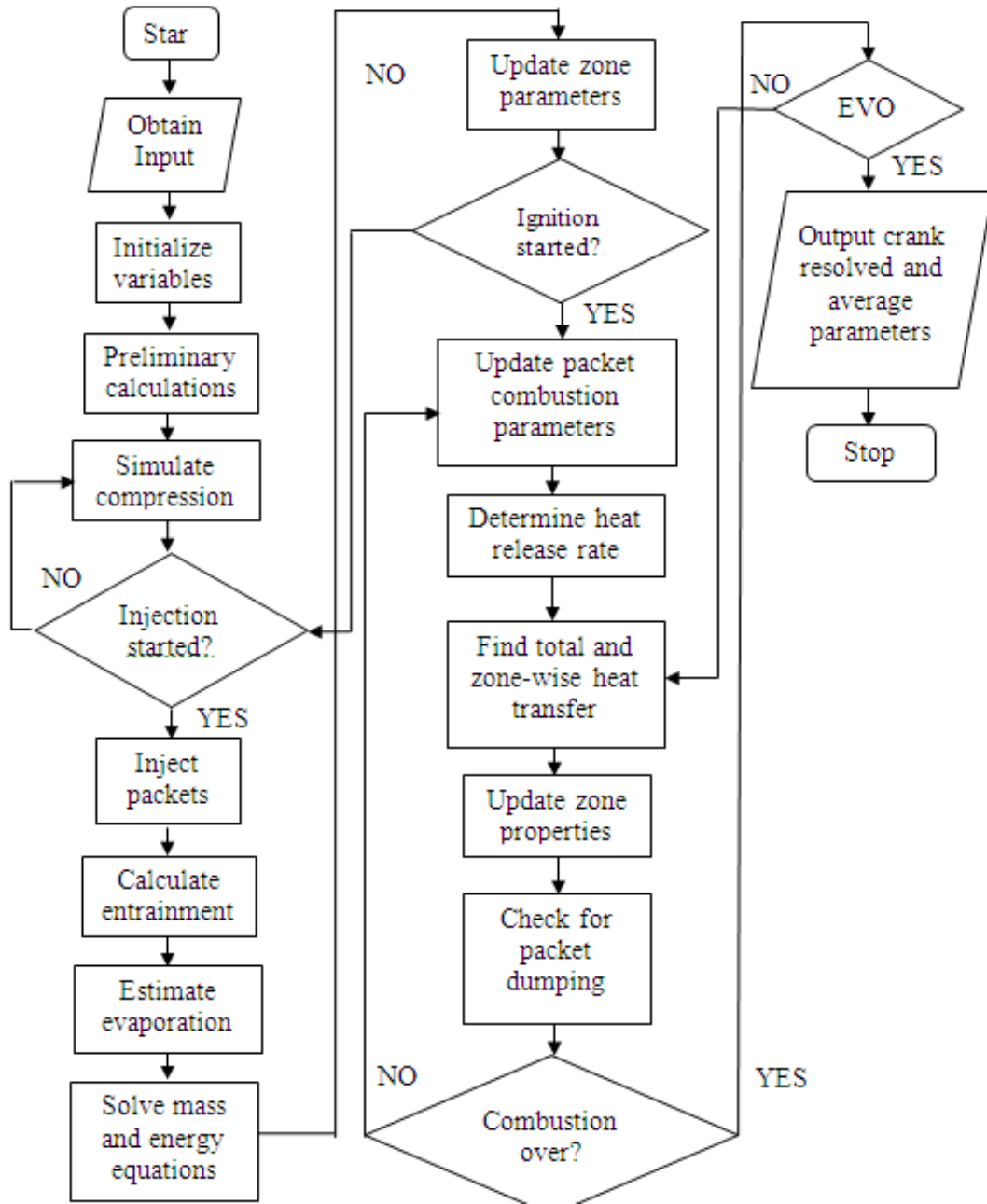
Figure 3.9   Flowchart illustrating the main processes (or sub-models) and the sequence
of execution of the simulation (Krishnan 2005)

Differential Equations (LSODE) (Hindmarsh, 1983). Once the zone temperatures

are evaluated, the average cylinder temperature is determined from the following

equation:

$$T_{avg} = \frac{\sum_i m_i C_{vi} T_i}{\sum_i m_i C_{vi}}$$

3.41

where m_i is the mass, c_{vi} the specific heat at constant volume, and T_i the temperature of zone i. The summation is taken over all zones present in the cylinder. Instantaneous cylinder pressure is determined using the average cylinder temperature, instantaneous cylinder volume, and the ideal gas relation for the overall cylinder contents. Zone volumes are then computed from individual zonal ideal gas relationships. The nominal computational time step during compression is 1 degree (at least 2 ms) and after BOI, the time step is reduced to 0.03125 degrees (at least 0.05 ms).

The overall sequence of execution of the computer simulation and the important processes modeled therein are illustrated as a flowchart in Figure 3.9. Briefly, the simulation may be summarized as consisting of three primary stages – preliminary calculations, modeling of the compression process (until the beginning of fuel injection) and detailed modeling of the combustion process in packets. Within these three stages, several sub-models are utilized to provide the required quantities at different crank angles. For example, the heat transfer model is used throughout the simulation, while the spray entrainment and diesel evaporation models are used only after BOI, and the packet combustion model is used only after ignition. Mass balance, energy balance, and ideal gas equations of state are solved throughout the simulation to obtain the mass, temperature, and volume of all zones present at a given crank angle and the instantaneous cylinder pressure is calculated. The thermodynamic properties (e.g., constant-pressure specific heats) for the instantaneous mix of species present in a zone are then evaluated from expressions provided by NASA coefficients for calculating thermodynamics and transport properties for individual species and updated every time step.

99

Experimental Set-up

All experiments in the present work were performed on a turbocharged direct-injected (TDI), 1.9L, in-line 4-cylinder compression ignition engine. Relevant engine details are provided in Table 3.3. The stock ECU of the engine was utilized in the experiments, thus limiting control of the engine. Engine speed was controlled with a Froude Hoffman AG80 (Imperial) eddy current dynamometer and engine torque was measured with a calibrated load cell. The ECU controlled biodiesel injection with a throttle position sensor, which was actuated by the Texcel 4.0 dynamometer control software. All gaseous exhaust emissions and smoke were measured downstream of the turbocharger turbine. Gaseous emissions were routed through an emissions sampling trolley to an integrated emissions bench (EGAS2M) manufactured by Altech Environnement S.A and smoke was measured using an AVL 415S variable sampling smoke meter.

Engine coolant temperatures, pre- and post-turbo air temperatures, intake mixture temperature, and post-turbo exhaust temperatures were measured with Omega Type-K thermocouples. The coolant temperatures were held between 85±2 degrees Celsius, while post turbo intake temperatures were held between 35±2 degrees Celsius. Intake air mass flow rates were measured with a FlowMaxx venturi flow meter. Diesel/Biodiesel mass flow rate was measured with a Max Machinery Model 213 piston flow meter. Absolute ressure in the test cell was measured with an Omega PX 429 sensor, differential pressure across the venturi flow meter was measured with a Validyne P55 differential pressure transducer (0.25% accuracy of full scale), and intake boost pressure was measured with a Setra 209 pressure transducer. In-cylinder pressure was measured using a Kistler 6056A piezo-electric pressure transducer mounted in a Kistler 6544Q series

100

glow plug adapter. The charge amplifier used was a Kistler 5010B using a medium time constant setting.

Needle lift was measured using a stock injector that was instrumented with a Wolff needle lift sensor coupled to a signal conditioner. In this study, the Start of Injection (SOI) is defined as the crank angle when the injector needle lift reaches 5% of its maximum lift for the cycle. Both in-cylinder pressure and needle lift measurements were recorded with National Instruments PXI S- Series hardware using a BEI encoder of 0.1° crank angle resolution. All in-cylinder data were recorded for 100 successive engine cycles after engine operation attained steady state. To ensure consistency over all cylinder pressure and heat release measurements, the engine was motored for 40 cycles before firing data were taken to ensure that no slippage of the encoder had occurred.

Table 3.3   Engine specifications

Engine Type	1997 4-cylinder TDI
Bore x Stroke (mm)	79.5 x 95
Aspiration	Turbocharged
Displacement	1.9 Liters
Nominal compression ratio	17:1
Number of valves per cylinder	4
Injection system	Stock mechanical; direct injection
Number of nozzle holes	5
Nominal orifice diameter (μm)	205
Nominal Injection timing (static)	4°BTDC
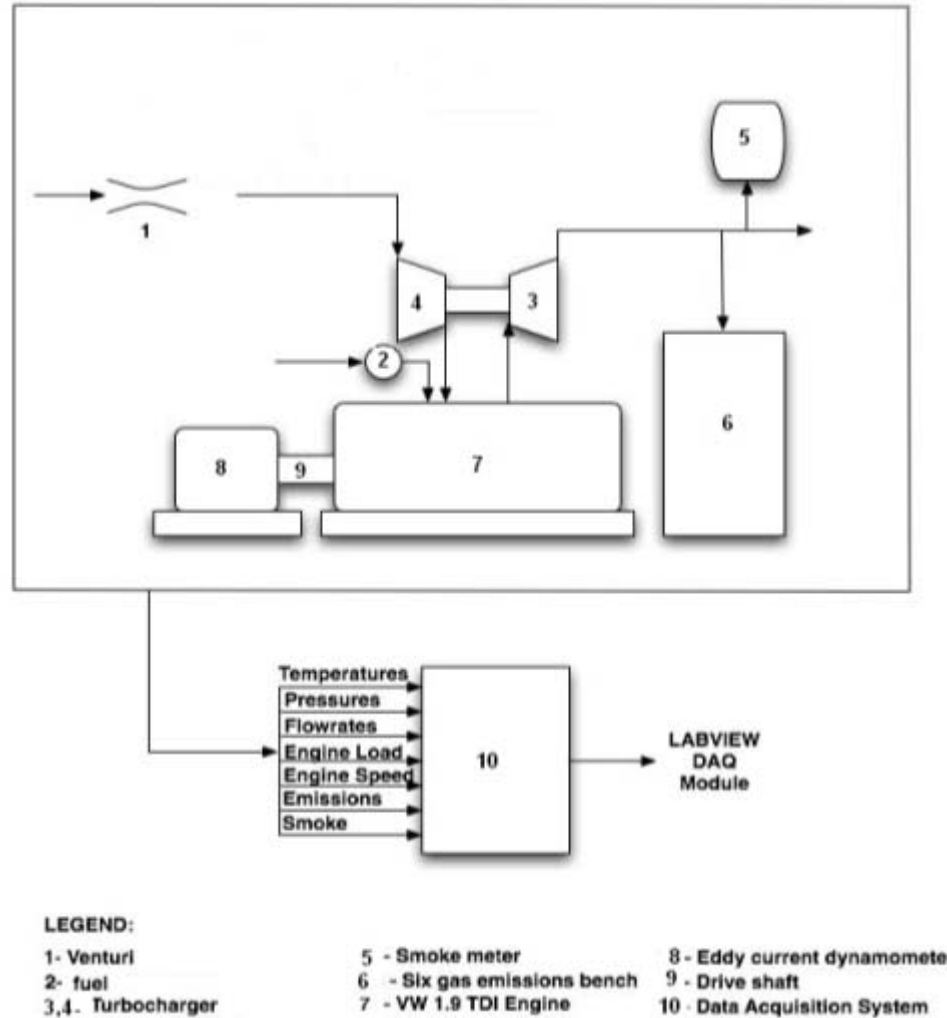
Figure 3.10   Schematic of experimental set-up (Gibson et al. 2010)

Matching Experimental and Predicted Motoring Pressure Curves

   A good comparison between the experimental and predicted motoring (without combustion) pressure curves helps in establishing a baseline. In this study, the simulation begins at inlet valve closure (IVC) and continues until exhaust valve opening (EVO). Initial air mass at IVC for the motoring case remains the same as that for the combustion case. The initial value of in-cylinder pressure at IVC is obtained from experiments and the intake manifold temperature is measured at IVC. The model parameters used for

simulating motoring are provided in Table 3.4. The experimental and simulated motoring pressure curves are compared in Figure 3.11.

Clearly, the baseline simulation under predicts pressure throughout the compression as well as the expansion stroke. To diagnose this issue, several measures including changing the compression ratio, modifying the heat transfer model parameters and reducing the computational time step were tried. The compression ratio of 17 led to a good match in peak pressures (not shown) but still the pressures during compression were well under predicted. Changing the heat transfer model parameters or computational time steps showed negligible impact on the motoring pressure predictions.

Later it was found that the intake manifold temperature at IVC could lead to considerable uncertainties. Since the ideal gas equation is used to compute the simulated pressure from the temperature, adjustment on in-cylinder total mass (MTOT) was done. This adjustment is justifiable since gas-exchange modeling is not considered in this study. Therefore, in order to capture the physics of the gas exchange process, an adjustment factor to adjust the MTOT in the cylinder is introduced. Accordingly, the motoring pressure predictions were compared to the measured pressures as MTOT was slowly increased. In this way, it was observed that for the specific initial conditions of pressure and temperature given in Table 3.4, the best match in between experimental and predicted pressures was obtained with a 4 percent higher MTOT, albeit with a slight over prediction of the pressures during expansion.
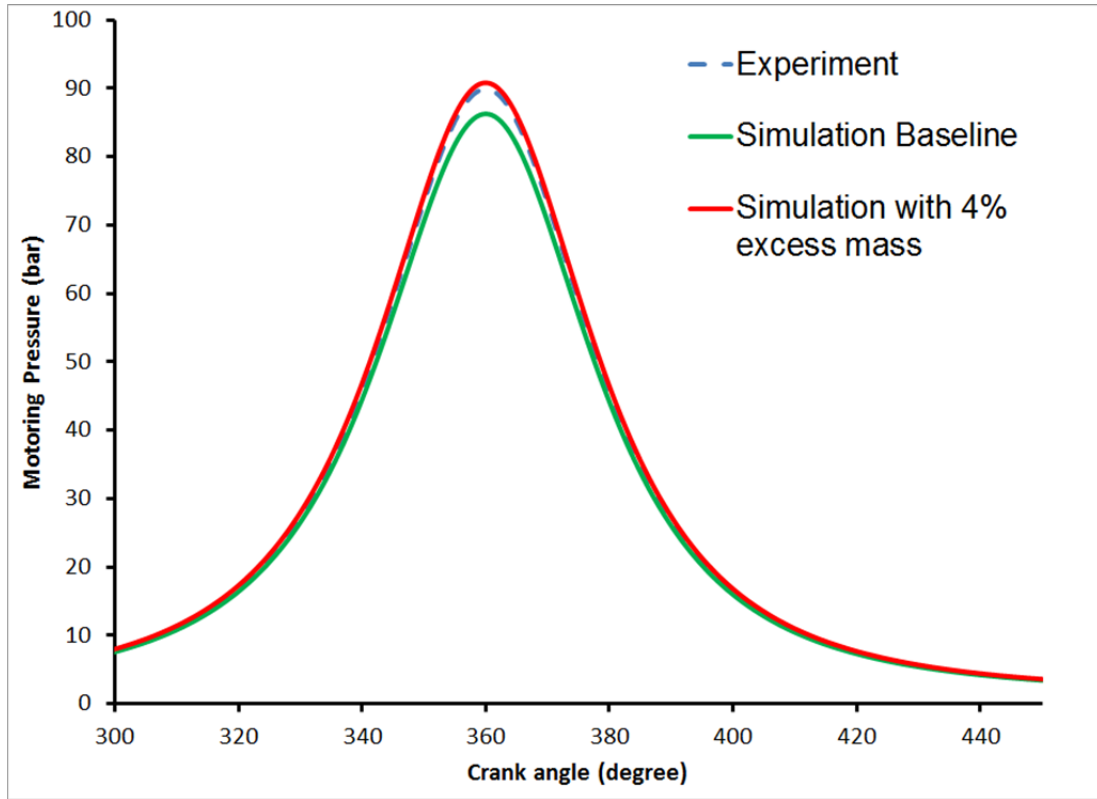
Figure 3.11   Experimental and predicted motoring pressures (for the baseline simulation and the simulation with trapped total mass, M_{TOT}, increased by 4 percent) for $P_{IVC} = 2.15$ bar, $T_{in} = 330$ K.

Table 3.4   Model Parameters for Motoring Pressure Comparisons

Parameter	Value
Compression ratio	17 : 1
Air flow rate (g/min)	2896
Initial pressure (obtained from experiments) at IVC (bar)	2.15
Initial charge temperature (K)	330
Computational time step for motoring, DCADM (crank angle degrees)	1.0

Single-zone simulation validation

A single-zone Wiebe function-based thermodynamic model of diesel/biodiesel combustion is presented below. The objective is to develop a simulation that predicts cylinder pressure histories by assuming a finite heat release (Wiebe function) model (Hiroyasu, 1988). The contents of an engine cylinder are modeled as a closed system. Applying energy conservation to the cylinder, the rate of change of cylinder pressure (P) with respect to crank angle (θ) can be expressed as a function of the cylinder volume (V), the ratio of specific heats (γ), the rate of chemical energy release during the combustion process (Q_c), and the rate of heat transfer through the cylinder walls (Q_{ht}):

$$\frac{dP}{d\theta} = -\gamma \frac{P}{V}\frac{dV}{d\theta} + \frac{\gamma-1}{V}\left(\frac{dQ_c}{d\theta} - \frac{dQ_{ht}}{d\theta}\right)$$

3.42

The chemical heat release rate is calculated using the assumed mass burn rate as follows:

$$\frac{dQ_c}{d\theta}(\theta) = Q_t \cdot \frac{dx_b}{d\theta} = m_d \cdot LHV_d \cdot \frac{dx_b}{d\theta}$$

3.43

where Q_t is the total chemical energy released during the combustion process and x_b is the mass burned fraction, m_d is the mass of diesel in the cylinder in one engine cycle and LHV_d is the lower heating value of diesel. The Wiebe function can be expressed as follows:

$$x_b(\theta) = x_{b,\max} \cdot \left(1 - \exp\left[-a\left(\frac{\theta-\left(\theta_{SOC}\right)}{\theta_d}\right)^{n+1}\right]\right)$$

3.44

According to Equations 3.43 and 3.44, the characteristics of the heat release rate depend on the injected fuel mass m_d, the start of combustion θ_{SOC}, the total combustion duration, $\Delta\theta_d$, the efficiency parameter "a" and the form factor "n". The injected fuel

mass is determined by the engine control module. It is also reasonable to maintain the combustion duration $\Delta\theta_d$ as constant. Therefore, the start of combustion, the efficiency parameter (a) and the form factor (n) largely control the accuracy of the wiebe model.

Heywood (1988) used the Wiebe function to calculate the mass fraction burned of the charge within the cylinder for each crank angle. Several values of a and n were used to obtain a good match for the experimental pressure curves and concluded that the set of $a = 5$ and $n = 2$ can provide a reasonable estimate for many conditions. The values suggested in their study can indeed achieve a reasonably good match for pressure curves at full operating range. To test the values of a and n in this study, cylinder pressures and the engine configuration of a Volkswagen 1.9L four cylinder turbocharged engine were used. In addition, when combustion proceeds to completion, $x_{b,max}$ reaches unity and therefore it is usually not considered in the Wiebe function for mass burned fraction. However, combustion is often incomplete and so $x_{b,max}$ must be considered. In addition, it is necessary to modify the Wiebe function parameters a and n. These values are provided in Table 3.5.

It is important to ensure that the Wiebe function-based combustion model faithfully reproduces the experimentally observed cylinder pressure histories in diesel/biodiesel combustion. The measured pressure curves were processed using a single-zone heat release analysis code to derive gross heat release rates and mass burned fraction curves. In fact, the Wiebe function parameters (Table 3.5) were chosen to minimize the least-squares error between the experimental and simulated mass burned fraction curves.

The heat release results for diesel fuel presented in Figure 3.12 provide validation of the overall combustion model. Again, the start and end of heat release and the overall

106

heat release rates from the simulation and experiments match quite well. The peak heat release rate is slightly under-predicted by the combustion model. The predicted heat release rates for biodiesel is compared with the experimentally derived heat release rates in Figures 3.13. Again, for biodiesel, the start and end of heat release are predicted well but the peak heat release is under-predicted. The simulated heat release curves shown in Figures 3.12 - 3.13 are the best predictions possible with the simple Wiebe function-based combustion model and some discrepancies between the predictions and measurements may be expected. It can be observed that the accuracy of the predicted heat release for all the fuels is maximum at half load and the accuracy decreases as the load is either increased or decreased.

Several fraction burned curves and the rate of fraction change are shown in literature for various a and n [Heywood 1988]. For a fixed form factor n, the larger the value of a, the more rapid the mass burned fraction change occurring around the midpoint of the total combustion duration. For larger value of a, the maximum heat release rate shifts to the first half of the combustion period. For a fixed efficiency parameter a, a larger n value causes the second half of the combustion period to have a larger heat release. According to the effects of these two parameters and the analysis of experimental data, a high efficiency parameter and form factor are suggested for high IMEP, while estimation in a low IMEP can be modeled with a low parameter a and low factor n. Even though a and n are adjusted for different IMEP levels, combustion variations can still cause modeling error to produce errors in pressure estimation. The information about the estimated combustion heat release and its rate can be utilized to identify an appropriate a and n.

Efficiency parameter a is higher for biodiesel than diesel in table 3.5. This shows that maximum heat release for biodiesel shifts more in the first half of combustion period than the diesel. Table 3.5 also shows that form factor n is higher for biodiesel in compare to diesel. It can be inferred that higher heat released in the second half of the combustion period for biodiesel than diesel. Higher a and n value for biodiesel clearly shows that overall heat release using biodiesel is more than diesel.

Table 3.5   Wiebe function parameters

IMEP	SOI	Diesel		Biodiesel	
		a	n	a	n
	10	4.49	0.18	4.88	0.33
2.5	4	5.15	0.19	5.55	0.27
	0	5.45	0.18	5.69	0.29
	10	4.77	0.27	4.75	0.25
5	4	5.22	0.36	5.55	0.43
	0	5.29	0.24	5.64	0.51
	10	4.62	0.43	4.62	0.68
7.5	4	5.37	0.45	5.50	0.46
	0	5.47	0.43	5.90	0.58
	10	4.53	0.50	4.49	0.58
10	4	5.46	0.68	5.31	0.42
	0	5.48	0.55	6.00	0.55
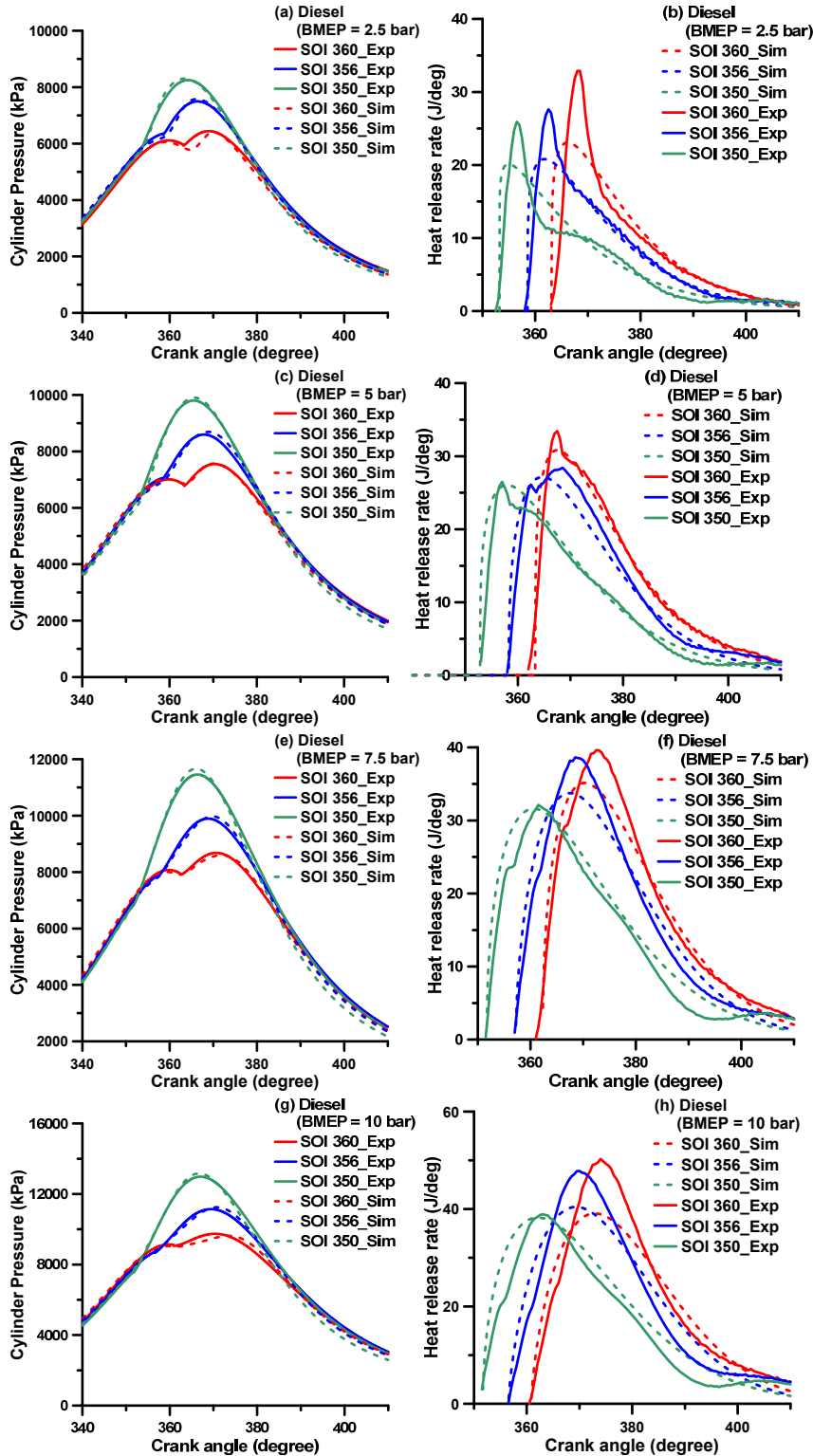
Figure 3.12   Comparison of experimental and simulated cylinder pressure (a, c, e, g) and
heat release rate (b, d, e, f) using single-zone wiebe model of diesel at
different load conditions

109
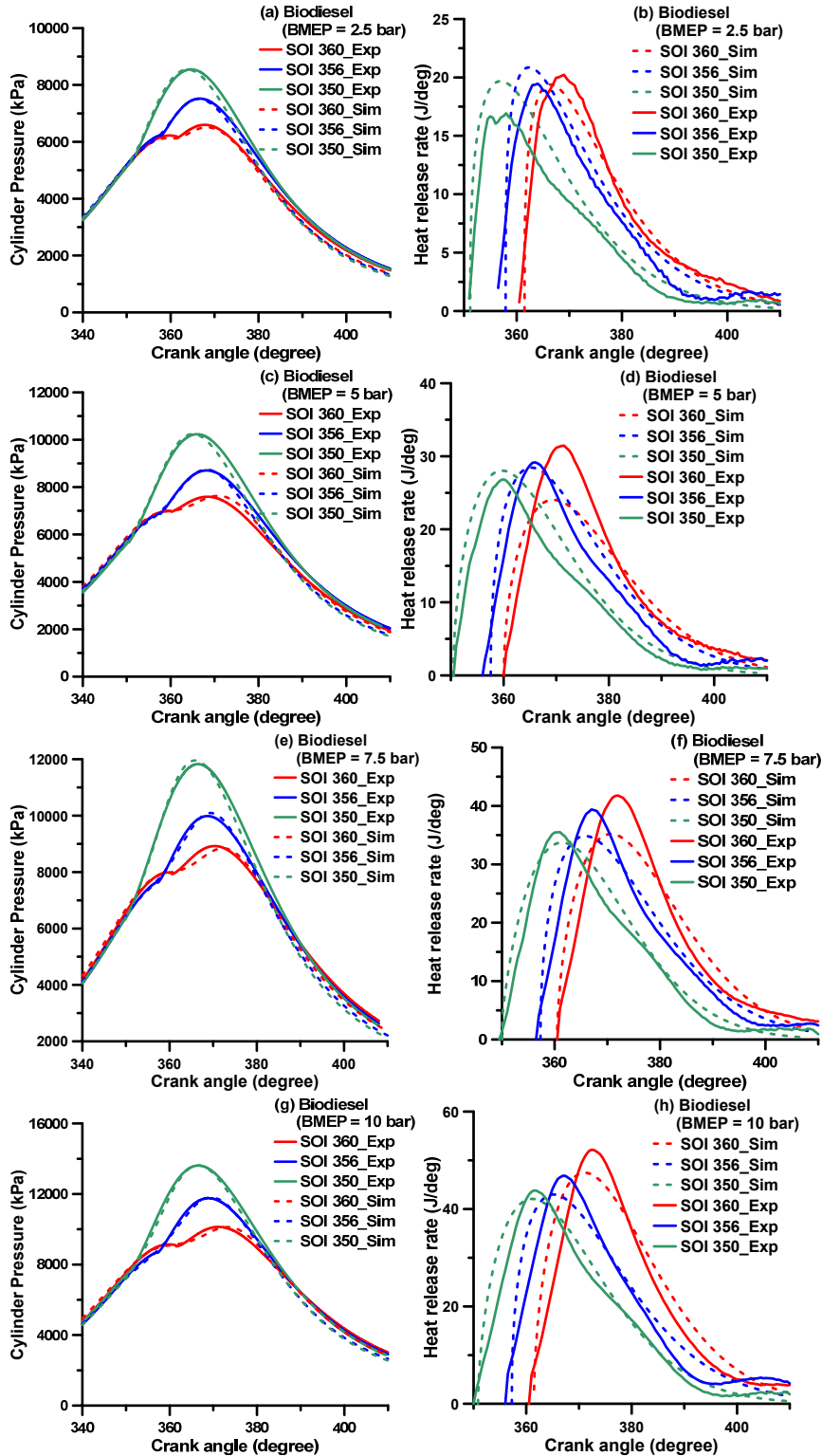
Figure 3.13   Comparison of experimental and simulated cylinder pressure (a, c, e, g) and heat release rate (b, d, e, f) using single-zone wiebe model of biodiesel at different load conditions

110

Multi-zone Simulation Results

The sub-models that were presented earlier in the chapter are grouped together for the purpose of model validation as follows:

- Spray evolution model and air entrainment

- Spray droplet diameter after breakup and evaporation model

- Ignition delay model

- Combustion model

Correlations for spray penetration play very important roles in the quasi-dimensional multi-zone model because they determine the spray shape and the location of packet zones. The multi-zone model is computationally much more efficient than the multi-dimensional model because it relies on empirical correlations to describe spray evolution, instead of solving the full momentum equation. In addition, spray penetration is the key factor that affects the air entrainment rate calculation. As can be seen in the momentum conservation equation for the air entrainment rate (equation 3.25), the air entrainment rate is a function of the first and second derivatives of spray penetration. Since the air entrainment rate subsequently affects the combustion process, the importance of the spray penetration correlation cannot be underestimated. The behavior of the various sub-models needs to be studied with respect to the experimental data taken from real diesel engines. The behavior of the model with respect to zonal resolution and time step choice will be determined.

The spray evaporation process occurs relatively faster compared to other processes. Evaporation takes place within a few crank angles after start of injection. The rate of evaporation determines the combustion characteristics as either mixing limited or evaporation limited.   The total mass of fuel injected, the total mass of fuel mixed with air

and the total mass of fuel evaporated are monitored with respect crank angle in the following sections.

Combustion models are validated by comparison of calculated cylinder pressure and apparent heat release rate with experimental data. By this approach, the start of combustion, the premixed combustion phase and the mixing controlled combustion phase can be checked at the same time. The engine operating conditions for the validation covered a wide range of engine speeds and engine loads.

Baseline Model Results

In this section, important predictions of the simulation such as cylinder pressure, heat release rate, and cumulative gross heat release histories will be presented for the baseline model constants shown in Table 3.6. Proper calibration of the simulation against experimental data may involve the simultaneous adjustment of several model parameters.In addition, the model predictions may be sensitive to different degrees for different model parameters. At first, it is important to discuss the selection of parameter values shown in Table 3.6. The diesel injection pressure and initial charge temperature are experimental values that are used as model inputs. As discussed in the previous sections of this chapter, air entrainment is one of the important phenomena that affect combustion. Two previously used air-entrainment models (Jung 2001; Krishnan 2005) are used to estimate the entrained air in the packet. The entrainment constant K_{Bell} was chosen as 2.0 instead of 0.05 as used by Krishnan (Krishnan 2005) to estimate the entrainment rate in the injected pilot fuel (diesel) in pilot-ignited natural gas combustion. The significant difference between the K values used by Krishnan and that of the present study may be due to the size of the fuel spray. The pilot fuel spray associated with

112

ALPING combustion by Krishnan (2005) was much smaller with significantly less

entrainment while, entrainment occurred into a much larger fuel spray in this study.

Table 3.6   Baseline Model Constants

Model Parameters	Value
Diesel injection pressure (bar)	160
Diesel injected quantity (g/min)	113
Diesel injection duration (crank angle degrees) (full load)	15
Initial charge temperature (K)	330
Entrainment constant (Krishnan, 2005), K_{Bell}	2.0
Entrainment constant (Hiroyasu, 1980), $K_{Hiroyasu}$	2.5
Constant factor in premixed phase reaction rate, B_1	1.5×10^6
Constant factor in mixing-controlled phase reaction rate, B_2	800000
Nozzle discharge coefficient, C_D	0.7
Total number of I packets, I_{tot}	61
Total number of J packets, J_{tot}	3
Shell model OSAM RON90 constant, A_Q (for diesel)	2.5×10^{13}
Shell model (methyl butanoate) constant, A_Q (for biodiesel)	3.0×10^{13}
Computational time step after BOI, DCAD (crank angle degrees)	0.03125

Air entrainment models based on spray penetration and momentum conservation

based on Jung and Assanis (2001) were used to evaluate the effects of air entrainment on

the whole combustion process. Jung and Assanis (2001) modified the spray penetration

correlation proposed by Hiroyasu and Arai (1980) to include discharge coefficients of

fuel injection nozzles. In this study, the entrainment model was further modified to

address the zonal variation in air entrainment rate. It is assumed that zones at the edge of

the spray will entrain more air than those chosen to the axis of the spray. In addition, it was found in this study that the baseline air entrainment rate using Hiroyasu and Arai (1980) model was low. Therefore, the baseline entrainment constant was adjusted by a factor of 2.5 to tackle the low entrainment rate issue.

The total number of injected packets (I_{tot}) depends on injection duration and injection time step. Injection duration is a measured engine variable. Therefore, it is important to vary the injection time step to fix the number of I_{tot}. For the chosen computational time step of 0.03125 degrees crank angle, the value of I_{tot} represents the maximum value possible. For injection duration of 15 CA degrees, the total number of injected packets equal to 183 (choosing the injection time step to be 0.25 CA degrees) is used to set the baseline for the selected J_{tot} of 3.

The experimental heat release rates are determined using a single-zone thermodynamic combustion model (Krishnan, 2001) and are dependent on the measured overall cylinder pressure. On the other hand, the predicted heat release rate is profoundly influenced by local (packet) reaction rates. Therefore, experimental and predicted heat release rates may not match due to fundamental differences between the combustion models used in the simulation and the experimental heat release analysis (Krishnan, 2005). This can be due to the difference in treatment (between the simulation and the single-zone model) accorded to the estimation of temperature and equivalence ratio distribution in different zones Hountalas et al. (2004).

The reaction rate during the premixed combustion phase is governed by Equation (3.30). It is assumed valid until the amount of fuel evaporated at the end of the ignition delay period has been consumed. According to Dec's model (1997), both premixed and mixing-controlled combustion regions occur simultaneously. Therefore, in this study, the

114

mixing-controlled phase starts in simultaneity with the premixed phase. Diesel mass evaporated after ignition delay mixes with air and burns during the mixing control phase. It should be mentioned here that the combustion model used in this study is referred from Jung (2001). Jung considered the mixing controlled phase to start after the premixed phase (when the entire initial fuel vapor has been consumed). The combustion rate of mixing controlled phase is determined using equation (3.31).
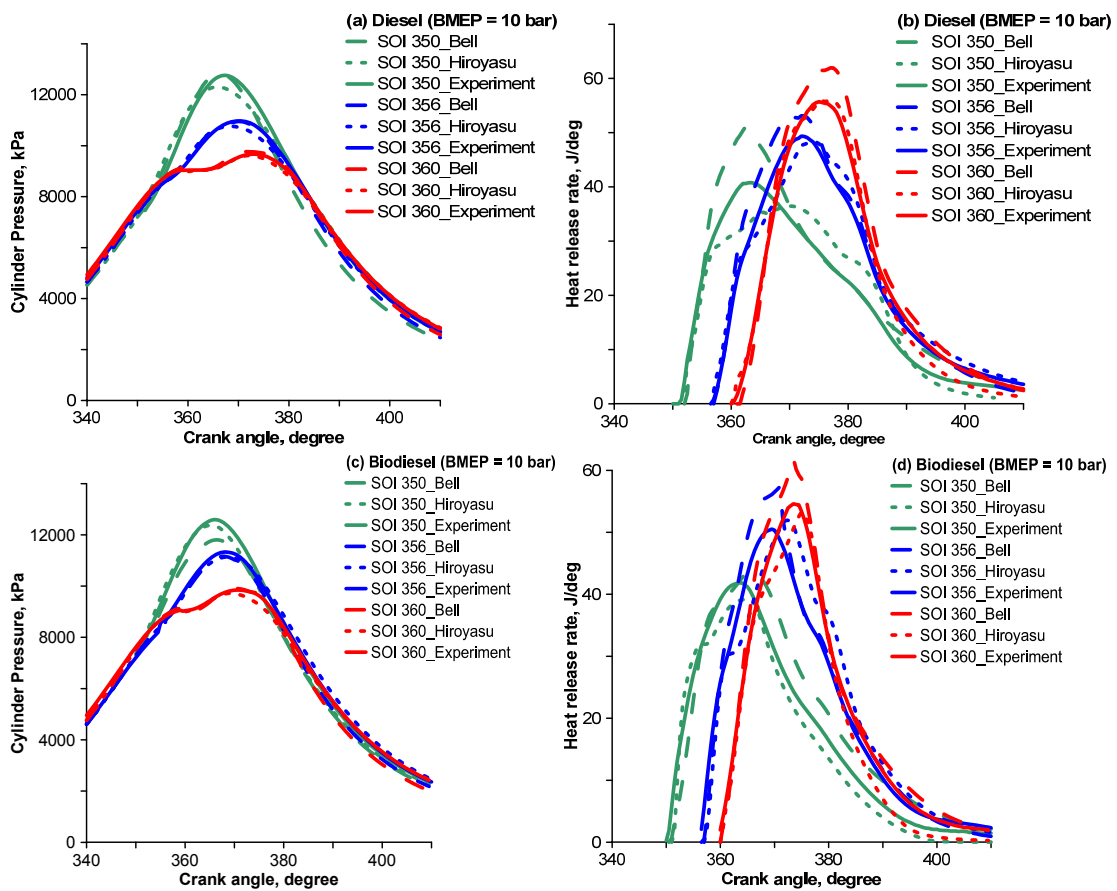
Figure 3.14   Comparison of experimental and predicted cylinder pressures (a, c) and heat release rates (b, d) for diesel and biodiesel at full load condition (BMEP = 10 bar).

115
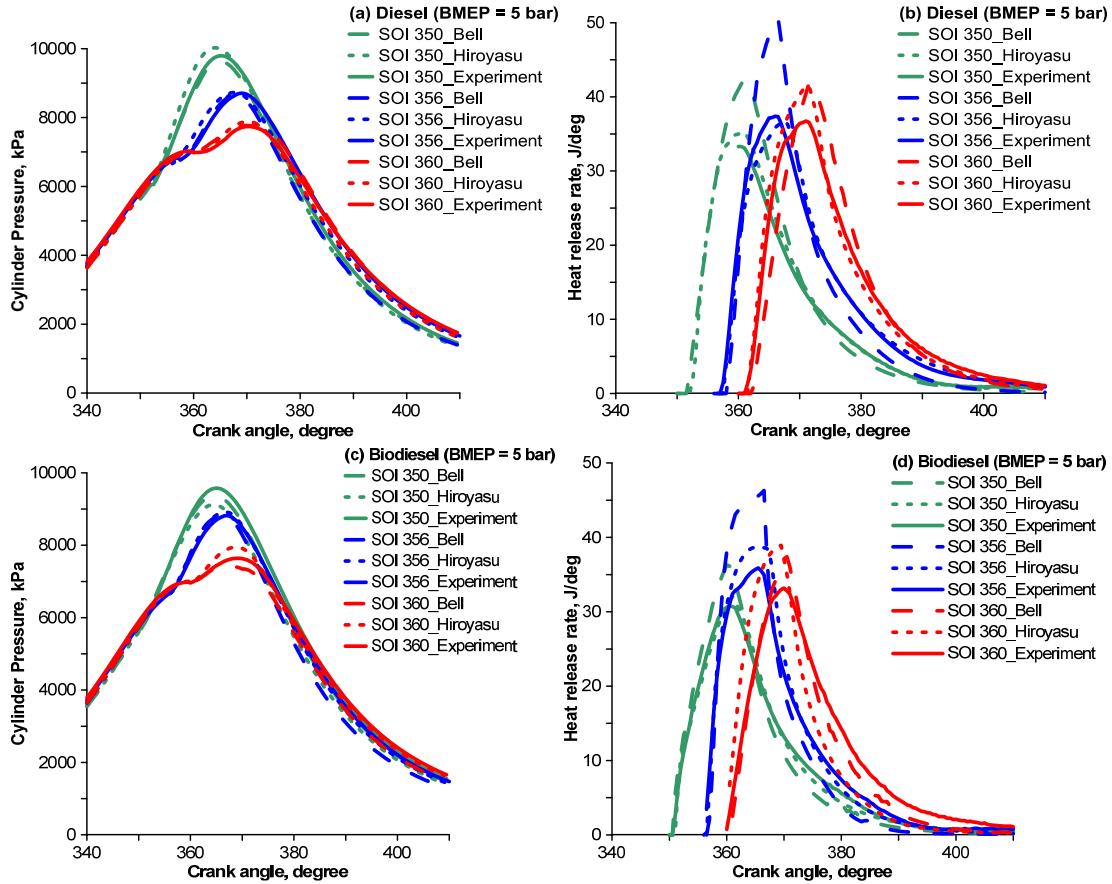
Figure 3.15   Comparison of experimental and predicted cylinder pressures (a, c) and
heat release rates (b, d) for diesel and biodiesel at engine half load
condition (BMEP = 5 bar).

The combustion model parameters, B_1 and B_2 are calibrated to match the

calculated pressure at an operating point of 1800 rpm and 10 bar load. The injection

timing of 0° BTDC is chosen as the representative timing for performing all the

sensitivity studies presented later. The B_1 and B_2 values of 1.5 x 10^6 and 800000 were

selected respectively for diesel fuel. These two values were used for different loads and

SOI. Figure 3.14 and Figure 3.15 compare experimental heat release rates and cylinder

pressures to model predictions (named Hiroyasu and Bell) over full and half loads and

SOIs. Both cylinder pressures and heat release rate predictions compare favorably to the

corresponding experimental values, with only the heat release duration being slightly

over-predicted. For all the operating conditions, the pressures, in general, were predicted satisfactorily.

The experimental and predicted cumulative gross heat release for all injection timings is illustrated in Figure 3.16 and Figure 3.17. The cumulative gross heat release allows us to understand the total combustion heat release for a given injection timing in a better way than does the apparent heat release rate. Evidently, the experimental and predicted cumulative heat release histories and the final values both match quite well for the SOIs of 0° BTDC and 10° BTDC. For 4° BTDC, the over-prediction of heat release rates led to very poor prediction of both the cumulative heat release history as well as the final heat release value.

The differences in the heat release rate and cumulative heat release prediction based on Hiroyasu and Bell entrainment models can be noticed. To explain the difference in the predictions between the two models, it is important to look into the predictions of cumulative air entrained and its effect on the cumulative fuel evaporated mass, equivalence ratio, and temperature of the first injected packet (XPAC = 1, YPAC = 1). It can be seen in Figure 3.19 that the modified Hiroyasu model predicts more air entrainment than the modified Bell model that affects the corresponding equivalence ratio of the packet. More the air entrained into the packet, the leaner is the packet. In addition, as more air from the unburned zone entrains into the packet, the temperature of the packet reduces and therefore evaporation rate of diesel reduces. It can be seen in Figure 3.18 that the diesel evaporation rate corresponding to the modified Hiroyasu model is lower than the modified Bell model. This rapid increase in evaporation rate is reflected in the peak heat release rate of Figure 3.14 and Figure 3.15 where heat release rate using modified Bell model is higher in most of the cases.

117
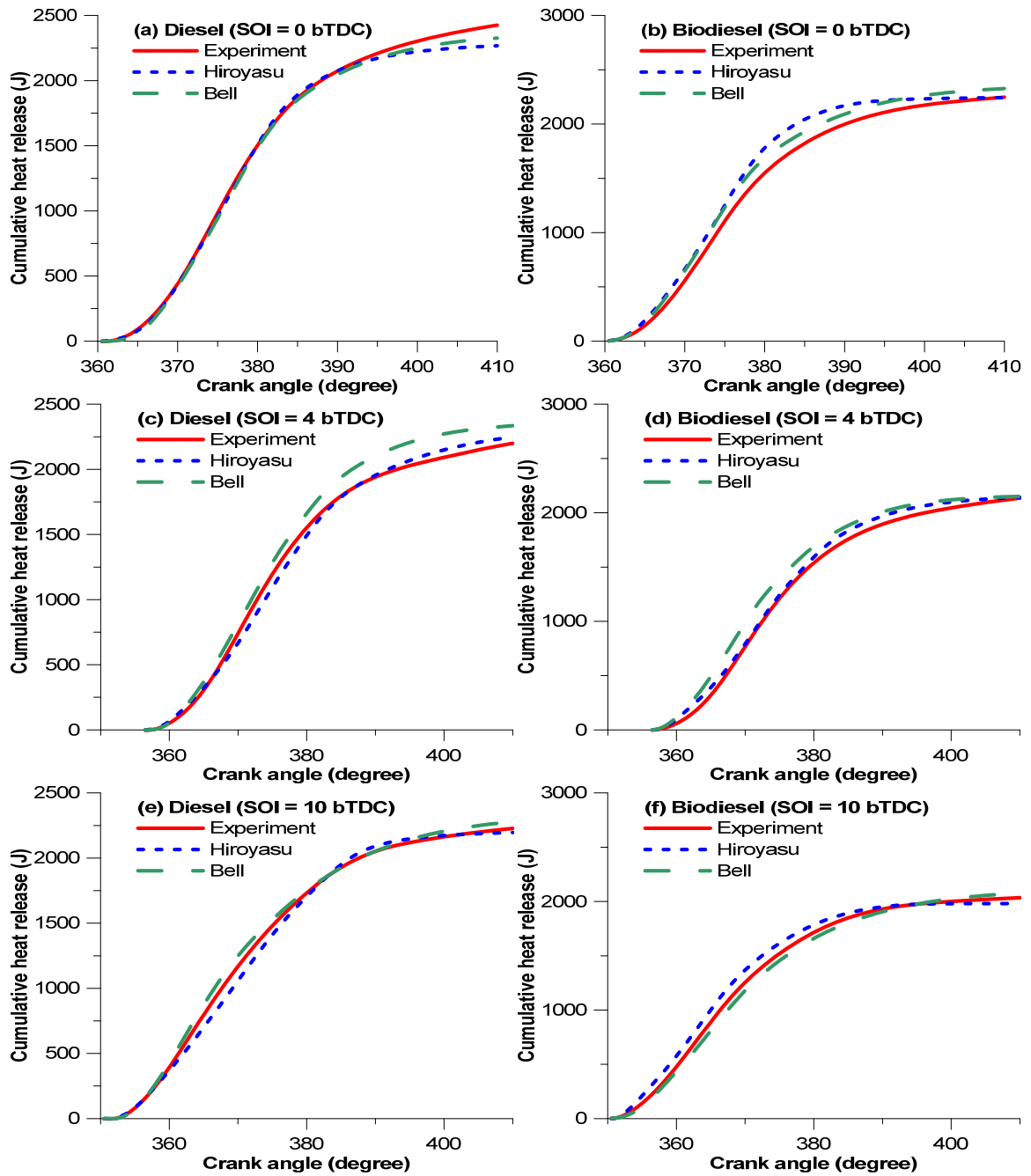
Figure 3.16   Comparison of experimental (HRcum-expt) and predicted (HRcum-Hiroyasu and HRcum-Bell) cumulative gross heat release with baseline model constants at full load condition (BMEP = 10 bar).
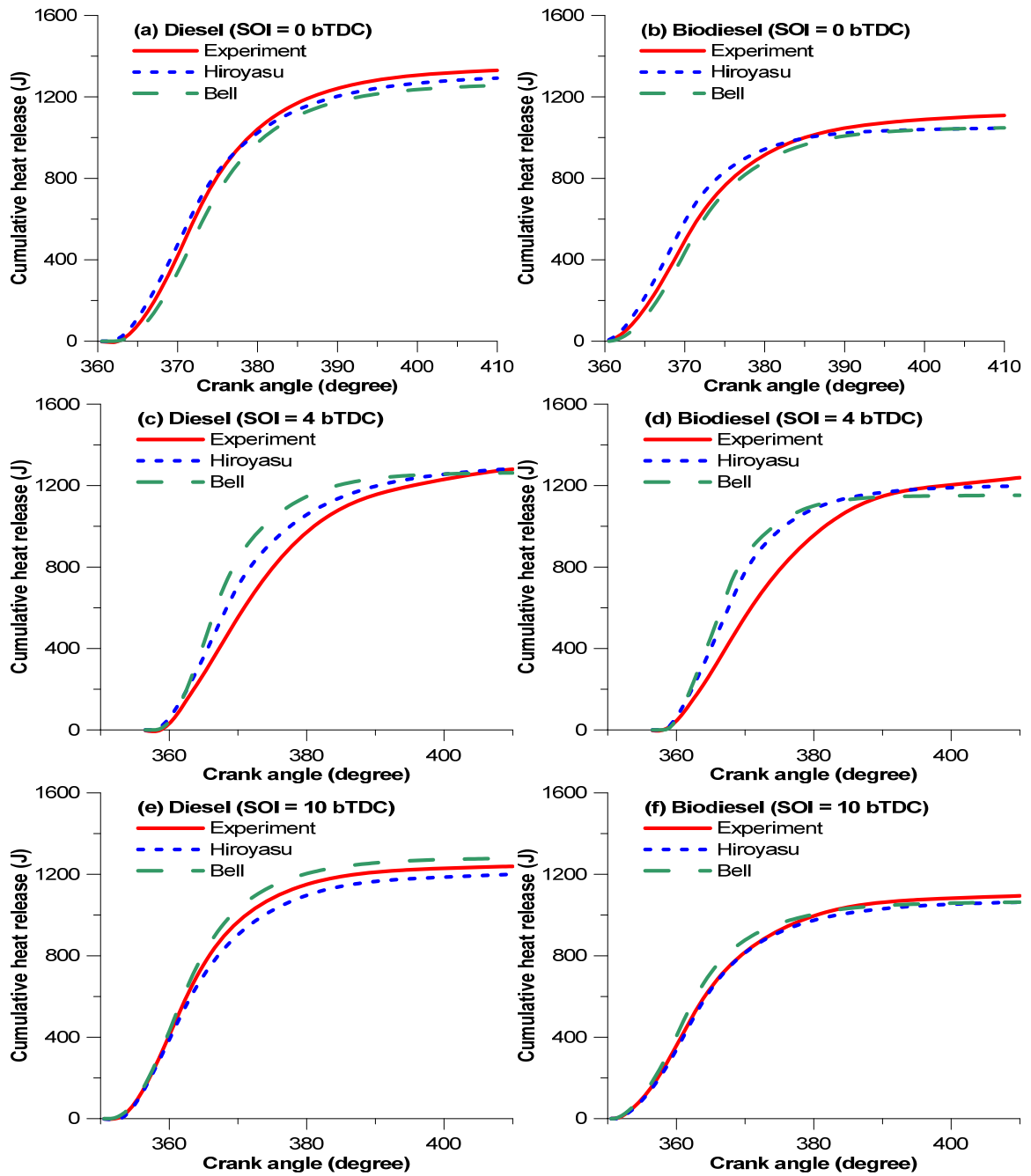
Figure 3.17   Comparison of experimental (HRcum-expt) and predicted (HRcum-Hiroyasu and HRcum-Bell) cumulative gross heat release with baseline model constants at half load condition (BMEP = 5 bar).
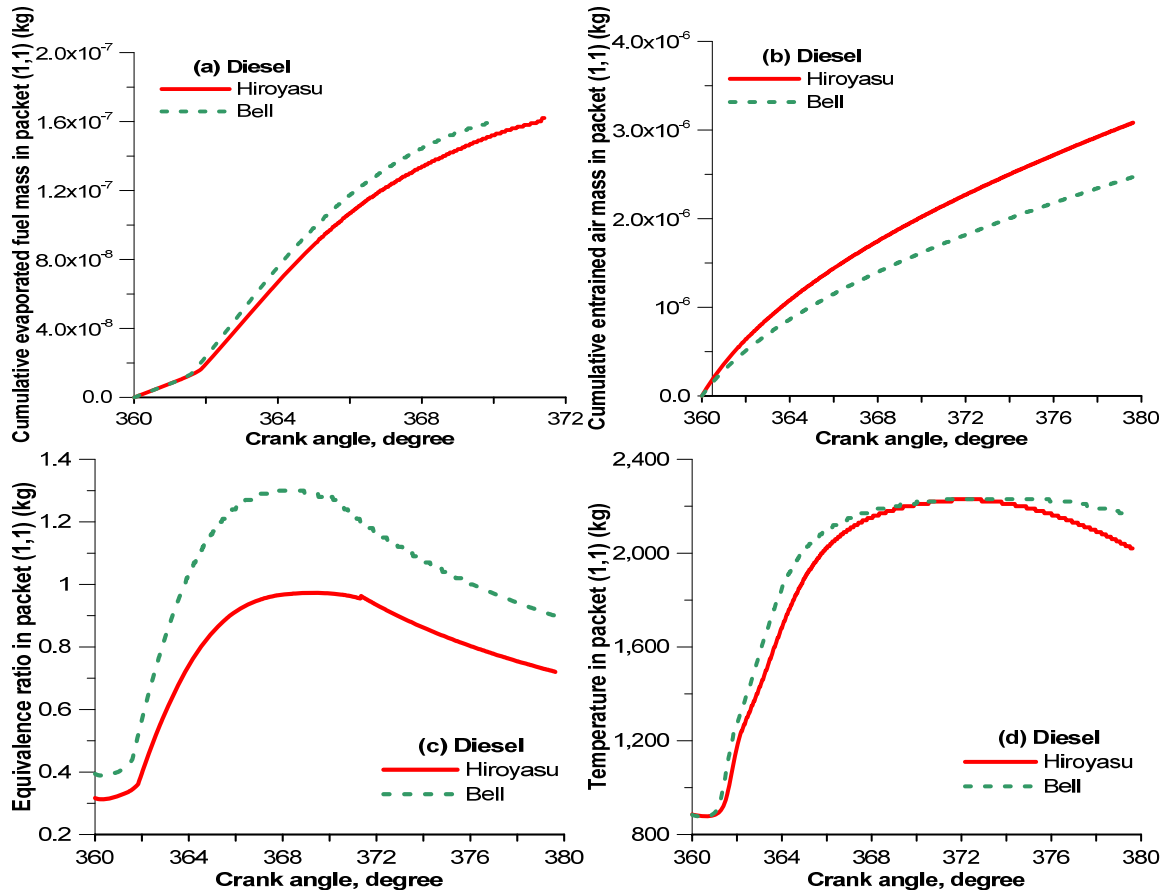
Figure 3.18   Cumulative fuel evaporated mass (a), cumulative air entrained (b),
equivalence ratio (c) and temperature (d) of the first injected packet (XPAC
= 1, YPAC = 1)
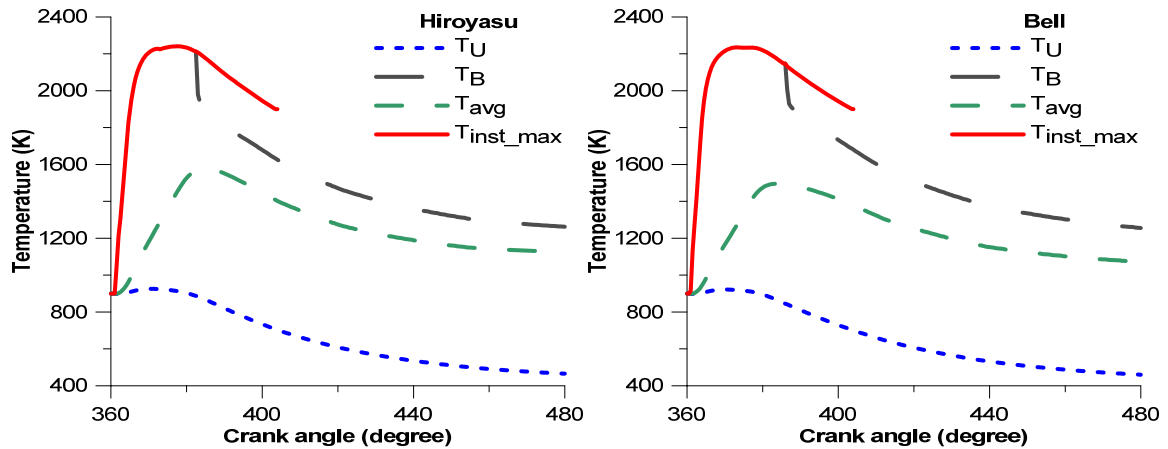
Figure 3.19   Temperature histories for full load condition for SOI at 0° BTDC (unburned zone temperature (T_U), burned zone temperature (T_B), average temperature (T_{avg}), maximum instantaneous packet temperature (T_{inst_max})

It is appropriate to examine the model predictions in greater detail. Zone-wise temperatures histories are illustrated in Figure 3.19. In this figure, the subscripts u, b, avg, and inst_max refer to the unburned zone, burned zones, average and maximum instantaneous respectively. The variables T_{avg} and $T_{inst\text{-}max}$ indicate the mass-averaged cylinder temperature and the instantaneous maximum temperature among all zones inside the cylinder, respectively. Burned zone starts forming at the moment when the first packet is "dumped". Packets are dumped when combustion of the evaporated diesel is 99% complete or if the packet temperature decreases below 1900K. It is evident that the peak temperatures of the packet zone and burned zone were approximately 2250 K. When combustion started, T_{avg} was equal to T_u but as it progressed, T_{avg} increased until dumping of the packet into burned zone begins. Towards the end of combustion T_{avg} equal to T_b since most of the cylinder contents had burned. The unburned zone temperature is quite close to simple compression. The temperature of unburned zone therefore reaches its peak close to TDC and drops as the piston moves down. The average temperature is average temperature of burned zone and unburned zone. As can

be seen in Figure 3.19, the average temperature is much lower than burned zone temperature. This explains why the zero-dimensional or single-zone model is not suitable for emission predictions.

Figure 3.20 shows a comparative analysis of packets in terms of ignition delay and evaporation duration of diesel. Each of the parameters has significant influence on the combustion performance. At the beginning, when the first few packets ignite, ignition delay is close to 3 crank angle degrees but as the ignition of more packets takes place there is a sudden decrease in the ignition delay value. Similar drop in droplet evaporation time is also observed. This is due to a sudden increase in the average temperature of the cylinder. The increase in temperature leads to faster evaporation rate and thus lower ignition delay. In addition, close observation of Figure 3.20 shows that initially packets close to the edge (YPAC = 1) of the spray evaporates and ignites before packets close to the axis of injection (YPAC = 3). The reason behind this can be explained in terms of greater air entrainment in the outermost packet and hence better availability of oxygen to ignite faster. Nevertheless, later on axial packets evaporate and ignite faster than packets at the edge. This is due to the reverse impact of entrained air on temperature of packet. As more air entrains from unburned zone into the packet, the rate of increase of packet temperature slows down due to lower unburned zone temperature and this lower temperature slows down evaporation rate and leads to increase in ignition delay. In this regard, Krishnan (2005) suggested that increasing the mixture entrainment in packets leads to two opposite possibilities: (a) a decrease in packet heat release due to "excessive leaning" of packets by the entrained mixture to equivalence ratios well below stoichiometric, or (b) an increase in packet heat release if the entrained mixture results in driving packet equivalence ratios from very rich values ($\varphi \gg 1$) toward stoichiometric

122

conditions. These observations can also be inferred from Figure 3.21. Figure 3.21 shows the variation of equivalence ratio and droplet sauter mean diameter among packets. The farther the packet is from the axis of injection, the faster the entrainment rate; also slower evaporation causes leaner mixture of air and fuel and therefore lesser is the equivalence ratio. Similarly, droplet diameter reduces at slower rate and consequently complete evaporation time increases for packets away from injection axis.

Figure 3.22 shows the wide variation in the dumping time of packets that is a very important parameter as it shows the variation in combustion duration. The packets that are injected early are dumped in earlier than the packets injected later. This means that early injected packets burn faster after ignition. However, the later the packets are injected; the longer the combustion duration. This may be due to a reduction in the average temperature and excess leaning of the packet. It can also be observed that the dump time increases for the packets closer to the injection axis. The simulated peak packet temperature trends are also shown in Figure 3.22, which shows the number of packets that fall within a given peak packet temperature range. Figure 3.22 also presents the peak packet temperatures and the corresponding normalized packet combustion durations (representing the in-cylinder residence times of hot regions) for all packets. In this figure, the actual combustion duration (from the SOC until the EOC) for each ignited packet was normalized with respect to the overall combustion duration to obtain the normalized packet combustion duration.
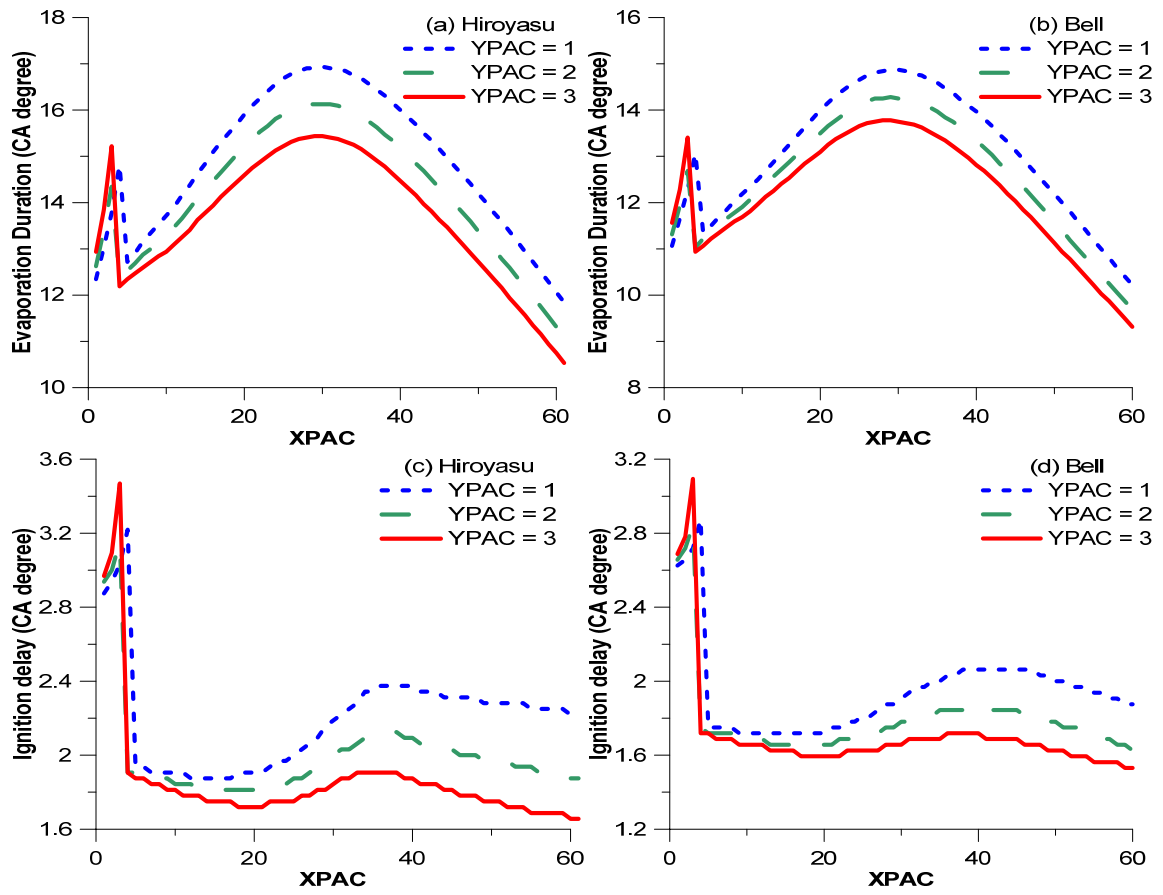
Figure 3.20   Packet wise variation of evaporation time (a, b) and Ignition delay (c, d)
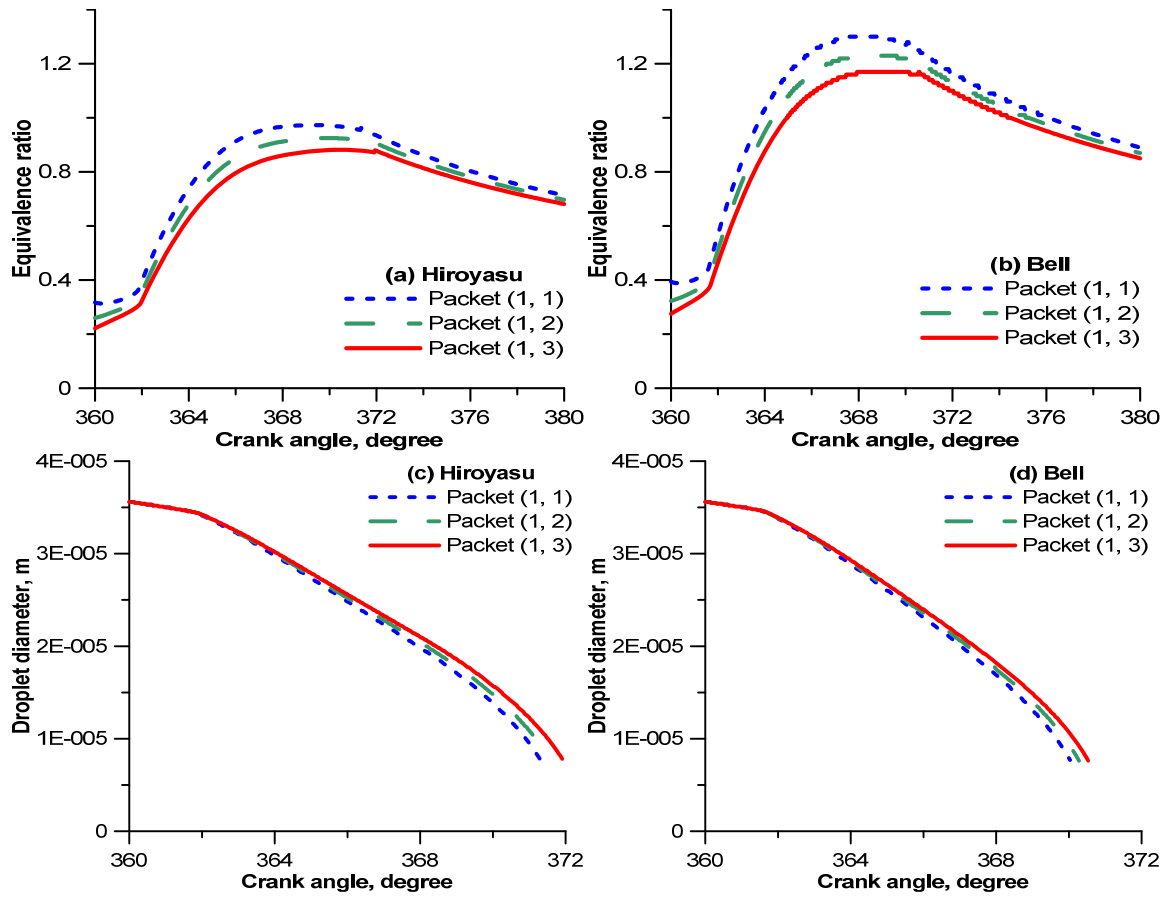
Figure 3.21 Packet wise variation in equivalence ratio (a, b) and droplet diameter (c, d).
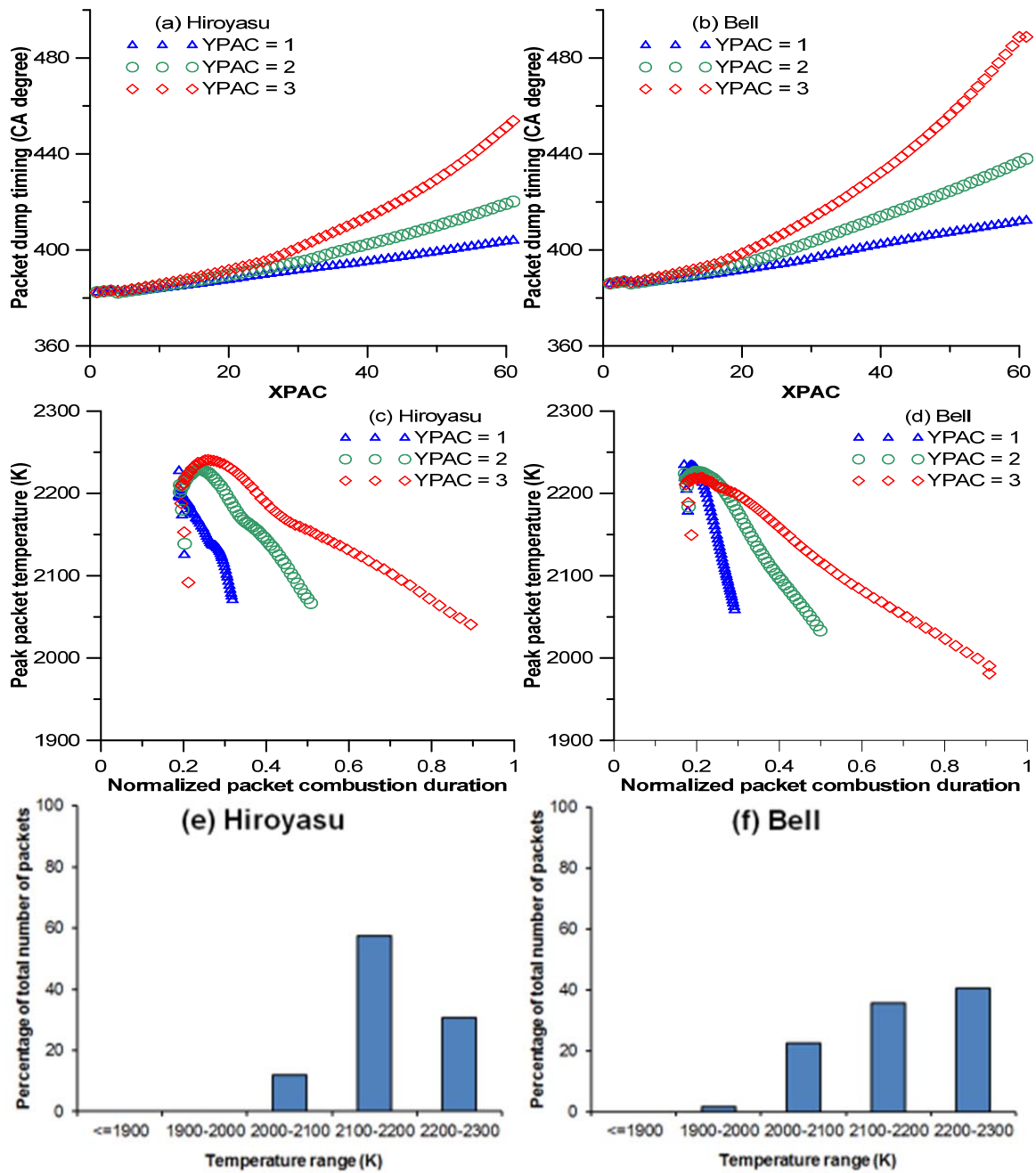
Figure 3.22   Packet wise variation in packet dump timing (a, b), peak packet
temperature relative to normalized packet combustion duration (c, d) and
percentage of number of packets in different temperature zones (e, f).

126

Sensitivity Analyses

For the sensitivity analysis studies in this section, the model parameters given in Table 3.6 were used. As mentioned before, the injection timing of 0° BTDC was chosen as the representative timing for performing all the sensitivity studies presented here. The various parameters that are investigated in the sensitivity analyses include Computational time step (DCAD), entrainment constant (K_{ent}), pre-exponential factor in the heat release rate model (B_1), exponential factor in the heat release rate model (B_2), nozzle discharge constant (C_D), total number of packets in axial direction, I_{tot}, and total number of packets in radial direction, J_{tot}.

The first parameter to be examined is the computational time step (DCAD) used after BOI. This study allows us to ascertain the minimum computational time step required to obtain time step-independent results. Later studies focus on important packet and combustion parameters as regards their effects on heat release and pressure predictions.

To compare the effects of DCAD alone, I_{tot} was fixed at 61 for all DCAD values. The predicted pressures did not change much when DCAD was increased from 0.03125 to 0.125 degrees. The heat release duration, however, showed a modest decrease when DCAD was increased from 0.0625 to 0.125 degrees. Nevertheless, both predicted heat release rates and onset of ignition for DCAD values of 0.03125 and 0.0625 degrees were virtually identical, providing reason to believe that a minimum DCAD value of 0.0625 degrees is required for obtaining time step-independent results. Truncation error starts increasing up as the time step decreases because the values of computational variables become too small. Moreover decreasing DCAD consumes increasing time in

127

computation. To maintain uniformity among all the results presented in this chapter, the computational time step after BOI was fixed at 0.03125 degrees.

After ascertaining the appropriate DCAD, sensitivity analysis of SAI model parameter, A_Q, is presented in Figure 3.23. Complete set of modified SAI model parameter is shown in Table 2 (Appendix). A_Q which determines the initian reaction in autoignition mechanism impacts the ignition delay value as discussed in the chapter 2. Although it does not show impact on largely on the overall heat release and cylinder pressure, it does show the impact on premixed heat release. Higher the A_Q value, larger is the ignition delay value and hence better fuel evaporation and air entrainment before ignition leads to more premixed heat release.

Later on, the effect of the mixture entrainment constant, K_{ent}, was examined. In addition to the baseline value of 2.5, one higher value (3.0) and one lower value (2.0) were tested. Figure 3.24 shows that increasing $K_{Hiroyasu}$ led to the higher peak pressures and vice versa. Similar effects were observed in the case of heat release rates. Both initial and peak heat release rates were increased as K_{ent} was increased from 2.0 to 3.0. The reason behind this can be the better air entrainment and thus better air and fuel mixing.
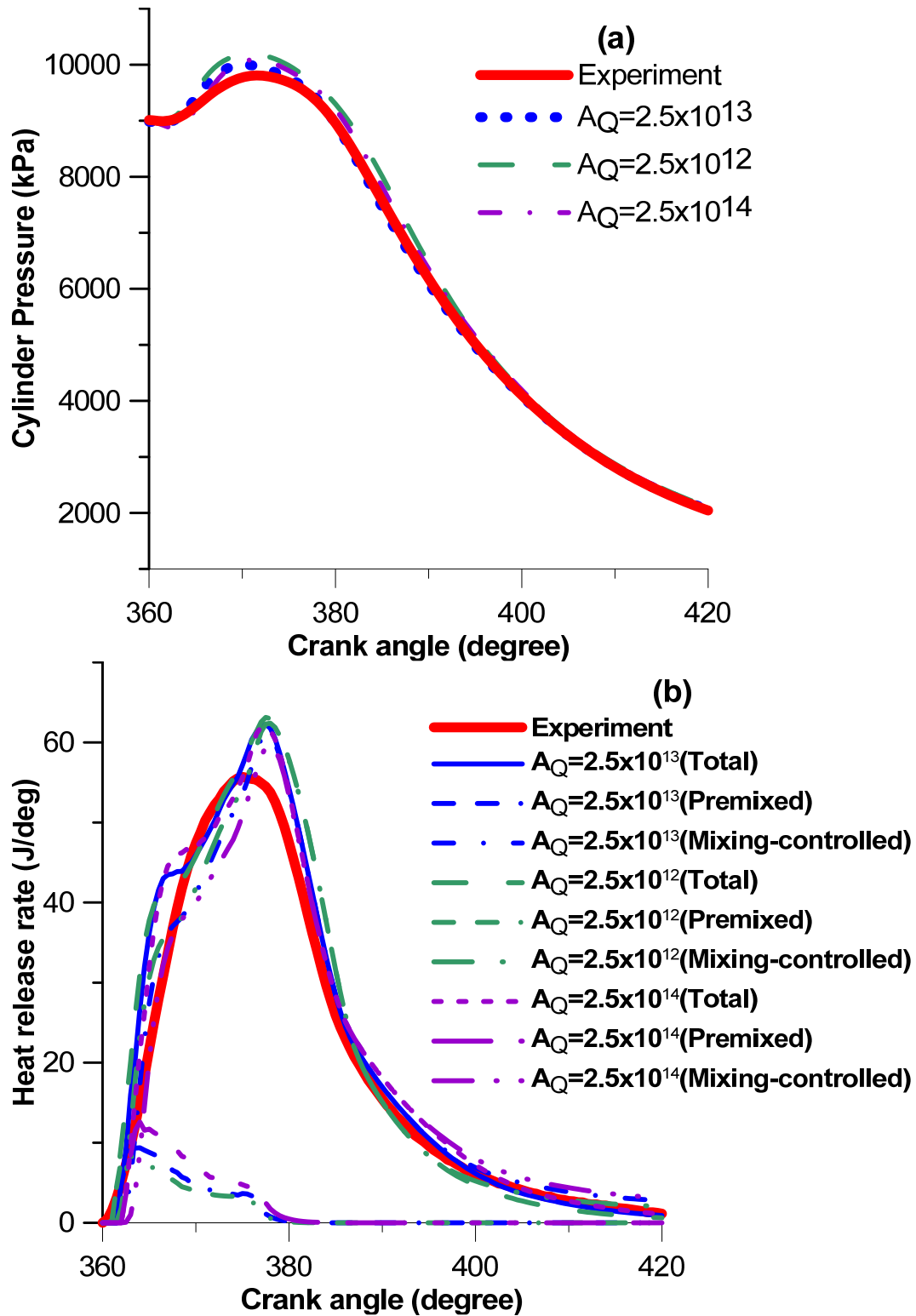
Figure 3.23   Sensitivity of predicted pressures (a) and heat release rates (b) to model parameters A_Q

Figure 3.25 shows the effect of model constant for premixed heat release rate model, B_1 on predicted pressure and heat release rates. Cylinder pressure increased on increasing B_1. B_1 does not show profound effect on the peak heat release rate and later part of heat release; however, it does have profound impact on the premixed phase of heat release. Since the evaporated diesel mass at the onset of ignition is a very small fraction of the total injected fuel mass, mass of fuel available for premixed burn is small and therefore B_1 does not have much impact on the overall heat release.

Figure 3.26 shows the impact of increasing model constant for mixing controlled heat release rate, B_2 on pressure and heat release. B_2 shows large impact on mixing control part of heat release. Peak cylinder pressure reduces as B_2 is decreased. Since major fraction of diesel evaporates after ignition, mixing control phase dictates the overall combustion phase. Hence changing B_2 will have a huge impact on the prediction of the entire combustion process.

The next important parameter used for sensitivity analysis was the coefficient of nozzle discharge, C_D. Coefficient of nozzle discharge plays a very important role in shaping the whole combustion process. C_D mainly influences the rate of injection into the cylinder that has major impact on the determination of the sauter mean diameter. Since the Hiroyasu model of entrainment is based on the conservation of spray momentum, C_D, which plays a very important role in the momentum of the injected spray, influences the rate of air entrainment too. As evident from Figure 3.27, reducing the C_D led to a decrease in cylinder pressure. As C_D is increased, peak heat release rate increased and the combustion duration reduced. On further analysis, it was found that increasing C_D decreases the liquid droplet SMD. In addition, higher value of C_D causes

higher momentum of injected fuel momentum and therefore the entrainment of air also improves in the packet zone.

Figure 3.24   Sensitivity of predicted pressures (a) and heat release rates (b) to model
parameters entrainment constant (K_{ent})
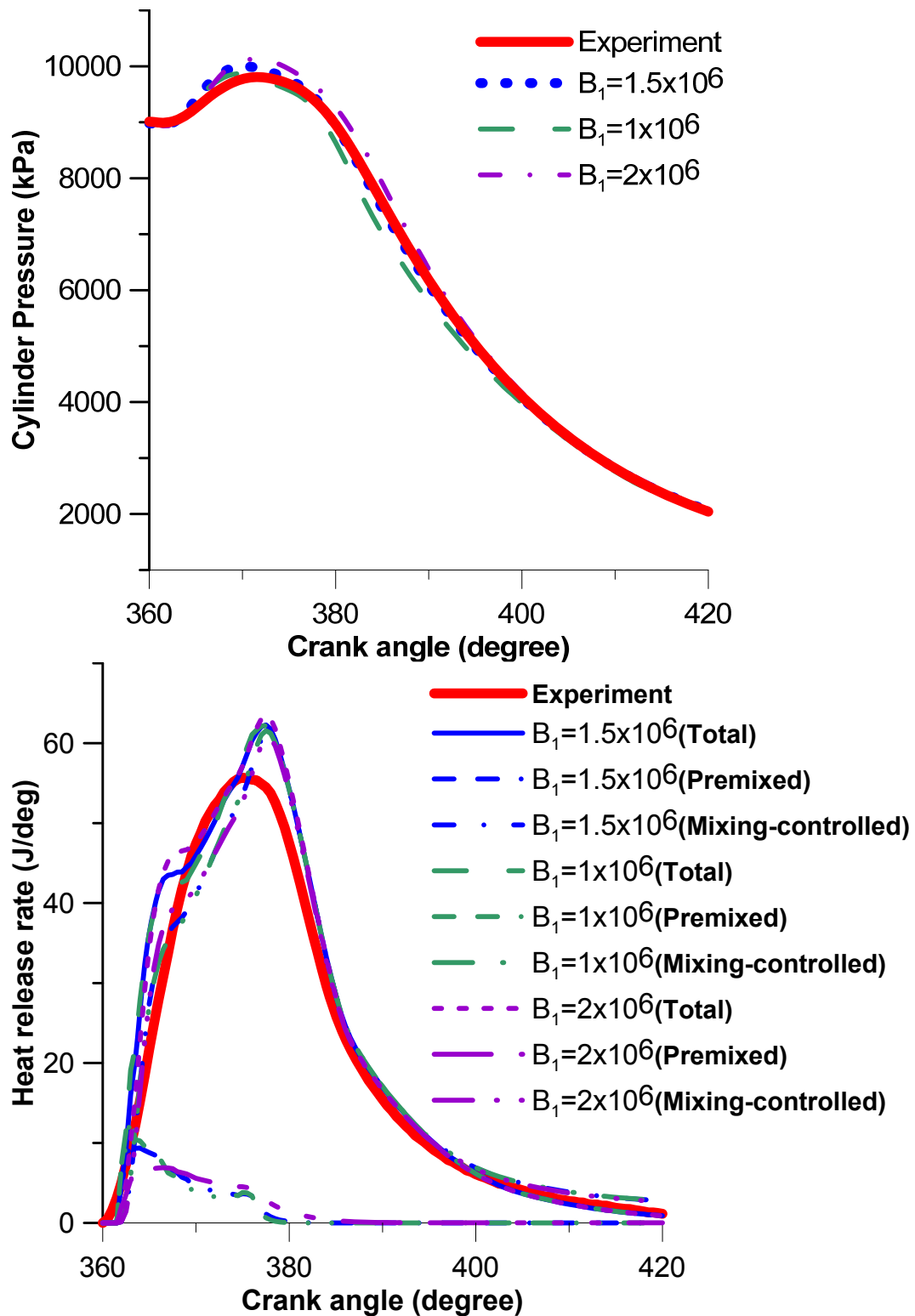
Figure 3.25   Sensitivity of predicted pressures (a) and heat release (b) rates to model
parameters pre-exponential factor in heat release rate (B_1)

133
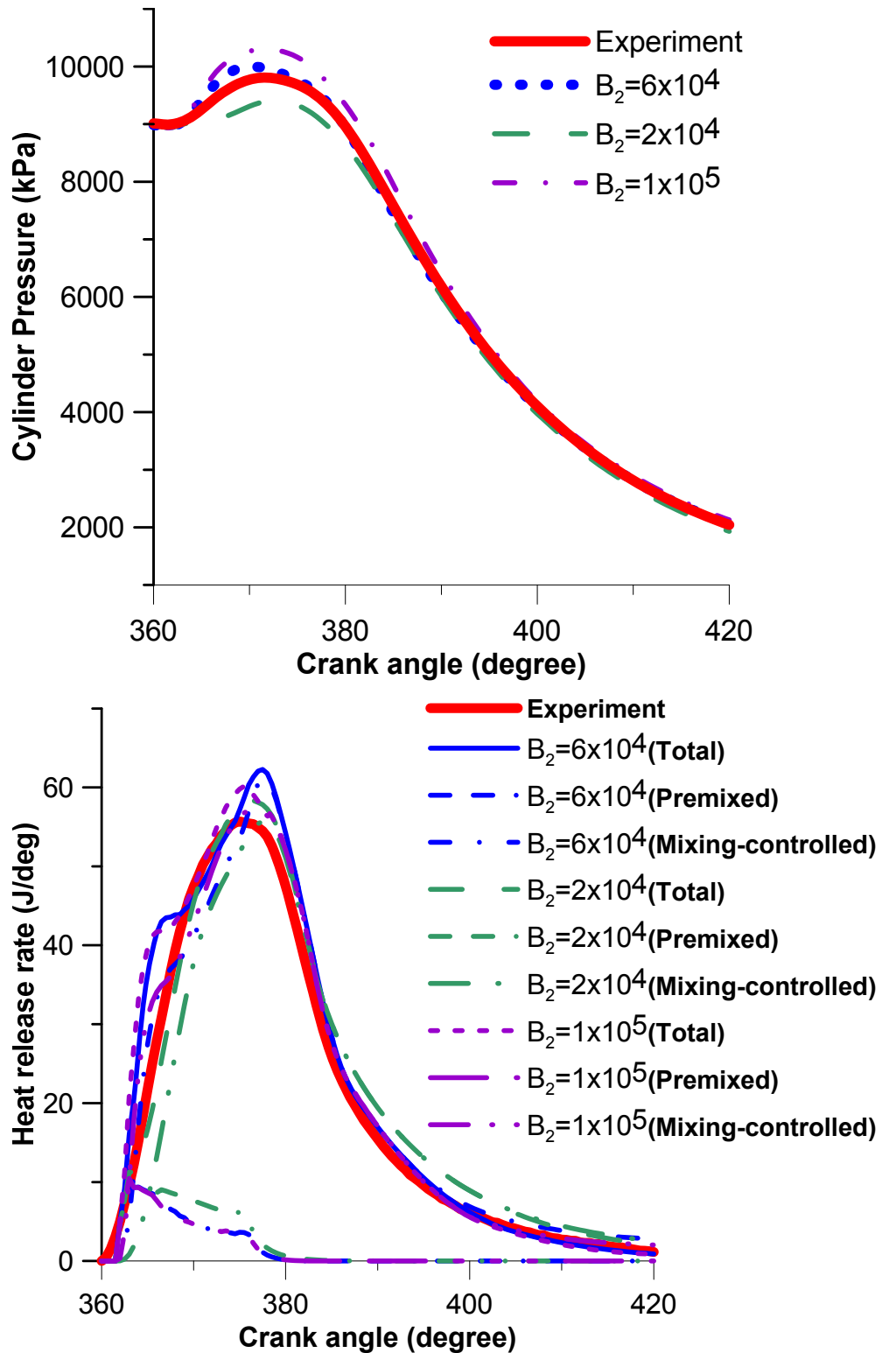
Figure 3.26   Sensitivity of predicted pressures (a) and heat release rates (b) to model
parameters exponential factor (B_2)
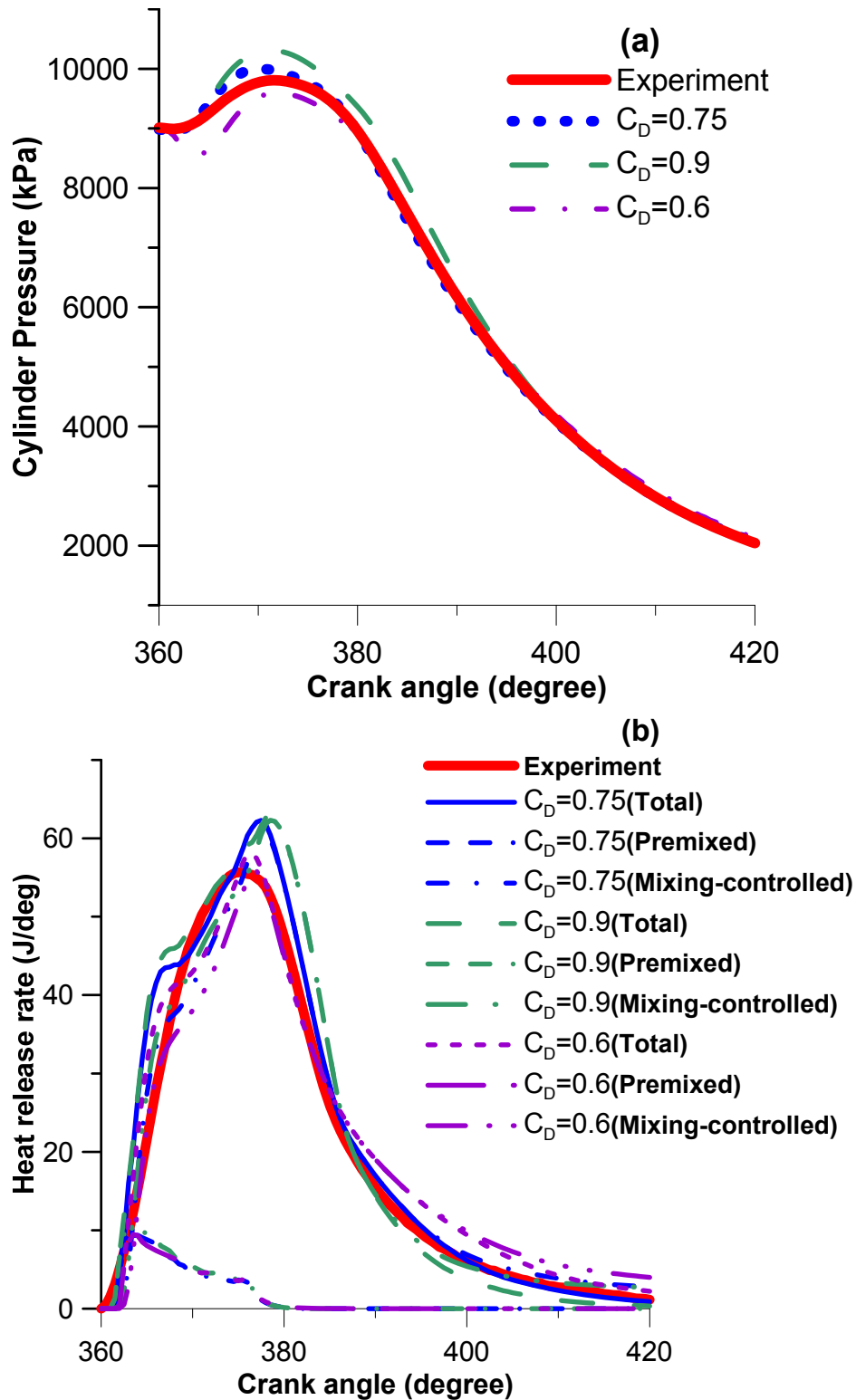
Figure 3.27   Sensitivity of predicted pressures (a) and heat release rates (b) to model
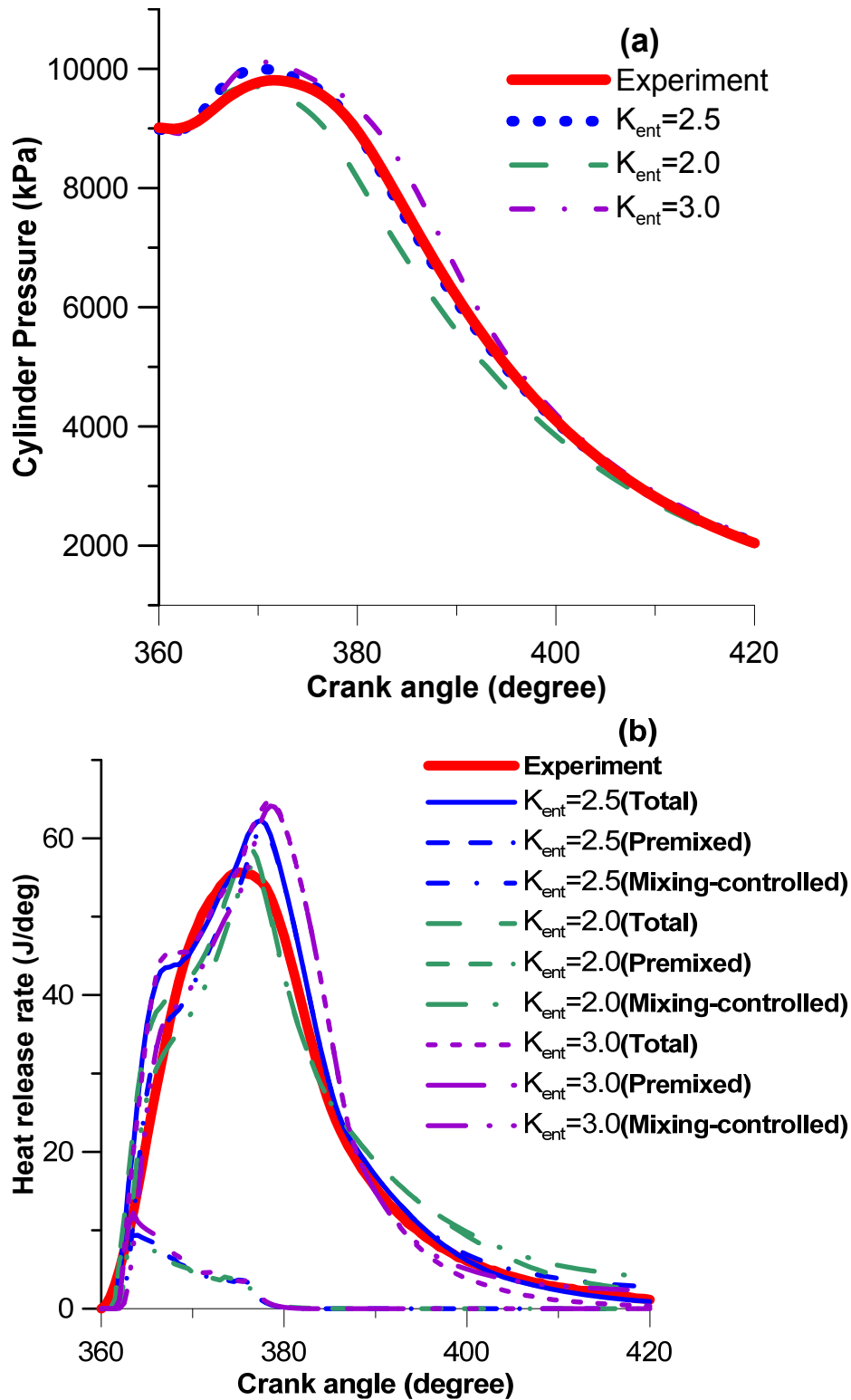   parameters nozzle discharge constant (C_D)
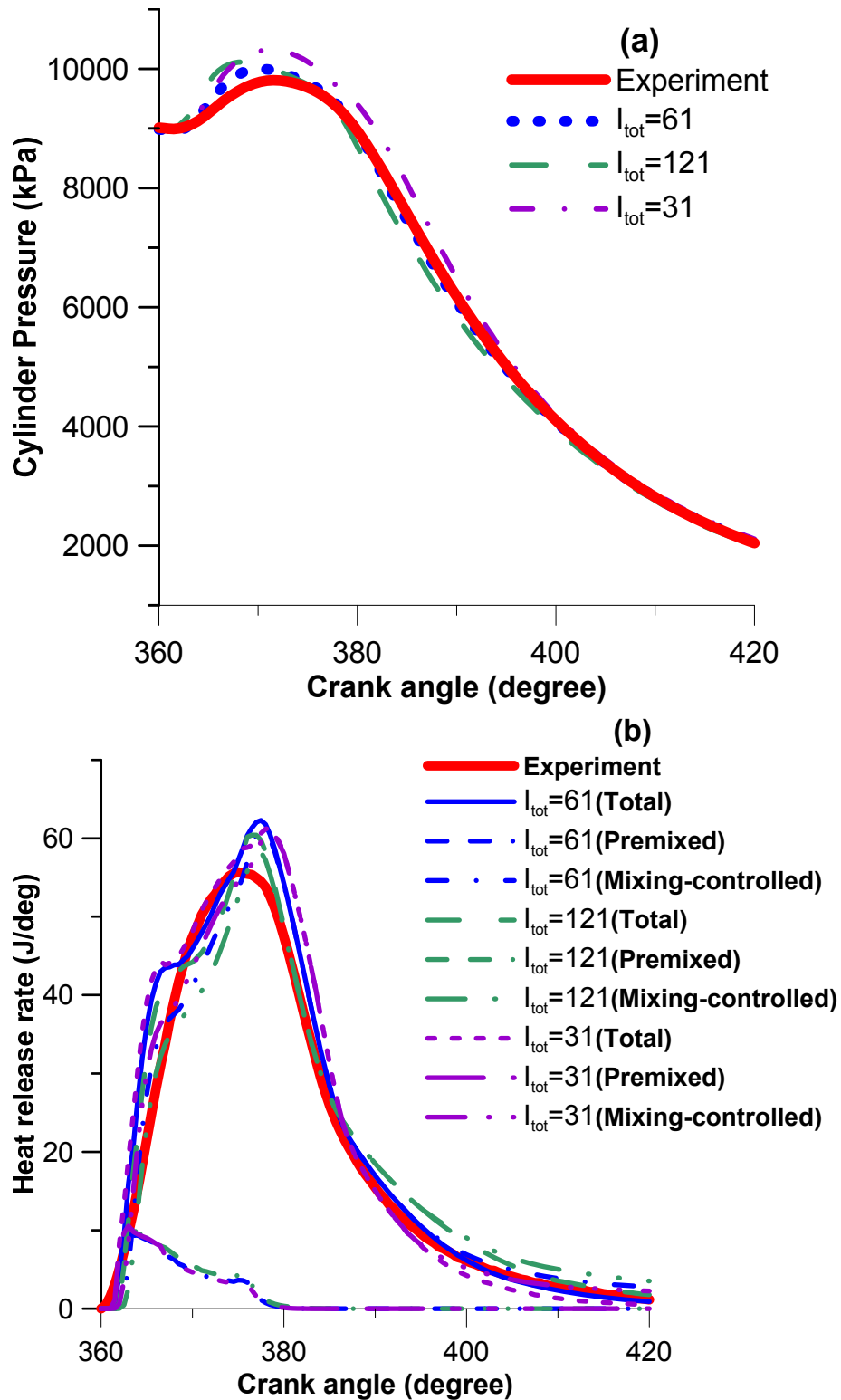
Figure 3.28   Sensitivity of predicted pressures (a) and heat release rates (b) to model
parameters I_{tot}
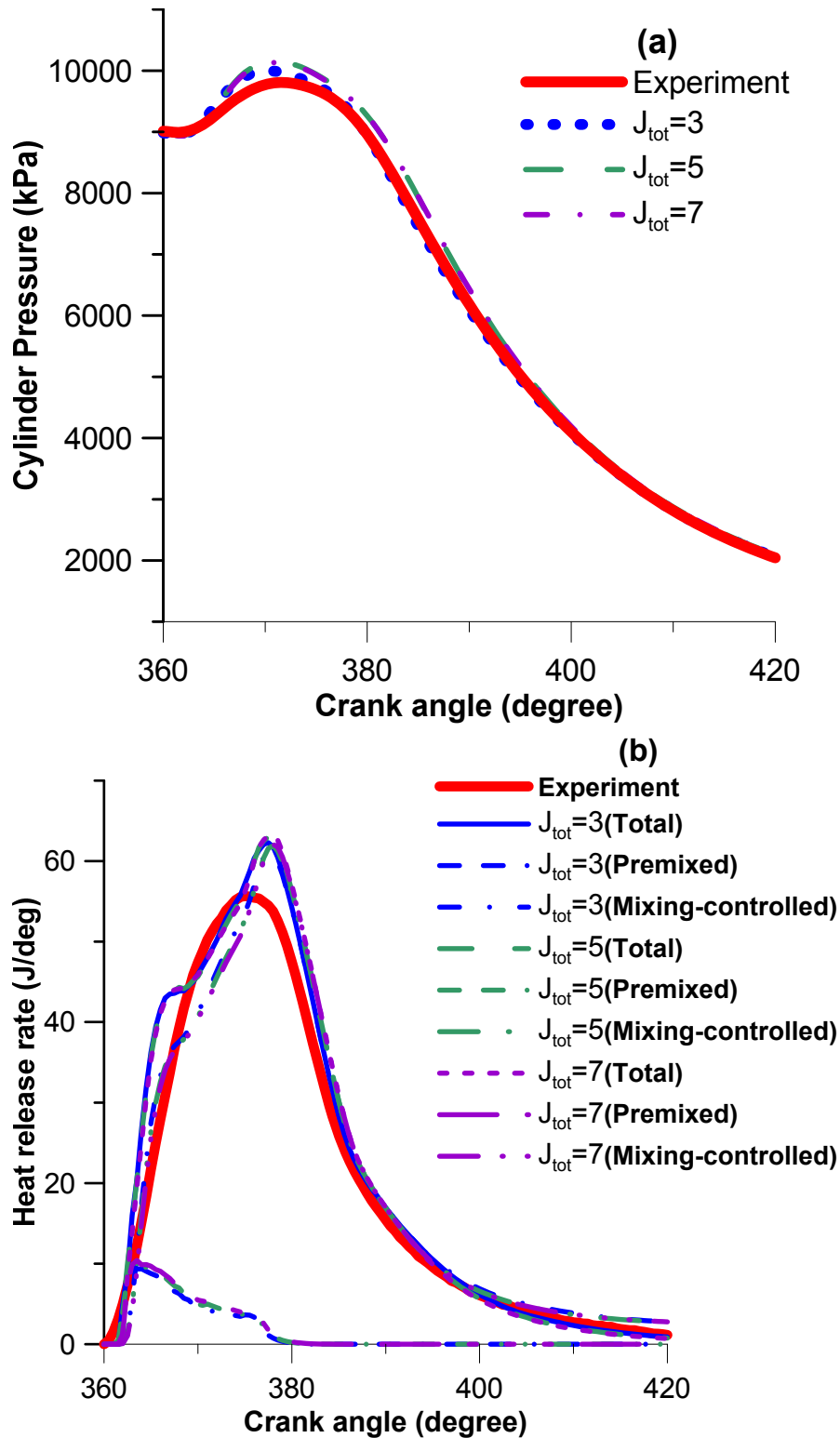
Figure 3.29   Sensitivity of predicted pressures (a) and heat release rates (b) to model
parameters J_{tot}

To investigate the behavior of the multi-zone model with respect to the zonal resolution, the number of packets in both the axial and radial directions of injection was varied. At first, the number of packets in the axial direction (I_{tot}) was changed by changing the injection time step. When I_{tot} was decreased from 121 to 31 while maintaining J_{tot} constant (equal to 3), the predicted peak pressures increased because the predicted heat release rates were also increased (Figure 3.28). Interestingly, changing I_{tot} did not appear to significantly alter the onset of ignition or the initial heat release rates immediately following ignition. Later J_{tot} was changed keeping I_{tot} constant (equal to 61). As can be seen in the Figure 3.29, there is not much difference in the pressure and heat release rates when J_{tot} is changed from 3 to 7. Thus it can be concluded that combustion performance can be predicted with a minimal number of packets ($J_{tot} = 3$) in the radial direction without losing much accuracy.

Multi-zone Model Validation

The model sensitivity and baseline calibration studies discussed above were useful in determining the model parameters to be readjusted to predict pressure and heat release histories at different injection timings and load conditions. In this study, a set of model constants for both diesel and biodiesel was determined which could be used to obtain an optimal match between experimental and predicted cylinder pressures and heat releases. For a different engine operating at different conditions, these constants may be modified, if necessary. The model constants can be readjusted to simulate diesel/biodiesel condition for different engine/conditions. The final set of model parameters that was used to obtain optimal combustion predictions in the present work is

138

given in Table 3.7. Most of the variables were retained at their baseline values shown in Table 3.6.

Simultaneous adjustment of multiple parameters was done to match the experimental and predicted heat release rates at a given injection timing and engine load. To obtain satisfactory predictions, the effects of all the parameters were observed for different injection timings and loads. Injection timing sweep at each load was performed to find how a slight change in one parameter affected the predictions over the entire experimental conditions.

Of the several parameters that were used in the model sensitivity studies, the nozzle discharge coefficient, C_D was very significant. C_D affects the sauter mean diameter of diesel/biodiesel droplets. It also determines the air entrainment into the packet calculated using momentum conservation equations. Therefore, it is very much necessary to calibrate the value of C_D which governs the entire process of combustion. A value of 0.75 was fixed for C_D to study the effect of other parameters.

To fix the number of packets, the injection time step was changed. Since injection duration for different load conditions are different, there will be different number of I_{tot} packets for each load conditions. Injection time step was fixed at 0.25 CA degrees. Therefore, for injection duration of 15 CA degree for full load conditions, the total number of packets in axial direction, I_{tot}, was 61. Since it was observed using sensitivity analysis that number of packets in radial-direction does not affect the prediction, j_{tot} was fixed at three to avoid complexity and to save computational time.

Table 3.7   Final Set of Optimized Model Constants

Model parameters	Value
Diesel injection pressure (bar)	160
Diesel injected quantity (g/min)	113
Diesel injection duration (crank angle degrees)	15
Initial charge temperature (K)	330
Entrainment constant (Bell), K_{Bell}	2.0
Entrainment constant (Hiroyasu), $K_{Hiroyasu}$	2.5
Constant in premixed phase reaction rate, B1	1.5×10^6
Constant in mixing-controlled phase reaction rate, B2 (Diesel)	200×10^3
Constant in mixing-controlled phase reaction rate, B2 (Biodiesel)	600×10^3
Nozzle discharge coefficient, C_D	0.75
Total number of I packets, I_{tot}	61
Total number of J packets, J_{tot}	3
Shell model OSAM RON90 constant, A_q (for diesel)	2.5×10^{13}
Shell model (methyl_butanoate) constant, A_q (for biodiesel)	3.0×10^{13}
Computational time step after BOI, DCAD (crank angle degrees)	0.03125

From the sensitivity analysis, it was found that constant factors B_1 and B_2 for premixed and mixing-controlled phase heat release rate are very important. Since each factor determines the rate of heat release of the corresponding phase, both the factors need to be calibrated simultaneously to match the peak heat release rates and combustion durations. Moreover, the evaporation rate influences the combustion phasing. The more rapid the evaporation rate, the greater the amount of evaporated fuel available in the premixed combustion phase. In this study, it was found that only 15-20 percent of the fuel mass was evaporated at the time of the onset of ignition. Therefore, the evaporated mass available for the premixed phase of combustion was limited compared to that

available for the mixing controlled phase. It can be observed in Figure 3.25 and Figure 3.26 that the premixed burn phase contributed only a small portion of the total heat release. Apart from this, B_1 and B_2 influence the rate of reaction during combustion, which determines the peak heat release rate and also combustion duration.

To match the cylinder pressures and the corresponding heat release rates, for both diesel and biodiesel, the value of B_1 was kept same i.e. equal to 1.5×10^6. However, for biodiesel, a higher value of B_2 than diesel was required.

Figures 3.30 and 3.31 show the comparison of the prediction and experimental heat release rates for diesel and biodiesel at three injection timings and two engine loads. Diesel or Biodiesel was injected at 0° BTDC, 4° BTDC and 10° BTDC. The load conditions selected for the study were half (BMEP = 5 bar) and full (BMEP = 10 bar) engine load. It can be seen that for a given load condition, the peak heat release rate is higher as the fuel is injected closer to top dead center. This might be due to the higher temperature at the onset of ignition.

Figure 3.32 shows predictions of cumulative air entrained and cumulative evaporated fuel mass in the first injected packet. The air entrainment rate increases as the fuel is injected closer to top dead center. However, the evaporation rate slows down as the injection timing is retarded. Air entrainment rate and evaporation rate are inter-related. The higher the evaporation rate, faster the air entrainment. Nevertheless, the rate of increase in air entrainment can play another role in influencing the evaporation rate. Better air entrainment will enable better mixing of evaporated fuel with the air by rapid removal of fuel vapor surrounding the fuel droplet. On the other hand, air from the lower temperature unburned zone will reduce the packet temperature and thus the evaporation rate will reduce. Thus, a complex interaction occurs between air entrainment and droplet

evaporation which needs a very good understanding of physics to understand the phenomena.
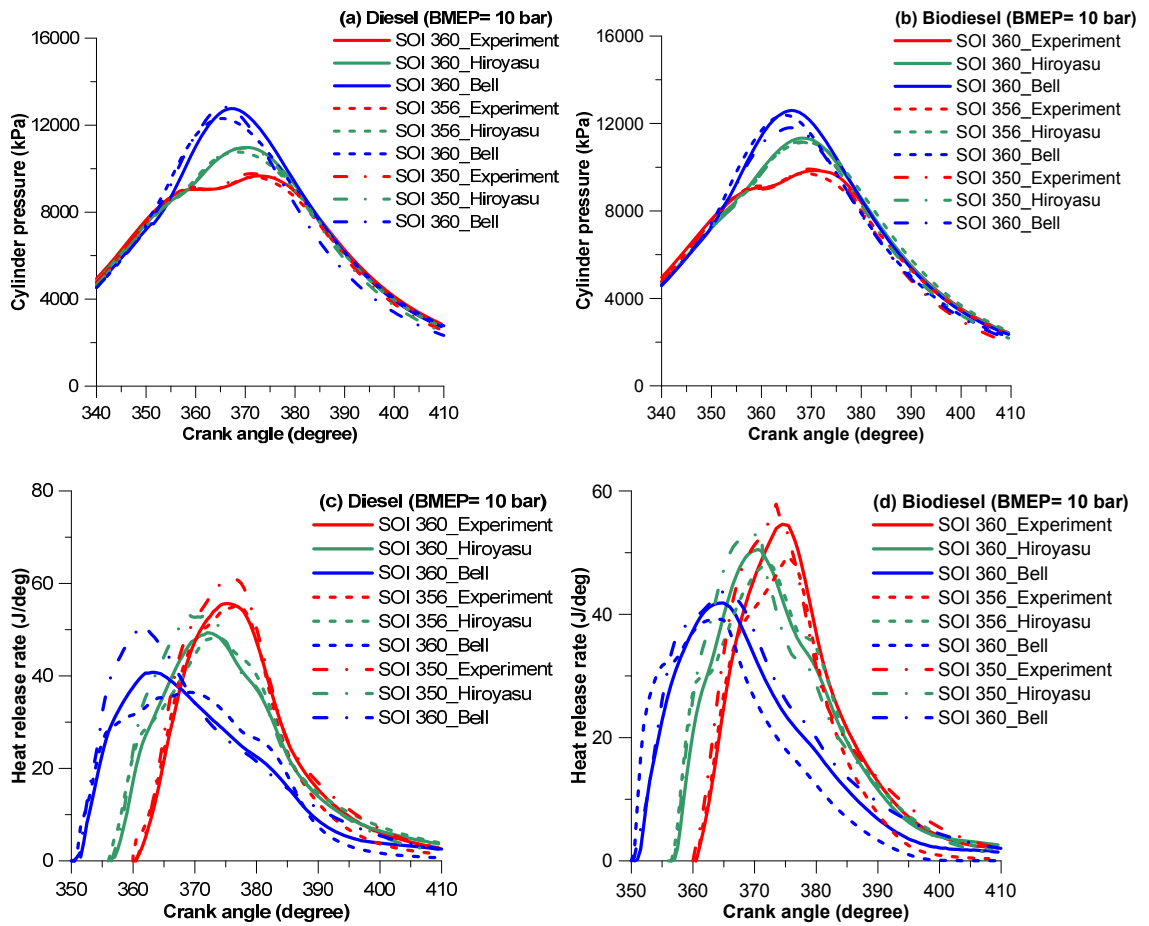
Figure 3.30   Comparison of experimental and predicted (multi-zone) cylinder pressures (a, b) and heat release rates (c, d) for diesel and bio diesel at full-load condition (BMEP = 10 bar)
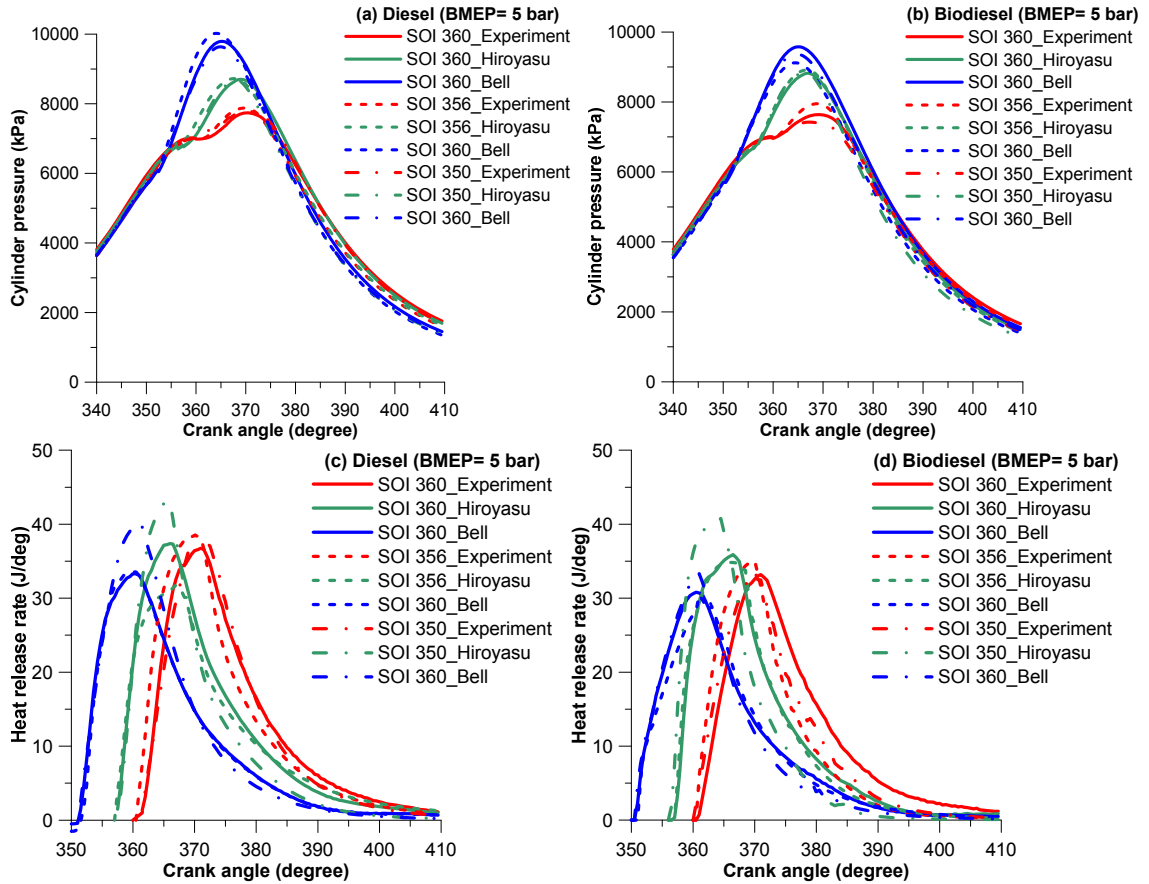
Figure 3.31   Comparison of experimental and predicted (multi-zone) cylinder pressures (a, b) and heat release rates (c, d) for diesel and biodiesel at half- load condition (BMEP = 5 bar).

Figure 3.33 shows the equivalence ratio and the temperature of the first packet. It can be seen that as the injection is advanced the equivalence ratio increases. This might be due to two facts. One, the ignition delay of first packet is less at 10° BTDC than 4° BTDC and 0° BTDC. This allows lesser air to get entrained before ignition. Other reason can be the faster evaporation rate at 10° BTDC. Maximum temperature of the first packet remains similar for all the injection timing. This can be observed in the packet wise variation of maximum temperature in figure 3.34.

Figure 3.34 clearly shows that the overall maximum temperature of the packet reduces as the injection timing is retarded from 10° BTDC to 0° BTDC. This might be

143

due to a portion of heat release occuring during compression when fuel is injected at 10°

BTDC where as in the case of the injection timing of 0° BTDC, heat release takes place

during expansion. Close observation of packet-wise variation of maximum temperature

shows that for initial few packets injected, the maximum temperature is highest at 4°

BTDC injection timing when the compression temperature is highest and the piston is in

compression stroke. Figure 3.34 also shows the packet-wise variation in ignition delay

and evaporation duration. On comparing the ignition delay of biodiesel and diesel, it is

clear that ignition delay of biodiesel is lower than that of diesel. Literature shows that the

biodiesel is composed of several esters which increases the availability of oxygenated

radical during ignition delay period. Thus increased radical formation rate for biodiesel

leads to shorter ignition delay.
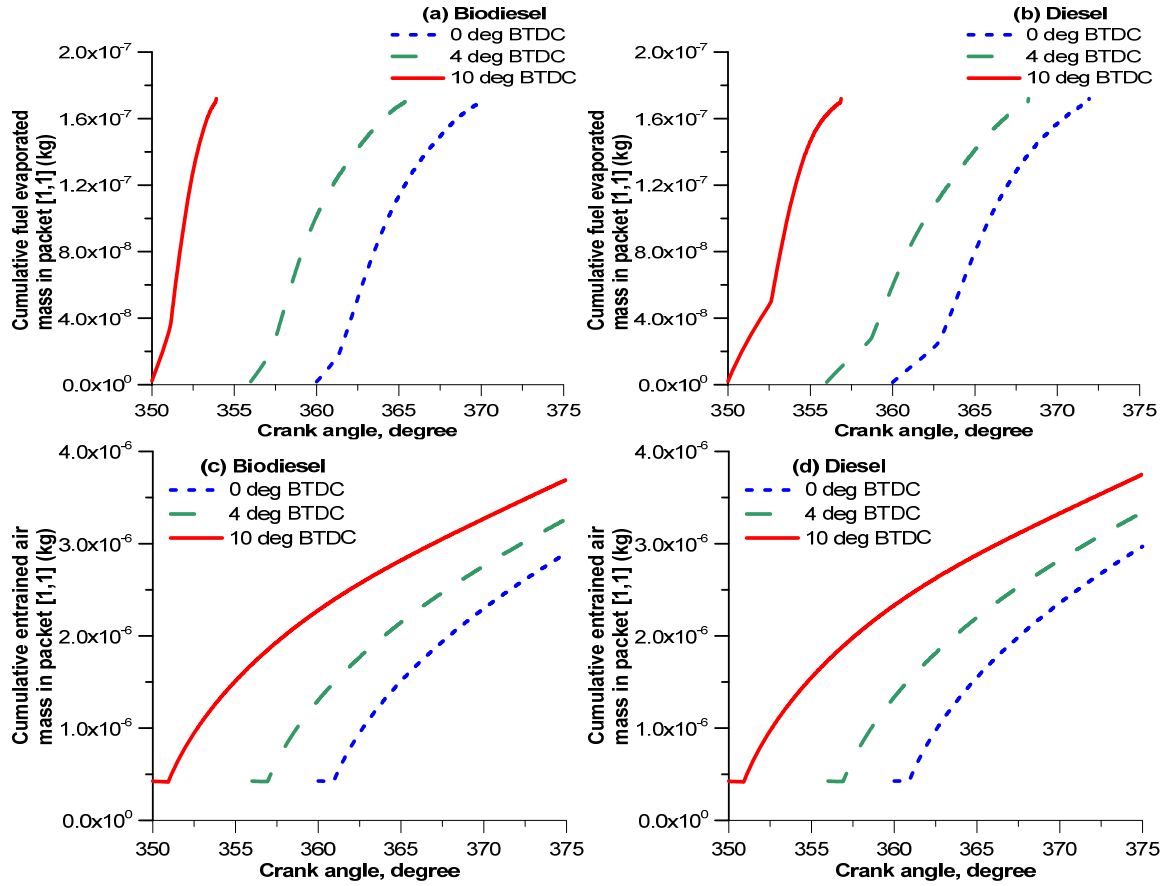
Figure 3.32   Prediction of cumulative evaporated fuel mass (a, b) and cumulative air entrained (c, d) in 1st injected packet (i=1, j=1) for three different injection timing at full engine load condition
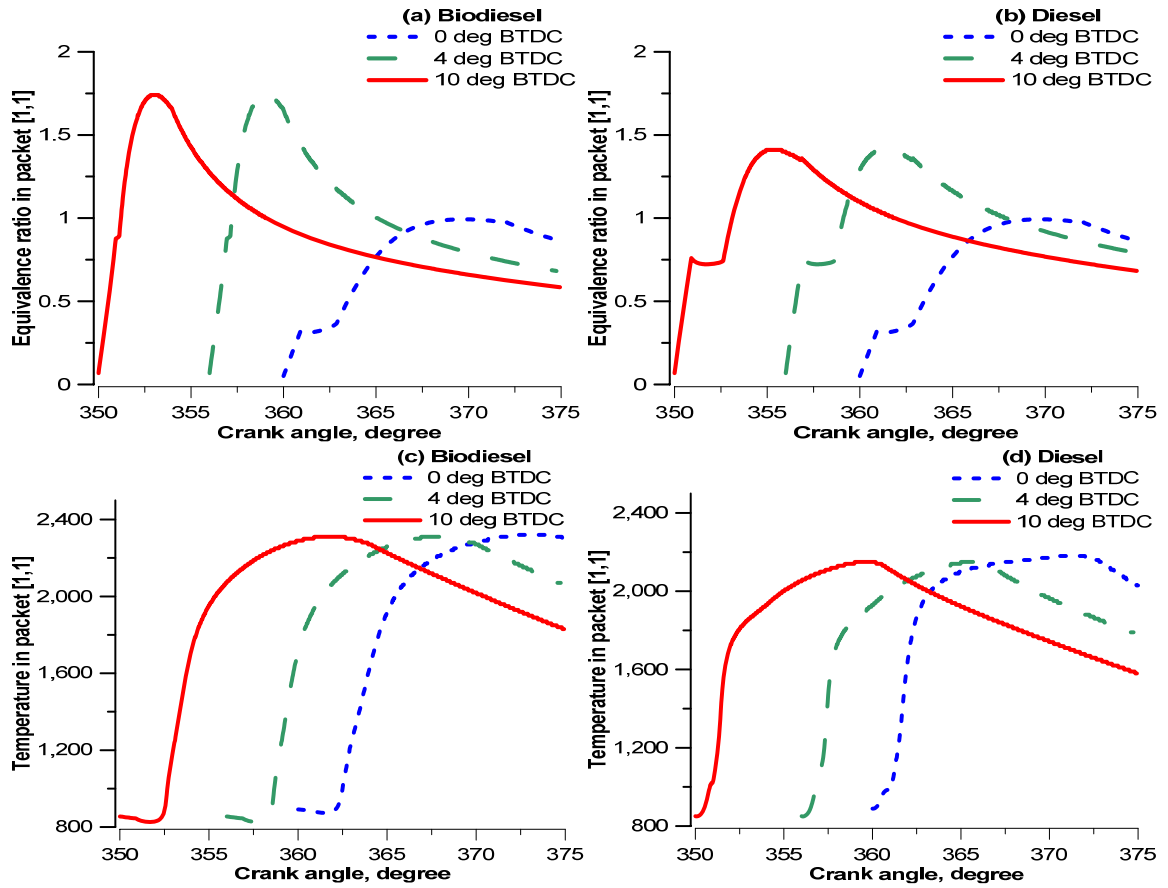
Figure 3.33   Prediction of equivalence ratio (a, b) and temperature (c, d) in first injected
packet (i=1, j=1) for three different injection timing at full engine load
condition.
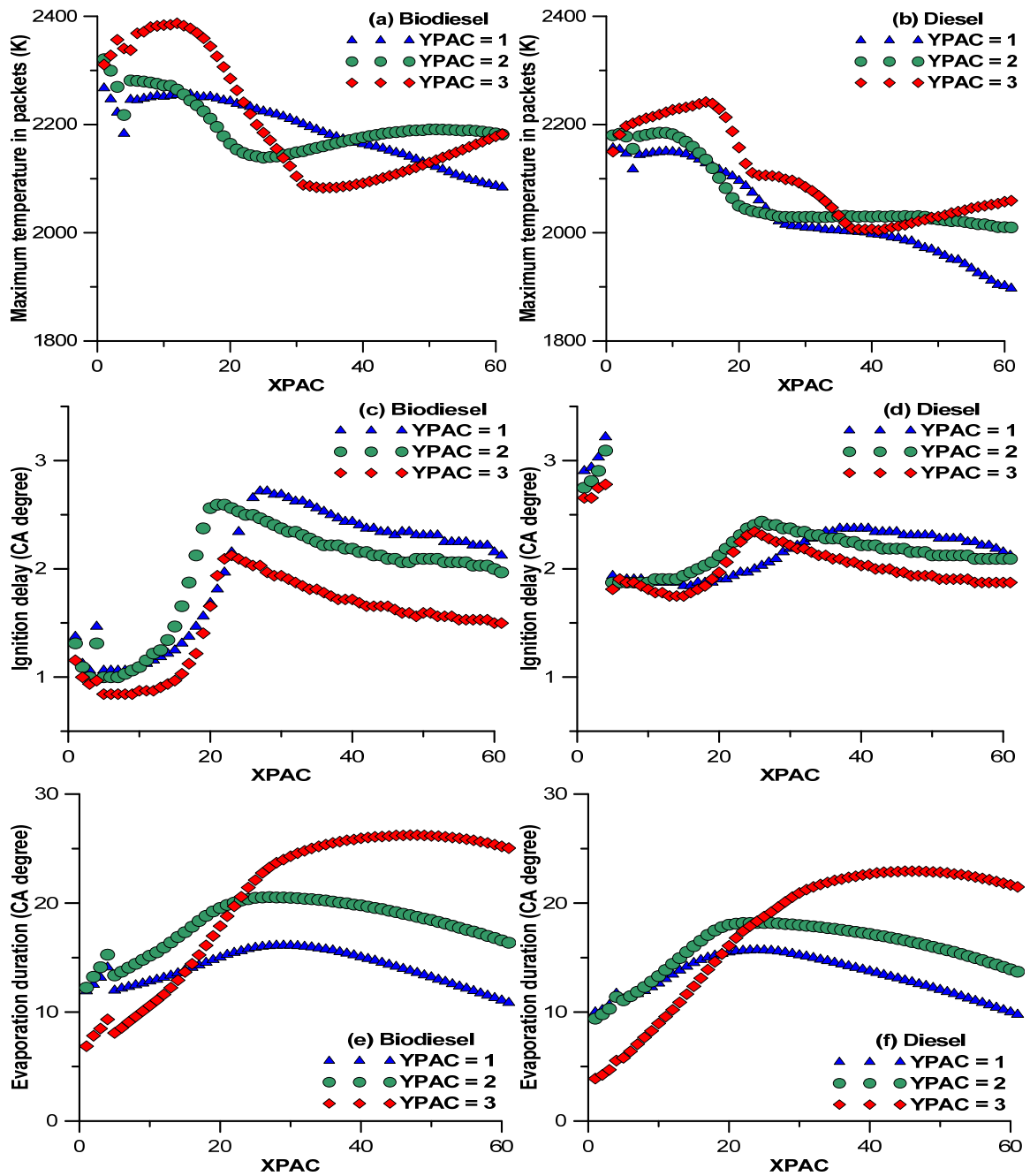
Figure 3.34   Packet wise variation in maximum temperature in packets (a, b), ignition delay (c, d) and evaporation duration (e, f) at three different injection timing at full engine load condition

147

Summary

In this chapter, development of the phenomenological simulation of diesel and biodiesel combustion was described in detail. Specifically, various sub-models used to simulate diesel/biodiesel combustion were discussed. At first, a brief literature review of previous research on diesel/biodiesel combustion was presented. Then, solution procedure followed by model calibration procedure was outlined. Thereafter, the results from model sensitivity studies performed with important model parameters were discussed. A "final" set of model constants were identified and used to validate the model predictions against experimental results over the entire range of injection timing and load condition for both diesel and biodiesel.

CHAPTER IV

CONCLUSIONS

Conclusions from Quasi Two-zone Simulation Results

A modified version of a generic hydrocarbon autoignition model was developed, validated and used in a quasi-two-zone combustion model to simulate diesel ignition delays (ID) for partially premixed Advanced Low Pilot Ignited Natural Gas Low Temperature Combustion (ALPING LTC). The effects of hot EGR on predicted and measured IDs in ALPING LTC were evaluated. Finally, a detailed uncertainty analysis of the ID model was performed to identify critical model parameters and experimental input variables. The following conclusions can be drawn from the predicted and measured ID results at a medium load (BMEP = 6 bar), engine speed of 1700 rpm, and intake manifold temperature (T_{in}) of 75°C:

- With the present ID model, the predicted IDs matched the measured IDs (within ± 10 percent error) over a range of BOIs from 20° to 60° BTDC, with only the pre-exponential constant for chain initiation (A_q) modified to 2.5×10^{13} from the baseline value of 5.74×10^{12}.

- Diesel evaporation times ($\Delta\theta_{evap}$) increased with increasing droplet sauter mean diameter (SMD). Initial droplet SMDs of the monodisperse diesel spray influenced IDs at retarded BOIs but had very little or no impact at advanced BOI.

- Increasing T_{in}, which was the most sensitive among all experimental input variables, led to a reduction in both the physical ($\Delta\theta_{evap}$) and chemical components of ID.

- Hot EGR led to shorter predicted and measured IDs over the range of BOIs, except 20° BTDC. In general, thermal effects of hot EGR were found to be more pronounced than either dilution or chemical effects for most BOIs.

- Uncertainty analysis results indicated that ID predictions were most sensitive to model parameters A_{P3}, A_q, and A_{fl}, and the experimental input variable T_{in}, which also contributed the most to overall uncertainties in IDs.

Conclusions from Phenomenological Multi-zone Simulation Results

A phenomenological, multi-zone, spray combustion model has been developed and used in a direct injection diesel engine for predicting combustion performance. The multi-zone spray combustion model includes details of spray evolution, evaporation, air entrainment, ignition and combustion. A broad validation of multi-zone model against experiments in a multi-cylinder engine has been conducted over a range of injection timings and engine loads for diesel and biodiesel.

The major conclusions are the following:

- The sensitivity analysis showed that engine performance could be predicted with a minimal number of zones in radial direction to be three with accuracy in the range of 95-98%.

- The total number of packets used in the simulation was recognized as an important model parameter.

150

- Igniton delay of biodiesel was found to be smaller than diesel. Furthermore, for both diesel and biodiesel, packets closer to the axis of spray ignite earlier than packets farther from the axis.

- The spray entrainment process was observed to have a strong effect on the combustion process in packets. In particular, the spray entrainment constant (K_{ent}) was found to immensely impact the packet combustion rates.

- The nozzle discharge coefficient (C_D) was found to be another very important parameter that has profound impact on estimation of combustion performance since it has a role in droplet size estimation and air entrainment into the packets.

- Residence time studies showed that both the magnitude of maximum temperatures and the time for which these temperatures persisted during combustion were higher for biodiesel combustion compared to diesel combustion. This is believed to be one of the reasons for higher nitrogen oxides emissions with biodiesel fuelling.

- The modified combustion models for premixed and mixing controlled phase have shown a great potential to estimate engine performance over a wide range of engine loads and injection timings for diesel and biodiesel. The predicted cylinder pressure and heat release from the phenomenological model were compared to and were found in close agreement (95-98% accuracy) with experimental data over a wide range of engine loads and injection timings for diesel and biodiesel

CHAPTER V

FUTURE WORKS AND RECOMMENDATIONS

The purpose of this research was to study the in-cylinder combustion process in diesel engines. It has focused mainly on developing the phenomenological models to simulate the ignition and combustion of diesel and biodiesel in diesel engine. Even with considerable encouraging initial results, there exists substantial scope for improvement. Following studies are recommended for future research:

- Ignition chemistry: Ignition model could be improved to include different ignition chemistry pathways, particularly low temperature chemistry for diesel autoignition, which is especially relevant in early injection low temperature combustion.

- Split-injection strategy: The present model should be validated for split injection and if needed modification should be done in the model to account for different injection strategies.

- Range of injection pressure: The model should be broadened to cover the impact of wide range of injection pressure on fuel atomization and hence on ignition and combustion process.

- Spray cone angle: Spray angle should be considered in estimating the number of packets in radial direction.

- Full cycle simulation: The present model should be extended to include the full engine cycle simulation. It will help in understanding the impact of variable valve

opening/closing timing on the effective compression and expansion ratio. It will also help in studying the role of trapped exhaust gas in the cylinder on the combustion process.

- Exhaust gas recirculation (EGR): The present simulation model can be modified to study the role of EGR on in-cylinder distribution of packet temperature and different emissions.

- Emission model: Improved phenomenological sub-models for NOx, HC,CO and soot emissions can be used to predict emissions behavior with diesel and/or biodiesel combustion.

REFERENCES

"Energy Information Administration." U. S. Department of Energy (http://www.eia.doe.gov/).

Agency, U. S. E. P. (2002). "A comprehensive analysis of biodiesel impacts on exhaust emissions." EPA420-P-02-001.

Aggarwal, S. K. (1998). "A review of spray ignition phenomena: present status and future research." Progress in Energy Combustion and Science 24: 565-600.

Alkidas, A. C. (1987). "On the Premixed Combustion in a Direct-Injection Diesel Engine

" Journal of Engine Gas Turbines Power 109(2): 187.

Amsden, A. A., et al. (1987). "KIVA-II Computer Program for Transient Multidimensional Chemically Reactive Flows with Sprays." Society of Automotive Engineers SAE 872072.

Amsden, A. A., et al. (1985). "KIVA: A Computer Program for Two- and Three-Dimensional Fluid Flow with Chemical Reactions and Fuel Sprays." Los Alamos National Laboratory Report LA-10245-MS.

Arrègle, J., et al. (1999). "The influence of injection parameters on Diesel spray characteristics." Society of Automotive Engineers SAE 1999-01-0200.

Assanis, D. N., et al. (2003). "A predictive ignition delay correlation under steady-state and transient operation of a direct injection diesel engine." Transactions of the American Society of Mechanical Engineers: Journal of Engineering for Gas Turbines and Power 125: 450-457.

ASTM (2002). "Standard Specification for Biodiesel Fuel (B100) Blend Stock for Distillate Fuels." American Society for Testing and Materials D6751-02.

Austen, A. E. W. and W. T. Lyn (1961). "Relation between fuel injection and heat release in a direct injection engine and the nature of the combustion processes." Proc Instn Mech Engng part D, J Autom Engg 1: 47-62.

Babinsky, E. and P. E. Sojka (2002). "Modelling drop size distribution." Progress in energy and combustion science 28: 303-329.

Badock, C., et al. (1999). "Investigation of cavitation in real size diesel injection nozzles." International Journal of Heat and Fluid Flow 20: 534-544.

Ban-Weiss, G., et al. (2007). "A numerical investigation into the anomalous slight NOx increase when burning biodiesel; a new (old) theory." Fuel Processing Technology 88: 659-667.

Barba, C., et al. (2000). "A phenomenological combustion model for heat release rate prediction in high-speed DI diesel engines with common rail injection." SAE Technical Paper 2000-01-2933.

Bazari, Z. (1992). "DI diesel combustion and emissions predictive capability for use in cycle simulation." SAE: 747-770.

Bergstrand, P. and I. Denbratt (2001). "Diesel combustion with reduced nozzle diameter." SAE paper no. 2001-01-2010.

Boehman, A. L., et al. (2004). "The Impact of the Bulk Modulus of Diesel Fuels on Fuel Injection Timing." Energy & Fuels 18: 1877-1882.

Bunger, J., et al. (2007). "Strong mutagenic effects of diesel engine emissions using vegetable oil as fuel." Arch. Toxicol. 81(8): 599-603.

Canacki, M. (2007). "Combustion characteristics of a turbocharged DI compression ignition engine fueled with petroleum diesel fuels and biodiesel." Bioresource Technology 98: 1167-1175.

Cao, L., et al. (2009). "Influence of Injection Timing and Piston Bowl Geometry on PCCI Combustion and Emissions." SAE International Journal of Engines October 2(1): 1019-1033.

Cheng, A. S., et al. (2006). "Investigation of the impact of biodiesel fuelling on NOx emissions using an optical direct injection diesel engine " International Journal of Engine Research 7: 297-318.

Cheng, A. S., et al. (2007). "Investigation of fuel effects on dilute, mixing-controlled combustion in an optical direct-injection diesel engine." Energy and Fuels 21(4): 1989-2002.

Chiu, H. H. (2000). "Advances and challenges in droplet and spray combustion. 1. Towards a unified theory of droplet and spray combustion." Progress in energy and combustion science 26: 381-416.

Chmela, F. and G. Orthaber (2004). "Rate of heat release prediction for direct injection diesel engines based on purely mixing controlled combustion." Oil and Gas Science and Technology, Rev. IFP 59(6).

Choi, C., et al. (1997). "Effects of Biodiesel Blended Fuels and Multiple Injections on D. I. Diesel Engines." SAE 970218.

Cloin, J. (2007). "Coconut oil as a fuel in the Pacific Islands." Natural Resources Forum 31: 119-127.

Coleman, H. W. and W. G. Steele (1999). "Experimentation and uncertainty analysis for engineers." John Wiley & Sons, New York.

Cox, R. A. and J. A. Cole (1985). "Chemical aspects of the autoignition of hydrocarbon-air mixtures." Combustion and Flame 60: 109-123.

Curran, H. J., et al. (2002). "A Comprehensive Modeling Study of iso-Octane Oxidation." Combustion and Flame 129: 253-280.

Curran, H. J., et al. (1998). "Oxidation of Automotive Primary Reference Fuels at Elevated Pressures." Proc. Combust. Inst. 27: 379-387.

Dagaut, P., et al. (2007). "Rapeseed oil methyl ester oxidation over extended ranges of pressure, temperature, and equivalence ratio: Experimental and modeling kinetic study." Proceedings of the Combustion Institute 31(2).

Dec, J. E. (1997). "A Conceptual Model of DI Diesel Combustion Based on Laser-Sheet Imaging." SAE Technical Paper 970873.

Dent, J. C. (1971). "Basis for the Comparison of Various Experimental Methods for Studying Spray Penetration." SAE Technical Paper 710571.

Dent, J. C. (1971). "A basis for the comparison of various experimental methods for studying spray penetration." Society of Automotive Engineers SAE 710571.

Dooley, S., et al. (2008). "Autoignition measurements and a validated kinetic model for the biodiesel surrogate, methyl butanoate." Combustion and Flame 153(1-2): 2-32.

EL-Hannouny, E., et al. (2007). "Spray characterization from common rail injection system for use in locomotive engines." Proceedings of ICEF07 Fall Technical Conference of the ASME Internal Combustion Engine Division ICEF2007-1637.

EPA (2002). "A Comprehensive Analysis of Biodiesel Impacts on Exhaust Emissions." U.S. Environmental Protection Agency, Draft Technical Report EPA420-P-02-001.

Epping, K., et al. (2002). "The Potential of HCCI Combustion for High Efficiency and Low Emissions." SAE 2002-01-1923.

Faeth, G. M. (1983). "Evaporation and combustion of sprays." Progress in energy and combustion science 9: 1-76.

FIE (2007). "Fatty Acid Methyl Ester Fuels as a Replacement or Extender for Diesel Fuels." FIE (Fuel Injection Equipment) Manufacturers Common Position Statement: Delphi, Stanadyne.

Fisher, E. M., et al. (2000). "Detailed chemical kinetic mechanisms for combustion of oxygenated fuels " Proceedings of the Combustion Institute 28(2): 1579-1586.

Flynn, P. F., et al. (1999). "Diesel Combustion: An Integrated View Combining Laser Diagnostics, Chemical Kinetics, and Empirical Validation." SAE Technical Paper 1999-01-0509.

Gaïl, S., et al. (2007). "A wide-ranging kinetic modeling study of methyl butanoate combustion." Proceedings of the Combustion Institute 31(1): 305-311.

García, M. T., et al. (2009). "A new Heat release rate (HRR) law for Homogeneous Charge Compression Ignition (HCCI) combustion mode." Applied Thermal Engineering 29.

Gerpen, J. V. (2001). "Combustion in Diesel Engines--Modeling and Simulation." SAE Engineering Academies Lecture Notes.

Gibson, C. M., et al. (2010). "Comparison of Propane and Methane Performance and Emissions in a Turbocharged Direct Injection Dual Fuel Engine." Proceedings of the ASME 2010 Internal Combustion Engine Division Fall Technical Conference ICEF2010-35128.

Graboski, M. S., et al. (2003). "The Effect of Biodiesel Composition on Engine Emissions from a DDC Series 60 Diesel Engine." U.S. Department of Energy, NREL Report, NREL/SR-510-31461

Gragg, K. (1994). "Effects of environmentally classified diesel fuels, RME and blends of diesel fuels and RME on the exhaust emissions." MTC (Sweden), Report 9209B.

Griffiths, J. F. (1995). "Reduced kinetic models and their application to practical combustion systems." Prog. Energy Combust. Sci. 21: 25-117.

Guo, H., et al. (2004). "Soot and NO formation in couterflow ethylene/oxygen/nitrogen diffusion flames." Combustion Theory and Modelling 8: 475-489.

Gupta, S., et al. (2000). "Effect of injection parameters on diesel sprays characteristic." Society of Automotive Engineers SAE 2000-01-1600.

Halstead, M. P., et al. (1975). "A Mathematical Model for Hydrocarbon Autoignition at High Pressures." Proc. R. Soc. London. A 346: 515-538.

Halstead, M. P., et al. (1977). "The autoignition of hydrocarbon fuels at high temperature and pressure - fitting of a mathematical model." Combustion and flame 30: 45-46.

Hamosfakidis, V. and R. D. Reitz (2003). "Optimization of a hydrocarbon fuel ignition model for two single component surrogates of diesel fuel." Combustion and Flame 132: 433-450.

Hardenberg, H. O. and F. W. Hase (1979). "An Empirical Formula for Computing the Pressure Rise Delay of a Fuel From Its Cetane Number and From the Relevant Parameters of Direct-Injection Diesel Engines." Society of Automotive Engineers 790493.

Hashimoto, M., et al. (2002). "Combustion of the Rape-Seed Oil in a Diesel Engine." SAE 2002-01-0867.

Hay, N. and P. L. Jones (1976). "Comparison of the various correlations for spray penetration." Society of Automotive Engineers SAE paper 720776.

Henein, N. A. and D. J. Patterson (1972). "Emissions From Combustion Engines And Their Control." Ann Arbor Science Publishers Inc.

Herbinet, O., et al. (2010). "Detailed chemical kinetic mechanism for the oxidation of biodiesel fuels blend surrogate." Combustion and Flame 157(5): 893-908.

Heywood, J. B. (1988). "Internal Combustion Engine Fundamentals." McGraw-Hill, New York.

Hill, J., et al. (2006). "Environmental, economic, and energetic costs and benefits of biodiesel and ethanol biofuels." Proceedings of the National Academy of Sciences of the United States of America 103(30): 11206-11210.

Hiroyasu, H. and M. Arai (1990). "Structure of fuel sprays in diesel engines." Transactions of the SAE 99(3): 1050-1061.

Hiroyasu, H., et al. (1989). "Empirical Equations for the Sauter Mean Diameter

of a Diesel Spray." Society of Automotive Engineers SAE 890464.

Hiroyasu, H., et al. (1980). "Supplementary comments: fuel spray characterization in diesel engines. In C. A. Amann and J. A. Mattavi (Eds.)." Combustion Modeling in Reciprocating Engines. New York: Plenum Press.: 369-408.

Hiroyasu, H., et al. (1983). "Development and Use of a Spray Combustion Model to Predict Diesel Engine Efficiency and Pollutant Emission." JSME 26(24): 569-575.

Howell, S. (1997). "U.S. Biodiesel Standards - An Update of Current Activities." SAE Technical Paper 971687.

Hu, H. and J. Keck (1987). "Autoignition of Adiabatically Compressed Combustible Gas Mixtures." SAE 872110.

Jung, D. (2001). "A multi-zone direct-injection diesel spray combustion model for cycle simulation studies of large-bore engine performance and emissions." A PhD Thesis: University of Michigan.

Kadota, T., et al. (1976). "Spontaneous Ignition Delay of a Fuel Droplet in High Pressure High Temperature Gaseous Environments." JSME 19(130): 437-445.

Kastengren, A. L., et al. (2008). "Study of Diesel Jet Variability Using Single-Shot X-Ray Radiography." Journal of Engine Gas Turbines Power 130(3).

Kimura, S., et al. (1999). "New Combustion Concept for Ultra-Clean andHigh-Efficiency Small DI Diesel Engines." SAE 1999-01-3681.

Kinast, J. A. (2003). "Production of Biodiesels from Multiple Feedstocks and Properties of Biodiesels and Biodiesel/Diesel Blends." U.S. Department of Energy, NREL Report, NREL/SR-510-31460.

Knothe, G. (2001). "Historical perspectives on vegetable oil-based diesel fuels." INFORM 12: 1103-1107.

Knothe, G., et al. (2006). "Exhaust Emissions of Biodiesel, Petrodiesel, Neat Methyl Esters, and Alkanes in a New Technology Engine." Energy & Fuels 20: 403-408.

Kobori, S., et al. (2000). "A study of ignition delay of diesel fuel sprays." International Journal of Engine Research 1(1): 29-39.

Krahl, J., et al. (1995). "Survey about Biodiesel Exhaust Emissions and their Environmental Effects." Institute of Biosystems Engineering, Federal Agricultural Research Centre, Braunschweig, Germany.

Krishnan, S. R. (2005). "Experimental investigations and phenomenological simulation of combustion in a low pilot-ignited natural gas engine with a focus on advanced injection timings." Ph.D. dissertation, University of Alabama, Tuscaloosa.

Krishnan, S. R., et al. (2004). "Strategies for reduced NOx emissions in pilot ignited natural gas engines." Trans. ASME: Journal of Engineering for Gas Turbines and Power 126: 665-671.

Kumar, K., et al. (2009). "Autoignition of n-decane under elevated pressure and low-to-intermediate temperature conditions." Combustion and Flame 156: 1278-1288.

Kuniyoshi, H., et al. (1980). "Investigation on the characteristics of diesel fuel spray." SAE paper no. 800968.

Kuo, K. K. (1986). "Priniciple of Combustion." John Wiley & Sons, New York.

Ladommatos, N., et al. (1998). "The effects of carbon dioxide in exhaust gas recirculation on diesel engine emission." Proc Instn Mech Engng part D, J Autom Engg 212: 25-42.

Laguitton, O., et al. (2002). "Spray development and combustion characteristics for common rail Diesel injection systems." Institute of Mechanical Engineer Conference on Fuel Injection Systems: 26-27.

Lahiri, D., et al. (1997). "Utilization of Oxygen-Enriched Air in Diesel Engines: Fundamental Considerations." Americal Society of Mechanical Engineers 97-ICE-72.

Li, Q. and D. N. Assanis (1993). "A Quasi-Dimensional Combustion Model for Diesel Engine Simulation." Americal Society of Mechanical Engineers ICE-Vol. 20.

Livengood, J. C. and P. C. Wu (1955). "Correlation of auto-ignition phenomena in internal combustion engines and rapid compression machines." Proceedings of the Combustion Institute 5: 347-356.

Loth, E. (2000). "Numerical approaches for motion of dispersed particles, droplets and bubbles." Progress in energy and combustion science 26: 161-223.

Lyn, W. T. (1963). "Study of burning rate and nature of combustion in diesel engines." Symposium (International) on Combustion 9(1): 1069-1082.

McCormick, R., et al. (2001). "Impact of biodiesel source material and chemical structure on emissions of criteria pollutants from a heavy-duty engine." Environmental Science and Technology 35: 1742-1747.

McCormick, R., et al. (2005). "Regulated emissions from biodiesel tested in heavy-duty engines meeting 2004 emission standards." SAE 2005-01-2200.

McCormick, R. L. (2002). "Renewable Diesel Fuels: Status of Technology and R&D Needs." US DOE, 8th Diesel Emissions Reduction Conference (DEER), San Diego, CA.

McCormick, R. L. (2006). "Deployment Issues for Biodiesel: Fuel Quality and NOx Emissions." National Renewable Energy Laboratory, Golden, CO, USA, Presentation, March 7, 2006.

McGill, R., et al. (2003). "Emission performance of selected biodiesel fuels." SAE Technical Paper 2003-01-1866.

Metcalfe, W. K., et al. (2007). "Experimental and Modeling Study of $C_5H_{10}O_2$ Ethyl and Methyl Esters." Journal of Physical Chemistry A 111: 4001-4014.

Minetti, R., et al. (1995). "A rapid compression machine investigation of oxidation and auto-ignition of n-heptane: Measurements and modelling." Combustion and Flame.

Mitchell, D. L., et al. (1993). "The effects of simulated EGR via intake air dilution on combustion in an optically accessible DI diesel engine." SAE 932798.

Monyem, A., et al. (2001). "The effect of timing and oxidation on emissions from biodiesel-fueled engines." ASAE Transactions 44(1): 35-42.

Morgan, R., et al. (2001). "The influence of injector parameters on the formation and break-up of a diesel sprays." Society of Automotive Engineers SAE 2001-01-0529.

Morgan, R., et al. (2001). "The influence of injector parameters on the formation and break up of adiesel spray." SAE Transactions - Journal of Engines 110(3): 389-399.

Naber, J. and D. L. Siebers (1996). "Effects of gas density and vaporization on penetration and dispersion of diesel sprays." Society of Automotive Engineers SAE 960034.

Naber, J. and D. L. Siebers (1996). "Effects of gas density and vaporization on penetration and dispersion of diesel sprays." SAE paper no. 960034.

Openshaw, K. (2000). "A review of Jatropha curcas: An oil plant of unfulfilled promise." Biomass and Bioenergy 19(1): 1-15.

Orme, M. (1997). "Experiments on droplet collisions, bounce, coalescence and disruption." Progress in energy and combustion science 23: 65-79.

Patterson, J., et al. (2006). "Experimental Study of DI Diesel Engine Performance Using Three Different Biodiesel Fuels." SAE 2006-01-0234.

Patterson, M. A., et al. (1994). "Modeling the Effects of Fuel Injection Characteristics on Diesel Engine Soot and NOx Emissions." Society of Automotive Engineers SAE Paper 940523.

Pepiot-Desjardinsa, P., et al. (2008). "Structural group analysis for soot reduction tendency of oxygenated fuels." Combustion and Flame 154: 191-205.

Ra, Y. and R. D. Reitz (2008). "A reduced chemical kinetic model for IC engine combustion simulations with primary reference fuels " Combustion and Flame 155(4): 713-738.

Rakopoulos, C., et al. (2008). "Performance and emissions of bus engine using blends of diesel fuel with Biodiesel of sunflower oil derived from Greek feedstock." Fuel 87(2): 147-157.

Ristori, A., et al. (2001). "The oxidation of n-Hexadecane: experimental and detailed kinetic modeling." Combustion and Flame 125(3): 1128-1137.

Sarathy, S. M., et al. (2007). "A comparison of saturated and unsaturated C4 fatty acid methyl esters in an opposed flow diffusion flame and a jet stirred reactor." Proceedings of the Combustion Institute 31(1): 1015-1022.

Sazhin, S. S., et al. (1999). "The Shell Autoignition Model: A New Mathematical Formulation." Combustion and Flame 117: 529-540.

Sazhina, E. M., et al. (2000). "A detailed modelling of the spray ignition process in diesel engines." Combust Science and Technology 160: 317-344.

Schapertons, H. and W. Lee. (1985). "Multidimensional modeling of knocking combustion in SI engines." SAE 850502.

Schroeder, O., et al. (1999). "Environmental and Health Effects Caused by the Use of Biodiesel." SAE Technical Paper 1999-01-3561.

Sharp, C. A., et al. (2000). "The Effect of Biodiesel Fuels on Transient Emissions From Modern Diesel Engines-Part I: Regulated Emissions and Performance." SAE Technical Paper 2000-01-1967.

Sheehan, J., et al. (1998). "Life Cycle Inventory of Biodiesel and Petroleum Diesel for Use in an Urban Bus." NREL/SR-580-24089.

Sheehan, J., et al. (1998). "An overview of biodiesel and petroleum diesel life cycles." NREL/TP-580-24772.

Shipinski, J., et al. (1968). "Experimental Correlation Between Rate-of-Injection and Rate-of-Heat-Release in a Diesel Engine." ASME Paper 68-DGP-11.

Singh, S., et al. (2004). "Effect of pilot injection timing, pilot quantity and intake charge conditions on performance and emissions for an advanced low pilot-ignited natural gas engine." Inter. J. Engine Res. 5(4): 329-348.

Sirignano, W. A. (1983). "Fuel droplet vaporization and spray combustion theory." Progress in energy and combustion science 9: 291-322.

Soteriou, C., et al. (1995). "Direct injection diesel sprays and the effect of cavitation and hydraulic flip on atomization." SAE paper no. 950080.

Soyhan, H. S., et al. (2002). "Chemical Kinetic Modeling of Combustion in Internal Combustion Engines using Reduced Chemistry." Combust. Sci. Technol. 174(73-91).

Spadaccini, L. J. and J. A. TeVelde (1982). "Autoignition characteristics of aircraft-type fuels." Combustion and Flame 46: 283-300.

Srinivasan, K. K., et al. (2006). "Improving low load combustion, stability, and emissions in pilot-ignited natural gas engines " Proc. of IMechE (Part D): Journal of Automobile Engineering 220: 229-239.

Srinivasan, K. K., et al. (2007). "Analysis of Diesel Pilot-Ignited Natural gas Low-Temperature combustion with Hot Exhaust Gas Recirculation." Combustion Science and Technology 179(9): 1737-1776.

Srinivasan, K. K., et al. (2006). "The advanced low pilot ignited natural gas engine - a combustion analysis." Trans. ASME: Journal of Engineering for Gas Turbines and Power 128: 213-218.

Stavinoha, L. L. and S. Howell (1999). "Potential Analytical Methods for Oxidative Stability Testing of Biodiesel and Biodiesel Blends." SAE Technical Paper 1999-01-3520.

Sze, C., et al. (2007). "Impact of test cycle and biodiesel concentration on emissions." SAE Technical Paper 2007-01-4040.

Szybist, J., et al. (2007). "Biodiesel combustion, emissions, and emission control." Fuel Processing Technology 88: 679{691.

Szybist, J. P. and A. L. Boehman (2003). "Behavior of a Diesel Injection System With Biodiesel Fuel." SAE Technical Paper 2003-01-1039.

Szybist, J. P., et al. (2005). "Evaluation of formulation strategies to eliminate the biodiesel NOx effect." Fuel Processing Technology 86(10): 1109-1126.

Tanaka, S., et al. (2003). "A reduced chemical kinetic model for HCCI combustion of primary reference fuels in a rapid compression machine." Combustion and Flame 133: 467-481.

Tat, M. (2003). "Investigation of Oxides of Nitrogen Emissions from Biodiesel-Fueled Engines." PhD thesis, University of Illinois at Urbana-Champaign.

Tat, M. E. and J. H. V. Gerpen (2003). "Measurement of Biodiesel Speed of Sound and Its Impact on Injection Timing." Report NREL/SR-510-31462, National Renewable Energy Laboratory, Golden, CO.

Tauzia, X., et al. (2000). "The Use of Phenomenological, Multizone Combustion Model to Investigate Emissions from Marine Diesel Engines." Americal Society of Mechanical Engineers ICE-325.

Taylor, J. D. (2004). "Report on the relationship between molecular structure and compression ignition fuels, both conventional and HCCI." National Renewable Energy Laboratory, Golden, CO, USA, Report NREL/MP-540-36726.

Theobald, M. A. and W. K. Cheng (1987). "A numerical study of diesel ignition." ASME Energy Sources Tech. Conf. and Exhibition, ASME 87-FE-2.

Toulson, E., et al. (2010). "Modeling the Auto-Ignition of Oxygenated Fuels using a Multistep Model." Energy and Fuels 24(2): 888-896.

Tyson, K. S., et al. (2004). "Biomass Oil Analysis: Research Needs and Recommendations." Report NREL/TP-510-34796, National Renewable Energy Laboratory, Golden, CO.

USEPA (2002). "A comprehensive analysis of biodiesel impacts on exhaust emissions." EPA420-P-02-001.

Varnavas, C. and D. N. Assanis (1996). "A High Temperature and High Pressure Evaporation Model for the KIVA-3 Code." Society of Automotive Engineers SAE 960629.

Vaughn, T., et al. (2006). "Ignition delay of bio-ester fuel droplets." Society of Automotive Engineers 2006-01-3302.

Wang, W., et al. (2000). "Emissions from nine heavy trucks fuel by diesel and biodiesel blend without modification." Environmental Science and Technology 34: 933-939.

Watson, N., et al. (1980). "A combustion correlation for diesel engine simulation." SAE 800029.

Westbrook, C. K., et al. (2011). "Detailed chemical kinetic reaction mechanisms for soy and rapeseed biodiesel fuels." Combustion and Flame 158(4): 742-755.

Westbrook, C. K., et al. (2009). "A Detailed Chemical Kinetic Reaction Mechanism for n-Alkane Hydrocarbons from n-Octane to n-Hexadecane." Combustion and Flame 156(1): 181-199.

Wolfer, H. H. (1938). "Ignition Lag in Diesel Engines." VDI-Forschungsheft, 392: Translated by Royal Aircraft Establishment, Farnborough Library no. 358, UDC 621-436.047 (Translation reprinted August 1959).

Wood, J., et al. (2004). "Long Term World Oil Scenario." an article published on (http://www.usgs.gov).

Xingcai, L., et al. (2006). "The effects of external exhaust Gas recirculation and Cetane number improver on the gasoline homogeneous charge compression ignition engines." Combust. Sci. and Tech. 178: 1237-1249.

Yuan, W. (2005). "Computational modeling of NOx emissions from biodiesel combustion based on accurate fuel properties." Ph.D. dissertation, University of Illinois, Urbana-Champaign.

APPENDIX A

AUTOIGNITION MODEL CONSTANTS

Table A.1   Original Autoignition Model Constants (Halstead et al. 1977)

Parameter	70 RON	90 RON	100 RON
A_{p1}	1×10^{12}	1×10^{12}	1×10^{12}
$E_{p}1$	0	0	0
$A_{p}2$	1×10^{11}	1×10^{11}	1×10^{11}
$E_{p}2$	1.5×10^{4}	1.5×10^{4}	1.5×10^{4}
$A_{p}3$	1×10^{13}	1×10^{13}	1×10^{13}
$E_{p}3$	8.5×10^{2}	8.5×10^{2}	8.5×10^{2}
A_{q}	6.96×10^{11}	1.2×10^{12}	3.96×10^{13}
E_{q}	3.5×10^{4}	3.5×10^{4}	4×10^{4}
A_{b}	3.35×10^{18}	4.4×10^{17}	6.512×10^{15}
E_{b}	4.7×10^{4}	4.5×10^{4}	4.0×10^{4}
A_{t}	2.5×10^{12}	3×10^{12}	3.5×10^{12}
E_{t}	0	0	0
A_{f1}	1.6×10^{-6}	7.3×10^{-4}	7.3×10^{-4}
$E_{f}1$	-1.5×10^{4}	-1.5×10^{4}	-1.5×10^{4}
A_{f2}	180	180	180
E_{f2}	-7.0×10^{3}	-7.0×10^{3}	-7.0×10^{3}
A_{f3}	0.75	1.47	2.205
E_{f3}	1×10^{4}	1×10^{4}	1×10^{4}
A_{f4}	1.21×10^{6}	1.88×10^{4}	1.7×10^{4}
E_{f4}	3×10^{4}	3×10^{4}	3×10^{4}
x_{1}	1	1	1
y_{1}	-0.5	0	0
x_{3}	0	0	0
y_{3}	0	0	0
x_{4}	-1	-1	-1.3
y_{4}	1.0	0.35	0.35

Table A.2   Modified Autoignition Model Constants

Parameter	Tetradecane (Hamosfakidis and Reitz 2003)	Methyl Butanoate (Toulson et al. 2010)
A_{p1}	3.98×10^{13}	1×10^{12}
$E_{p}1$	9.25×10^{2}	0
$A_{p}2$	8.95×10^{12}	1×10^{11}
$E_{p}2$	2.092×10^{4}	1.5×10^{4}
$A_{p}3$	2.17×10^{13}	1×10^{13}
$E_{p}3$	6.92×10^{3}	850
A_{q}	2.5×10^{13}	3×10^{13}
E_{q}	4.159×10^{4}	5×10^{4}
A_{b}	4.90×10^{17}	6.512×10^{15}
E_{b}	4.972×10^{4}	6×10^{4}
A_{t}	1.10×10^{13}	3×10^{5}
E_{t}	7.57×10^{3}	0
A_{f1}	6.80×10^{-4}	9.3
$E_{f}1$	-3.39×10^{3}	-1.5×10^{4}
A_{f2}	2.68×10^{2}	180
E_{f2}	-7.19×10^{3}	-7.0×10^{3}
A_{f3}	8.19	1.205
E_{f3}	1.45×10^{4}	1.5×10^{4}
A_{f4}	3.70×10^{5}	1.88×10^{4}
E_{f4}	$3.264. \times .10^{4}$	4×10^{4}
x_{1}	0	1.5
y_{1}	0	0
x_{3}	0	0
y_{3}	0	0
x_{4}	0	-0.3
y_{4}	0	0.35